

# 1 **Bidirectional coupling of a long-term integrated assessment model**

## 2 **REMINd v3.0.0 with an hourly power sector model DIETER v1.0.2**

3 Chen Chris Gong<sup>1</sup>, Falko Ueckerdt<sup>1</sup>, Robert Pietzcker<sup>1</sup>, Adrian Odenweller<sup>1,3</sup>, Wolf-Peter Schill<sup>2</sup>, Martin  
4 Kittel<sup>2</sup>, Gunnar Luderer<sup>1,3</sup>

5 <sup>1</sup> Potsdam Institute for Climate Impact Research (PIK), Potsdam, Germany

6 <sup>2</sup> German Institute for Economic Research (DIW Berlin), Berlin, Germany

7 <sup>3</sup> Global Energy Systems Analysis, Technische Universität Berlin, Berlin, Germany

8 *Correspondence to:* Chen Chris Gong ([chen.gong@pik-potsdam.de](mailto:chen.gong@pik-potsdam.de))

9

10 **Abstract.** Integrated assessment models (IAMs) are a central tool for the quantitative analysis of climate change mitigation  
11 strategies. However, due to their global, cross-sectoral and centennial scope, IAMs cannot explicitly represent the temporal and  
12 spatial details required to properly analyze the key role of variable renewable electricity (VRE) for decarbonizing the power  
13 sector and enabling emission reductions through end-use electrification. In contrast, power sector models (PSMs) can  
14 incorporate high spatio-temporal resolutions, but tend to have narrower sectoral and geographic scopes and shorter time  
15 horizons. To overcome these limitations, here we present a novel methodology: an iterative and fully automated soft-coupling  
16 framework that combines the strengths of a long-term IAM and a detailed PSM. The key innovation is that the framework uses  
17 the market values of power generations as well as the capture prices of demand flexibilities in the PSM as price signals that  
18 change the capacity and power mix of the IAM. Hence, both models make endogenous investment decisions, leading to a joint  
19 solution. We apply the method to Germany in a proof-of-concept study using the IAM REMIND v3.0.0 and the PSM DIETER  
20 v1.0.2, and confirm the theoretical prediction of almost-full convergence both in terms of decision variables and (shadow)  
21 prices. At the end of the iterative process, the absolute model difference between the generation shares of any generator type for  
22 any year is <5% for a simple configuration (no storage, no flexible demand) under a “proof-of-concept” baseline scenario, and  
23 6-7% for a more realistic and detailed configuration (with storage and flexible demand). For the simple configuration, we  
24 mathematically show that this coupling scheme corresponds uniquely to an iterative mapping of the Lagrangians of two power  
25 sector optimization problems of different time resolutions, which can lead to a comprehensive model convergence of both  
26 decision variables and (shadow) prices. The remaining differences in the two models can be explained by a slight mismatch  
27 between the standing capacities in the real-world and optimal modeling solutions purely based on cost competition. Since our  
28 approach is based on fundamental economic principles, it is applicable also to other IAM-PSM pairs.

### 29 **1 Introduction**

30 Thanks to decade-long policy support in many regions of the world and technological learning, the costs of both wind power  
31 and solar photovoltaics have plummeted (IEA, 2021; Lazard, 2021). These types of variable electricity generation are now  
32 highly cost competitive against other alternatives, such that their deployment is increasingly driven by market forces instead of  
33 climate policies. Among the newly added renewable generations in 2020, nearly two thirds were cheaper than the cheapest new  
34 fossil fuel (IRENA, 2020). Due to both cost declines and pressing concerns over climate change, investing in these clean and  
35 abundant resources has become a crucial part of national and regional strategies to decarbonize the power sector (The White  
36 House, 2021; Cherp et al., 2021; National long-term strategies, 2022; Rechsteiner, 2021; ICCSD Tsinghua University, 2022).

37 Given this dramatic development in the power sector over the past two decades, a universal consensus has emerged among  
38 energy transition scholars and policy makers: emissions in the power sector are relatively “easy-to-abate” (Luderer et al., 2018;  
39 Azevedo et al., 2021; Clarke et al., 2022). Compared with other primarily non-electrified end-use sectors such as buildings,  
40 transport and industry, the technologies required to transform the power sector are low-cost, mature and readily available. This  
41 trend has in recent years led to a second emerging consensus: the power sector will be the fundamental basis of a future low-  
42 cost, efficient and climate-neutral energy system (Brown et al., 2018b; Ram et al., 2018; Ramsebner et al., 2021; Luderer et al.,  
43 2022a). In addition to direct electrification, which requires end-use transformations of currently non-electrified demand,  
44 emerging technological developments in hydrogen and e-fuels produced from renewable electricity have also contributed to the  
45 broadening of potential technology portfolios for the “hard-to-abate” sectors, such as high temperature heat and chemical  
46 productions (Parra et al., 2019; Bhaskar et al., 2020; Griffiths et al., 2021). Together, direct and indirect electrification support a  
47 broad concept of “sector coupling”, which facilitates decarbonization by powering end-use demand with variable renewable  
48 energy sources (Ramsebner et al., 2021).

49 Due to the pivotal role of electrification and sector coupling in mitigation scenarios, there is an increasing demand on the scope  
50 and level of detail of energy-economy models used to guide the energy transition and climate policies. The models would  
51 ideally encompass a global, multi-decadal and multi-sectoral scope, such that the scenarios are relevant for international and  
52 regional climate policies, while simultaneously incorporating a high level of spatio-temporal detail. The latter is important to  
53 account for the specifics of variable renewable electricity generation as well as its physical and economic interplay with the  
54 electrification of energy demand (Li and Pye, 2018; Brunner et al., 2020; Prol and Schill, 2020; Böttger and Härtel, 2022;  
55 Ruhnau, 2022). This need for improved modeling methods or frameworks, which has to overcome the trade-off between scope  
56 and detail, is a substantial methodological challenge. It entails realizing two main objectives:

57 Objective 1) Accurately model the power sector transformation over long time horizons in terms of investment and dispatch,  
58 especially at high shares of variable renewable energy (VRE) sources. Long-term pathways for the following power  
59 sector quantities and prices should accurately incorporate short-term hourly details:  
60 a) capacity and generation mix of the power sector,  
61 b) market values (annual average revenues per power generation unit) for variable and dispatchable plants,  
62 c) capacity factors of the dispatchable plants and the curtailment rates of variable renewables,  
63 d) storage capacity and dispatch.

64 Objective 2) Accurately model direct electrification of end-use sectors as well as indirect electrification technologies such as  
65 green hydrogen production, where existing and emerging sources of power demand can be in-part flexibilized.

## 66 **1.1 Current modeling approaches and limitations**

67 Current energy system models broadly fall into two distinct categories, carried out by two research communities with little  
68 institutional overlap: integrated assessment models (IAMs) and power sector models (PSMs), each with its own strengths and  
69 weaknesses. IAMs are comprehensive models of global scale and span multiple decades, linking macroeconomics, energy  
70 systems, land-use and environmental impacts (Stehfest et al., 2014; Calvin et al., 2017; Huppmann et al., 2019; Baumstark et al.,  
71 2021; Keppo et al., 2021; Guivarc et al., 2022), therefore providing an “integrated assessment” of multiple factors (Rotmans and  
72 van Asselt, 2001). IAMs substantially shape the IPCC assessments on long-term climate mitigation scenarios, and play an  
73 important role in policy making (Rogelj et al., 2018; UNEP, 2019; NGFS, 2020; P.R. Shukla et al., 2022). In comparison to IAMs,  
74 PSMs typically have narrower spatial and sectoral scopes and shorter time horizons, but provide higher resolutions and increased  
75 technological detail (Palzer and Henning, 2014; Zerrahn and Schill, 2017; Brown et al., 2018a; Ram et al., 2018; Sepulveda et al.,

76 2018; Blanford and Weissbart, 2019; Böttger and Härtel, 2022; Ringkjøb et al. 2018; Prina et al. 2020). (Also see Supplemental  
77 Material S5 for a comparison of model specifications of a few selected PSMs). This allow PSMs to more accurately model the  
78 power sector under high VRE shares (Bistline, 2021; Chang et al., 2021). Note that we use the term “power sector model” here to  
79 represent all general smaller-scope models than IAMs (usually by geographical or time horizon measures), even though many of  
80 them have sector-coupling aspects and do not only contain the traditional power sector.

81  
82 IAMs and PSMs are therefore limited by a lack of spatio-temporal detail and a lack of scope, respectively. IAMs usually have a  
83 temporal resolution no shorter than a year (Keppo et al., 2021) and therefore include simplified representations of hourly power  
84 sector variability, which mimic the real-world dynamics to varying degrees of success (Pietzcker et al., 2017). In general, a lack  
85 of high temporal resolutions can lead to difficulties when estimating the optimal level of variable renewable generation, often  
86 either over- or underestimating the market value of solar or wind generation, the challenges of variable renewable integration,  
87 the peak hourly residual demand, and the need for energy storage and baseload (Pina et al., 2011; Haydt et al., 2011; Ludig et  
88 al., 2011; Kannan and Turton, 2013; Welsch et al., 2014; Luderer et al., 2017; Pietzcker et al., 2017; Bistline, 2021). While  
89 approximate methods such as parameterization via residual load duration curves (RLDCs) are able to capture the supply-side  
90 dynamics of VREs, they remain methodologically limited for representing the flexible demand-side dynamics (Ueckerdt et al.,  
91 2015; Ueckerdt et al., 2017; Creutzig et al., 2017). Besides limited temporal resolutions, IAMs also usually have coarse spatial  
92 resolutions, which can lead to an under- or overestimation of transmission grid bottlenecks, geographical variability of wind and  
93 solar resources, and of the flexibility requirements to balance supply and demand (Aryanpur et al., 2021; Frysztacki et al., 2021;  
94 Martínez-Gordón et al., 2021). PSMs, on the other hand, usually lack the global and sectoral scope required for addressing  
95 global climate mitigation, in part because of limited availability of detailed data, and due to computational challenges.  
96 Furthermore, PSMs with a short-term horizon may lack the vintage tracking of standing capacities, capacity evolution over time,  
97 as well as long-term perfect foresight, which can help policy makers and companies to look ahead beyond the short-term  
98 business cycles, to invest early and to actively drive technical progress. In contrast, in IAMs such as REMIND, proactive early  
99 investment is a built-in feature, because the optimization is done from a long-term social planner’s perspective. In IAMs,  
100 investing early in the technological learning phase results in lower costs of energy expenditure later, avoiding the severity of  
101 punishment to economic growth later in time in the form of lower consumption, which raises the welfare which the model  
102 optimizes.

## 103 **1.2 Iterative coupling for full model convergence**

104 IAMs and PSMs differ in scope and resolution across three main modeling dimensions: temporal, spatial and technological. A  
105 soft-coupling approach can tap into these complementarities and combine their strengths, at potentially only a moderate increase  
106 in computational cost. The main challenge of the soft-coupling approach is to show that the two models can converge under  
107 coupling, which leads to a joint equilibrium that maximizes regional interannual intertemporal welfare in the IAM and  
108 minimizes total power system costs in the PSM. Ideally, the converged model offers the “best of both worlds”: it has both the  
109 broad scope required to assess global long-term energy transitions, as well as the technical resolution required to capture the  
110 interplay between VREs, storage and newly electrified demand on a much shorter time scale.

111 Approaches aiming to bridge the “temporal resolution gap” between long-term energy system models and hourly PSMs have  
112 been proposed in the past (Deane et al., 2012; Sullivan et al., 2013; Alimou et al., 2020; Brinkerink et al., 2020; Seljom et al.,  
113 2020; Guo et al., 2022; Younis et al., 2022; Brinkerink et al., 2022; Mowers et al., 2023). While these achieved some aspects of  
114 Objective (1) with adequate results, none attempted to incorporate and achieve Objective (2). In addition, there is a

115 methodological gap in the previous attempts to a full harmonization of the multiscale models. By a full harmonization, we mean  
116 a comprehensive coupling of the power sector dynamics, and an eventual model convergence in capacities, generation, and  
117 prices. In only a few previous studies, price information has been fed back into the long-term models from the short-term  
118 models: in one study only partial price information has been exchanged (Seljom et al., 2020); in another study some subset of  
119 price information is exchanged but they are not fully endogenized (instead they are parametrized), the exchange is also one  
120 directional (Mowers et al., 2023). Without a feedback mechanism through prices, the investment in the coupled model will very  
121 likely be sub-optimal due to two effects: 1) because of the misalignment in prices in the two models, there is a mismatch in  
122 investment incentives, resulting in a mismatch for optimal capacities if both models are completely endogenous; 2) in all  
123 previous studies, the capacities are fixed in the PSM and only the long-term model is allowed to invest in new capacities. This  
124 implementation can further propagate and sustain the price mismatch due to (1) via nontrivial shadow prices from these capacity  
125 bounds, and create in turn price distortions in the PSM that can be passed on to the IAM. Therefore, the methodological gap in  
126 previous work prevented a comprehensive convergence of the coupled models of both quantities and prices. As we show later in  
127 this study, without a comprehensive coupling of price information, no system-wide convergence can be achieved. However,  
128 with price coupling as our method proposes, we could achieve all aspects of Objective (1), as well as Objective (2) for one type  
129 of flexible demand with adequate numerical results, and therefore represents a first step to bridge the previous methodological  
130 gap.

131 Compared to previous studies, our approach features three main innovations: 1), the coupling is achieved by linking market  
132 values, and not hard fixing quantities, allowing both models to invest “as endogenously as possible”; 2), the market values of all  
133 power sector technologies are coupled, not just the electricity price of the system or the market value of a particular technology,  
134 allowing models to achieve close to full convergence; 3) under idealized coupling assumptions and for a simplified “proof-of-  
135 concept” model without storage, we can mathematically derive the necessary conditions under which comprehensive model  
136 convergence can be reached, which puts multiscale coupling on firm theoretical footing. Our coupling approach is bi-  
137 directional, iterative and fully automated.

138 One should note that our methodology bears certain mathematical similarities to Benders Decomposition from the discipline of  
139 Operation Research (Conejo et al., 2006), which is used in long-term energy system model PRIMES to obtain hourly detail  
140 (E3Mlab, 2018). There are however, crucial differences. For example, the optimization in our work is carried out iteratively  
141 outside solver time, whereas the Benders Decomposition is carried out iteratively during solver time. In addition, our approach  
142 can function even when the objective function is convex, whereas the Benders Decomposition cannot, allowing our approach to  
143 be applied in more general cases. Mathematically, the subproblems in Benders Decomposition have fixed capacities obtained  
144 from master problems, therefore are not endogenous, but the shadow prices of these constraints are iteratively passed to the  
145 master problems, ensuring mathematical convergence. The exact ways our methodology is connected to Benders Decomposition  
146 or other similar methods are yet to be fully explored.

147 To showcase such a framework and its ability to achieve iterative convergence, we couple the PSM DIETER, which has an  
148 hourly resolution (8760 hours in a year) and the IAM REMIND for a single-region Germany. Germany is a well-suited case  
149 study for exploring high VRE shares in the power sector. The country is expected to meet stringent climate targets despite the  
150 country’s high level of residential and industrial power demand, relatively small geographical size and lack of solar endowment  
151 during winter seasons. Nevertheless, the German government has set very ambitious targets for the expansion and use of  
152 variable renewable energy sources (Schill et al., 2022). A viable zero-carbon power mix in Germany must include an adequate  
153 amount of storage and transmission for the renewable generation, as well as “clean firm generation” such as geothermal,  
154 biomass or gas with carbon capture and storage (CCS) (Sepulveda et al., 2018).

155 **2 Models**

156 The models used in this study are well-documented open source models (REMIND is an open source model but requires  
157 proprietary input data to run). A side-by-side comparison of the scope, resolution and other specifications of the two models can  
158 be found in Appendix A. The coupling scope can be found in Appendix B. Details on model input data can be found in  
159 Supplemental Material S-1.

160 **2.1 IAM: REMIND**

161 REMIND (REgional Model of INvestments and Development) is a process-based IAM, which describes complex global energy-  
162 economy-climate interactions (Baumstark et al., 2021). REMIND has been frequently used in long-term planning of  
163 decarbonization scenarios, most notably in the IPCC (IPCC, 2014; Rogelj et al., 2018; P.R. Shukla et al., 2022). The REMIND  
164 model links different modules, which describe the global economy, the energy, land and climate systems, with a relatively  
165 detailed representation of the energy sector compared to non-process-based IAMs. The model is formulated as an interannual  
166 intertemporal optimization problem. Due to the computational complexity of nonlinear optimization, the model simulates a time  
167 span from 2005 to 2100 with a temporal resolution of either 5 years (between 2005 to 2060) or 10 years (between 2070 to 2100).  
168 The years in REMIND are representative years of the surrounding 5 or 10-year period, e.g. year “2030” represents the 5-year  
169 period 2028 to 2032. Spatially, the model represents the world composed of aggregated global regions (Fig. B1). For each  
170 region, using a nested constant elasticity of substitution (CES) production function, the model maximizes interannual  
171 intertemporal welfare as a function of labor, capital, and energy use (Baumstark et al., 2021). The macro-economic projections  
172 of REMIND come from various established global socio-economic scenarios jointly used by social scientists and economists –  
173 the so-called Shared Socioeconomic Pathways (SSPs) (Bauer et al., 2017).

174 By default, REMIND runs in a regionally decentralized iterative “Nash mode”, where all regions are run in parallel and the  
175 interannual intertemporal welfare is maximized for each region for each internal “Nash” iteration. Trade flows between the  
176 regions are determined between the Nash iterations. During the Nash algorithm, REMIND regions share partial information  
177 between each other, which are trade variables in primary energy products and goods. The Nash algorithm is said to converge,  
178 when all markets are cleared and no region has the incentive to change their behavior regarding their trade decisions, i.e. no  
179 resources can be reallocated to make one region better off without making at least one region worse off. A successfully  
180 converged run of stand-alone REMIND under “Nash mode” usually consists of 30 to 70 iterations of single-region models in  
181 parallel. Each parallel single-region model usually takes 3-6 minutes to solve. A typical REMIND run in the Nash mode lasts  
182 2.5-6 hours depending on the level of sectoral details included. The latest version REMIND (v3.0.0) is published as an open-  
183 source version on github (Release REMIND v3.0.0 · remindmodel/remind, 2022). REMIND is implemented as a nonlinear  
184 programming (NLP) mathematical optimization problem. In REMIND, the nonlinearity consists of the welfare function, the  
185 CES production functions, adjustment costs, technological learning, the extraction cost functions, the bioenergy supply function  
186 and nonlinear constraints, among others.

187 **2.2 PSM: DIETER**

188 DIETER (Dispatch and Investment Evaluation Tool with Endogenous Renewables) is an open-source power sector model  
189 developed for Germany and Europe. In a long-run equilibrium setting (i.e. a competitive benchmark), the model minimizes  
190 overall system costs of the power sector for one year. DIETER determines the least-cost investment and hourly dispatch of  
191 various power generation, storage, and demand-side flexibility technologies. In previous literature, different versions of the

192 model have been used to explore scenarios with high VRE shares, where storage (Zerrahn et al., 2018; Zerrahn and Schill, 2017;  
193 Schill and Zerrahn, 2018), hydrogen (Stöckl et al., 2021), power-to-heat (Schill and Zerrahn, 2020), or solar prosumage (Say et  
194 al., 2020; Günther et al., 2021) are evaluated with a high degree of technological detail. DIETER recently also contributed to  
195 model comparison exercises that focused on power sector flexibility for VRE integration and sector coupling (Gils et al., 2022b,  
196 a; van Ouwerkerk et al., 2022).

197 As a first step to building a model coupling infrastructure, we implemented an earlier and simpler version of DIETER (v1.0.2),  
198 which is purely based on the General Algebraic Modeling System (GAMS). It has limited features on ramping constraints,  
199 flexible demand, and storage. The model minimizes total investment and dispatch cost of a power system for a single region,  
200 considering all consecutive hours of one full year. The technology portfolio contains conventional generators such as coal and  
201 gas power plants, nuclear power, as well as renewable sources such as hydroelectric power, solar PV and wind turbines.  
202 Endogenous storage investment and dispatch, as well as demand flexibilizations are offered as additional features that can be  
203 turned on or off. DIETER, like many PSMs, is a linear program (LP). A typical stand-alone run (with essential features) lasts  
204 from several seconds to several minutes for a single region. See Zerrahn and Schill, 2017 for a detailed documentation of the  
205 initial model, which was implemented purely in GAMS. Later, DIETER's GAMS core was embedded in a Python wrapper for  
206 enhanced scenario analysis and post-processing, but the model can still be run in a GAMS-only mode (Gaete-Morales et al.,  
207 2021).

### 208 **3 A novel coupling approach**

209 It is central to our approach that the price-based variables, such as the market values of electricity generation, are exchanged  
210 between the models. This approach ensures full convergence – including both quantity convergence as well as price  
211 convergence in the market equilibrium. Here, we first introduce the intuition behind this approach, then conduct a deep dive into  
212 the economic theory behind energy system modeling.

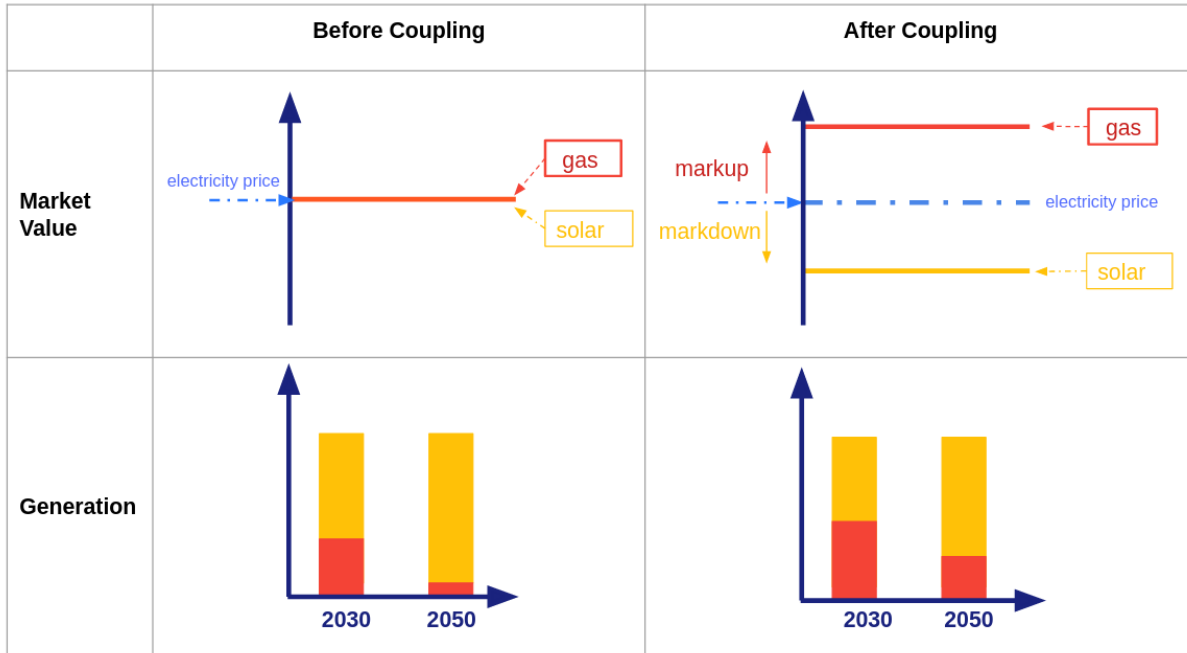
213 Economic concepts such as market values or capture prices (Böttger and Härtel, 2022), as key variables in our coupling,  
214 translate the physical characteristics of variable power generation or flexible consumption into economic ones. For example,  
215 generation technologies differ with respect to physical features and constraints – solar and wind generation depends on current  
216 weather conditions as well as diurnal and seasonal patterns, whereas this is less the case for dispatchable power plants such as  
217 coal, gas, biomass, nuclear or storage (López Prol and Schill, 2021). One consequence of this is that, for example, prices in  
218 hours where PV does not produce will be essentially set by other, and usually more expensive forms of generation. In cost-  
219 minimizing PSMs, the shadow prices of the energy balance are interpreted as wholesale market prices (Brown and Reichenberg,  
220 2021; López Prol and Schill, 2021). Therefore in general, hourly-resolution PSMs are well equipped to translate such physical  
221 constraints of generation into (wholesale) power market price time series. By providing such prices generated by PSMs (among  
222 other variables of the power sector dynamics) to IAMs, the latter can be indirectly informed about power market dynamics  
223 happening on much shorter time scales, even if they lack hourly resolutions. Over iterations, the prices from PSMs act as “price  
224 signals” to induce investment decision changes in IAMs, which can in turn provide feedback to the PSMs until the two models  
225 converge.

226 One innovation of our method is that the prices used for the model coupling can be symmetrically applied on the power supply  
227 side as well as the demand side. On the supply side, the coupling method mainly utilizes the concept of market value (i.e. annual  
228 average revenue per energy unit of a generator) in a competitive market at equilibrium. Generally speaking, market values of  
229 generation usually convey the degree of variability intrinsic to a given source of power supply, and reflect the generator's ability  
230 to meet an inflexible hourly demand, especially given lower cost of variable generation compared to dispatchable technologies.

231 Mirroring the concept of the market value, on the demand side, there is the concept of the “capture price” of electricity demand,  
232 which conveys the degree of demand-side flexibility. Note that there may be multiple terminologies for demand-side electricity  
233 prices, we use “capture price” to be consistent with one of the literatures on this topic. The capture price is the average  
234 electricity price that a flexible demand technology pays over a year. For example, flexible demand technologies such as heat  
235 pumps, electrolyzers or electric vehicles (EVs) can take advantage of electricity at hours when the generation is cheap to obtain  
236 a lower “capture price”, whereas inflexible demand has to pay a higher price on average. Price information given from a PSM to  
237 an IAM from both the supply and demand sides can change the IAM’s inherent investment and dispatch decisions of power  
238 generation as well as inflexible and flexible demand-side technologies.

239 For an intuitive understanding of our innovative coupling scheme, we take the supply-side as an example, and use a toy model  
240 to visualize the approach of coupling via market values. The market values of electricity generating technologies have been  
241 studied in depth (Sensfuß, 2007; Sensfuß et al., 2008; Hirth, 2013; Mills and Wiser, 2015; Hildmann et al., 2015; Koutstaal and  
242 va. Hout, 2017; Figueiredo and Silva, 2018; Hirth, 2018; Brown and Reichenberg, 2021). The general idea of the coupling is  
243 illustrated in Fig. 1 for a simplified case of only two types of generators – dispatchable gas turbines and solar photovoltaics with  
244 variable output. Note that we assume the system is at a solar share of > 50% and no storage, such that the solar market value is  
245 below average electricity price, and that of gas generation is above. Before the coupling, for a general IAM with coarse temporal  
246 resolution and without any VRE integration cost parameterizations, there is no differentiation between the market values of gas  
247 and solar generators – they are both equal to the electricity price. Thus, there is no differentiated revenue for one MWh  
248 generated by variable sources and dispatchable sources. The lack of market value differentiation is a direct consequence of the  
249 limited temporal resolution in IAMs, which cannot represent hourly dynamics. However, through a market-value-based  
250 coupling, the IAM can be informed by the PSM via a price “markup”. The annual price markup is defined as the difference  
251 between the market value of a specific technology and the annual average revenue that all generators together earn for one unit  
252 of generation (i.e. the annual average electricity price that a user pays). Under our soft-coupling approach, the markups from the  
253 PSM act as price-signals that change the composition of the energy mix in the next iteration of the IAM. Since in this simple  
254 example with a lot of PV and no storage, the gas generator is “more valuable” to the system, as it can generate electricity in  
255 times of scarcity (night), and thus it will receive a positive markup. When this positive price incentive is transferred from the  
256 PSM to the IAM, it increases the optimal level of investment into gas generation in the next IAM iteration. At the same time,  
257 solar generation receives a negative price incentive, reducing the optimal level of investments in the next iteration. Ultimately,  
258 the higher market value of gas turbines is due to: 1) its higher cost compared to solar (when gas is at <50% market share), 2) its  
259 ability to set prices in hours of low solar output and inflexible electricity demand. As we later show through mathematical  
260 theory of model convergence, other information besides markups also needs to be transferred such as capacity factors (annual

average utilization rates of the generators).



263 **Figure 1: Schematic illustration of the coupling approach for a simple power system in an IAM with coarse temporal**  
 264 **resolution, consisting of only gas and solar generators (no storage). Left column: before coupling; right column: after**  
 265 **coupling. Top row: endogenous prices (electricity price, market values of solar and gas generators); bottom row:**  
 266 **endogenous quantities (generation mix). The markups (as part of a larger set of interfaced variables) are the differences**  
 267 **between market values and electricity prices, and are given by the PSM of high temporal resolution as price signals to**  
 268 **the IAM. Usually, it is called a “markup” when the market value is higher than the annual average electricity price, and**  
 269 **“markdown” if it is the other way around. For simplicity, in the rest of the text we only refer to “markup” and**  
 270 **“markdown” collectively as “markup”, regardless of whether the market value is higher or lower than the average**  
 271 **electricity price.**

273 There are several advantages to this new coupling approach centered on linking prices. First, instead of simply prescribing  
 274 quantities such as yearly generation and capacities, the approach allows endogenous investment decisions to be made by both  
 275 models as they converge towards a joint solution. This gives maximal freedom to the coupled models, while minimizing  
 276 unnecessary distortions from one model to the other when some necessary quantities are being prescribed. Second, our coupling  
 277 scheme provides an elegant treatment of both supply- and demand-side technologies using the concept of “market values” on the  
 278 one hand and “capture prices” on the other. Third, from a theoretical point of view, transferring the market values of all the  
 279 generation types in a system alongside mappings of other relevant system parameters can lead to a convergence of the solutions  
 280 of the two models under idealized coupling circumstances. It can be rigorously shown that our method contains an exhaustive  
 281 list of interfacing parameters and variables for full model convergence of both quantities and prices. To the authors’ best  
 282 knowledge, the last point has not been explored or shown in any previous work.

283 In certain IAMs, VRE integration cost parameterization has been implemented to mimic the economic consequences of  
 284 variability of VRE, especially when the models have lower temporal resolution. Such VRE integration costs are contained in the  
 285 uncoupled default REMIND power sector modeling. However, the exact parameterization always depends on a particular set of  
 286 technological costs and parameters which might be subject to changes (Pietzcker et al., 2017), and the parameterization often

287 needs to be carried out anew under new assumptions and scenarios. In contrast, the model coupling approach is more general,  
288 and no such bespoke parametrization is needed.

289 Inspired by the theoretical framework based on the Karush–Kuhn–Tucker (KKT) conditions for power sector optimization  
290 problems (Brown and Reichenberg, 2021), we develop the theoretical basis for the coupling method in this section, which we  
291 use for validating convergence in numerical coupling in later sections. In Section 3.1, we analytically formulate the fundamental  
292 economic theory of the coupling approach. We first introduce the power sector formulations in the two uncoupled models (Sect.  
293 3.1). Then we carry out a derivation of the convergence conditions and criteria, where we map the Lagrangians of the two  
294 power-sector problems at different time resolutions, and derive the equilibrium condition for the coupled models (Sect. 3.2). In  
295 Sect. 3.3, we introduce the iterative coupling interface which contains all the previously derived convergence conditions. For  
296 REMIND information being passed on to DIETER (Sect. 3.3.1), and DIETER information being passed on to REMIND (Sect.  
297 3.3.2), we list and define the variables and parameters being exchanged at the interface, as well as additional constraints and  
298 implementations which serve to improve the coupling.

299 A complete list of mathematical symbols and list of abbreviations can be found in the appendices.

300 In the following sections, we first formulate the two uncoupled models, then move onto discussing coupled models. The  
301 theoretical tools we develop here are the foundation to the numerical implementation of coupling, and serve to validate and  
302 assess the model convergence in the result sections.

### 303 **3.1 Descriptions of uncoupled models**

304 REMIND and DIETER are both optimization models. REMIND maximizes interannual global welfare from 2005 to 2150,  
305 whereas DIETER minimizes the power sector system cost for a single year and a single region. For a given REMIND “Nash”  
306 iteration (see Sect. 2.1), the single-region economy is in long-term equilibrium after the optimization problem is solved. Since  
307 given fixed national income, lower energy system costs mean higher consumption which leads to increased welfare (see  
308 Appendix C for details), maximizing welfare can be assumed to correspond to minimizing energy system costs, a part of which  
309 is power sector costs. Therefore, to reduce the complexity of our analysis, we formulate an uncoupled REMIND model based  
310 solely on the power sector cost minimization and not the total welfare maximization. For stand-alone REMIND, the multi-year  
311 power system cost for a single region equals the sum of all variable and fixed costs of generation,

$$312 Z = \sum_{y,s} (c_{y,s} P_{y,s} + o_{y,s} G_{y,s}), \quad (1)$$

313 where  $c$  represents the fixed cost for capacity,  $o$  represents the variable cost of running power generation,  $P$  denotes endogenous  
314 capacity, and  $G$  denotes endogenous generation (defined as including curtailment in REMIND).  $P$  and  $G$  are the decision  
315 variables of the problem. The sum in the objective function is over time index  $y$  and power generating technology type  $s$ . The  
316 REMIND time index  $y$  stands for one representative year, which represents 5 or 10 years centered around it. So even though the  
317 time step is 5 to 10 years, the time resolution is one year. For example, “y=2020” represents the years 2018-2022. Capital letters  
318 (both Latin and Greek) denote independent decision variables of the optimization problem. We classify an endogenous decision  
319 variable as independent if it is not uniquely determined by one or more other decision variables, and has no binding constraints  
320 applied to itself that is not already accounted for by the constraints on the decision variable(s) it depends on. Note that for  
321 simplicity, we treat all costs in REMIND in this formulation as if they are exogenous. In reality, REMIND has endogenous fixed  
322 costs due to technological learning as well as endogenous interest rate. Some types of variable costs such as fuel costs are also  
323 endogenous, which are determined based on primary energy balance equations for oil, gas and biomass. CO2 prices can also be  
324 endogenous under emission constraints.

325 Under the simplifying assumptions made for the derivation in this paper, the only independent decision variables are capacities,  
 326 generations and curtailments. Small letters denote either exogenously given parameters or endogenous shadow prices.

327 For stand-alone DIETER which has a year-long time horizon, the power system cost is:

328 
$$\underline{Z} = \sum_s c_s \underline{P}_s + \sum_h [\underline{\varrho}_s (\underline{G}_{h,s} + \underline{\Gamma}_{h,vre})], \quad (2)$$

329 where  $\underline{G}_{h,s}$  is the endogenous hourly power generation (excluding curtailment, note that this is different from the generation  
 330 variable definition in REMIND),  $h$  is the hourly index in a year from 1 to 8760,  $s$  is the index for the power generating  
 331 technology in DIETER.  $\underline{\Gamma}$  is hourly curtailment, only applicable in the case of variable renewables  $vre$  ( $vre \subset s$ ). Technology  
 332 type  $s$  can be subdivided into two subsets:  $vre$  and  $dis$  (“dispatchables”). For simplicity, we abbreviate the index subscript from  
 333  $s|s = vre$  to  $vre$  and  $s|s = dis$  to  $dis$ . Here in order to differentiate from REMIND notations, we use underscore  $\underline{\cdot}$  to denote  
 334 DIETER parameters and variables. Note that for simplicity, in the derivation we treat the technology types in both models as  
 335 being identical, although in fact the technologies in the two models are not one-to-one mapped (Fig. B2). During the coupling  
 336 all interface parameters and optimal decision variables need to be upscaled or downscaled when transferred from one model to  
 337 the other.

338 The cost minimization of total power sector cost  $Z$  and  $\underline{Z}$  under constraints yields the optimal values of the decision variables,  
 339 denoted as  $(P_{y,s}^*, G_{y,s}^*)$ , and  $(\underline{P}_s^*, \underline{G}_{h,s}^*, \underline{\Gamma}_{h,s}^*)$ .

340 Without coupling and under a baseline scenario, there are several constraints for each model. In the following equations we  
 341 denote the shadow price (i.e. the Lagrangian multiplier) of a constraint by the symbol following  $\perp$ . We use small greek letters to  
 342 denote endogenous shadow prices, and small Latin and Greek letters to denote exogenous parameters. The major constraints are  
 343 as follows (“c” stands for “constraint”):

344 c1) Constraint on generation for meeting demand, a.k.a. “supply-demand balance equation”, or “balance equation” in short:

345 REMIND (annual):  $d_y = \sum_s G_{y,s} (1 - \alpha_{y,s}) \perp \lambda_y ,$

346 DIETER (hourly):  $\underline{d}_h = \sum_s \underline{G}_{h,s} \perp \underline{\lambda}_h ,$

347 where  $d_y$  denotes annual REMIND power demand, and  $\underline{d}_h$  denotes DIETER hourly demand. The shadow prices (Lagrange  
 348 multipliers)  $\lambda_y$  and  $\underline{\lambda}_h$  represent the annual and hourly electricity prices in REMIND and DIETER, respectively, and are  
 349 equal to the marginal cost of one additional unit of electricity generation.  $\alpha_{y,s}$  is the annual VRE curtailment ratio in  
 350 REMIND. Note that technically speaking, REMIND electricity demand  $d_y$  is determined endogenously, partially via  
 351 competition with other energy carriers at the final energy consumption level, such as the competition between electricity and  
 352 gaseous carriers such as natural gas or hydrogen in household heating. But because here we have reduced REMIND to only  
 353 intra-power sector dynamics for the purpose of mathematical analysis, we treat demand as exogenous.

354 c2) Constraint on maximum capacity by the available annual potential  $\psi_s$  in a region:

355 REMIND:  $P_{y,s} \leq \psi_s \perp \omega_{y,s} ,$

356 DIETER:  $\underline{P}_s \leq \underline{\psi}_s \perp \underline{\omega}_s .$

357 Note that the resource constraint in REMIND is only relevant for wind, solar and hydro, and is assumed to be constant over  
 358 the model horizon. Biomass availability is not modeled via a regional potential constraint. Instead the availability of biomass  
 359 is priced in through the soft-coupling to the land-use model MAgPIE via a supply curve.

360 c3) Constraint on generation being non-negative:

361 REMIND:  $-G_{y,s} \leq 0 \perp \xi_{y,s} ,$

362 DIETER:  $-\underline{G}_{h,s} \leq 0 \perp \underline{\xi}_{h,s} .$

363 Note that there are several other similar constraints on other positive variables such as capacities and curtailment. In practice,  
 364 during the derivation they behave similarly to this positive generation constraint, therefore for simplicity, we do not include  
 365 them in the derivation.

366 c4) Constraint on maximum generation from capacity:

367 REMIND:  $G_{y,s} = \phi_{y,s} P_{y,s} * 8760 \perp \mu_{y,s}$ ,

368 DIETER: (variable renewables)  $\underline{G}_{h,vre} + \underline{L}_{h,vre} = \underline{\phi}_{h,vre} \underline{P}_{vre} \perp \underline{\mu}_{h,vre}$

369 (dispatchables)  $\underline{G}_{h,dis} \leq \underline{P}_{dis} \perp \underline{\mu}_{h,dis}$ ,

370 where  $\phi_{y,s}$  is the exogenous annual average capacity factor of the power plant  $s$  in REMIND in year  $y$ , and  $\underline{\phi}_{h,vre}$  is the  
 371 exogenously given hourly theoretical capacity factor (i.e. before curtailment) of VRE in DIETER. Note that strictly  
 372 speaking, curtailments in the uncoupled REMIND and DIETER are endogenous decision variables but are not independent  
 373 variables. However, here we use capital letter to denote hourly curtailment in DIETER as an independent decision variable to  
 374 account for curtailment costs and other curtailment constraints that can arise from a more general formulation of the model.

375 c5) “Historical” constraints on capacities in REMIND. This makes REMIND a so-called “brown-field model”, i.e. a model  
 376 accounting for the standing capacities in the real-world. Past capacities ( $y < 2020$ ) are hard-fixed, i.e. the variable capacities  
 377 are fixed to certain numeric values. Current capacities ( $y = 2020$ ) are “soft-fixed”, i.e. the variable capacities are fixed to a  
 378 corridor around certain standing numeric values: the lower bounds guarantee the already planned capacities, and the upper  
 379 bounds reflect the finite physical capabilities of scaling up, defined by 5% above the 2020 real-world data. For simplicity,  
 380 we use only one constraint for both past and current capacities,

381  $P_{y,s} \geq p_{y,s} \perp \sigma_{y,s}$  for  $y \leq 2020$ ,

382 where  $p_{y,s}$  represents the standing capacities of technology  $s$  at time  $y$  in REMIND in the past and present years.

383 c6) Near-term upscaling constraint on VRE capacity expansion, represented by an upper bound on near-term capacity addition  
 384 in model period  $(y - \Delta y, y)$ ,  $\Delta P_{y,s} := P_{y,s} - P_{y-\Delta y,s}$ , where  $\Delta y$  is the REMIND model time step:

385  $\Delta P_{y,s} \leq q_{y,s} \perp \gamma_{y,s}$  for  $y = 2025$ ,

386 where  $q_{y,s}$  is equal to twice the added capacity during the 2010-2020 period (only applied to Germany in default REMIND).

387 Note that constraints (c5) and (c6) introduce interannual intertemporality into the power sector of REMIND. This additional  
 388 interannual intertemporality determines that the model equilibrium can only be strictly satisfied across the sum of all model  
 389 periods and not for a single period. Another source of intertemporality in REMIND is due to the adjustment cost, which we  
 390 ignore in the main text of this study since it introduces non-linearity in the power sector and also plays a relatively small role in  
 391 the overall dynamics.

392 Note that regarding the simplification of REMIND above, to the authors’ best knowledge, there is no theoretical or empirical  
 393 concept that addresses the validity of drawing equivalence between welfare maximization and energy system cost minimization  
 394 in IAMs. Naively, given GDP is unchanged, decreasing energy system cost raises consumption and therefore welfare. However,  
 395 this is only valid under the assumption that energy is a substitute (and not a complement) to capital and labor, i.e. one usually  
 396 cannot raise economic output (GDP) simply by spending more on higher energy expenditure (while satisfying the same level of  
 397 energy demand). Nevertheless, this is likely a necessary condition and not a sufficient one for proving the equivalence. More  
 398 theoretical research will be needed to draw a precise and rigorous equivalence. However, in practice, we see that during our  
 399 numerical calculation the model is well behaved according to this reduced theory, which means that the parameters in the  
 400 models are in a regime where such an assumption is valid, at least in the case of IAM REMIND.

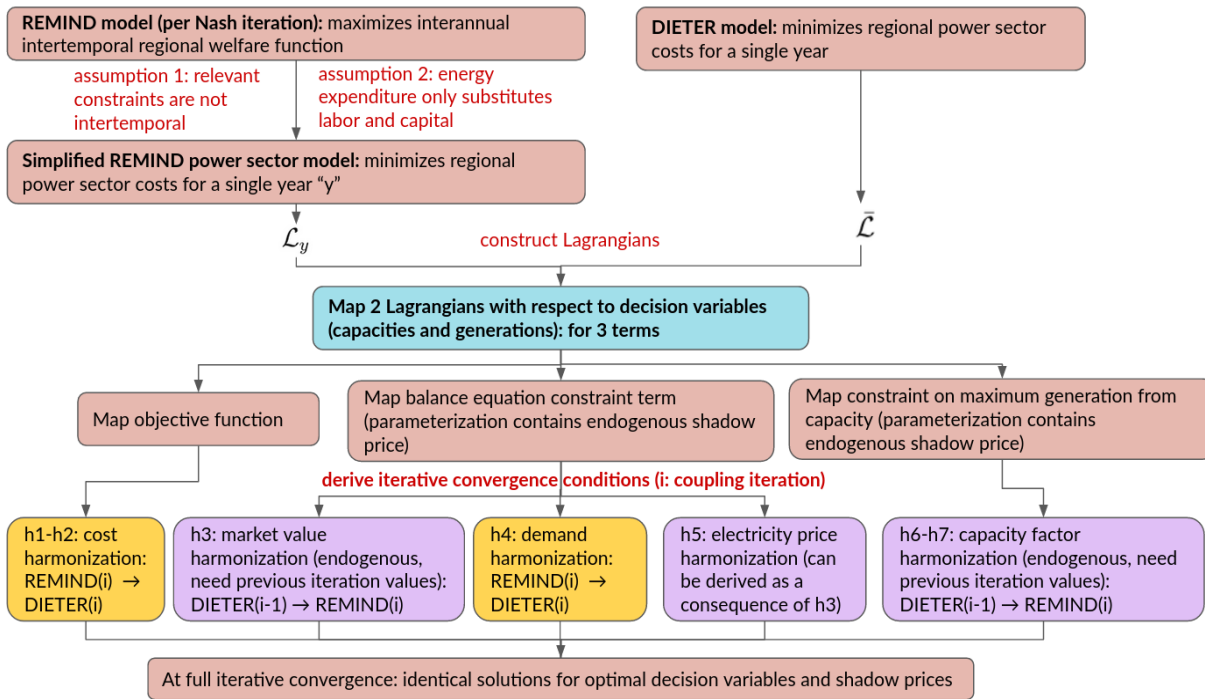
401 **3.2 Economic theory of model convergence**

402 In the last section we have discussed the stand-alone uncoupled power sector formulations in REMIND and DIETER. In this  
403 section we discuss the coupled models and its convergence. Under simplified assumptions, we first derive the mapping between  
404 the models which are necessary for a convergence (Sect. 3.2.1-2), then we derive theoretical relations which are later used to  
405 validate the numerical results of the coupled run (Sect. 3.2.3).

406 **3.2.1 Derivation of convergence conditions**

407 Our aim is to develop a method under which comprehensive convergence can be reached for soft-coupled multiscale models.  
408 We achieve this by deriving a mapping of the two problems, such that their decision variables have identical optimal solutions  
409 and the endogenous shadow prices are also equal across the models. The convergence conditions of the coupled REMIND-  
410 DIETER model for the power sector are the result of such a mapping. Below, we first define what is meant by a “comprehensive  
411 model convergence”, and then sketch the workflow of the derivation of a coupling framework which would result in a  
412 comprehensive model convergence of both decision variables and shadow prices. The detailed derivation is in Appendix D.  
413 Here, we derive the conditions under which the endogenous decision variables are identical at each model's optimum, i.e.  $P_{y,s}^* =$   
414  $\underline{P}_{y,s}^*$ , and  $G_{y,s}^*(1 - \alpha_{y,s}^*) = \sum_h \underline{G}_{y,h,s}^*$  (or equivalently pre-curtailment generation  $G_{y,s}^*$  and  $\sum_h (\underline{G}_{y,h,s}^* + \Gamma_{y,h,s}^*)$ ). A convergence of  
415 the solutions of these two sets of annual decision variables for each technology  $s$  and for each year  $y$ , along with the  
416 convergence of shadow prices gives rise to “comprehensive model convergence”. We show below that this can only be achieved  
417 if there is a harmonization at the level of the KKT Lagrangians of the two problems, following the methods first developed by  
418 Karush, Kuhn and Tucker (Karush, 1939; Kuhn and Tucker, 1951).

419 Our coupling approach fundamentally relies on mapping the parameterization of the Lagrangians for both optimization  
420 problems. It is trivial to show that as long as the KKT Lagrangians are identical with respect to the decision variables, the  
421 solutions of the problem are identical. For example, if an optimization problem A has Lagrangian  $L_1 = a_1*x + b_1*y$  and  
422 another problem B has Lagrangian  $L_2 = a_2*x + b_2*y$ , where  $x$  and  $y$  are decision variables of the optimization problems.  
423 Then if we let  $a_1 = a_2$ ,  $b_1 = b_2$ , the two problems are identical, and they must have identical optimal solutions for the  
424 decision variables  $x^*$  and  $y^*$ . This is the basic logic behind the Lagrangian-based method. The challenge in the case of  
425 REMIND and DIETER is to show that when a decision variable representing the same physical quantity, for example, the  
426 annual power generation from a technology is defined with low resolution in one problem, and is defined with high resolution in  
427 another, that there is nevertheless a viable mapping between the two Lagrangians. In this case, the parameterization of the  
428 Lagrangian is not only limited to exogenous parameters of the model, but also includes endogenous shadow prices and  
429 endogenous decision variables from the other model. Due to the endogenous nature of the latter two, the parametrization in the  
430 current-iteration model A must come from the solved results from the last iteration from model B, and vice versa. Fig. 2  
431 illustrates the workflow of the analytical derivation of the convergence conditions.



432

433 **Figure 2: The schematics of the Lagrangian-based derivation procedure for a simplified version of REMIND-DIETER**  
 434 **iterative convergence. After simplifying assumptions, we can construct the Lagrangians of the reduced REMIND model**  
 435 **and the full DIETER model for a single year (Eqs. (3)-(4)). Comparing and mapping terms in the Lagrangians (a key**  
 436 **step in bold), we discover that iterative exchange of a broad range of information is needed for a fully harmonized**  
 437 **parameterization of the Lagrangians. Under the harmonization specified in the seven convergence conditions (color**  
 438 **coded for directions of information flow), the coupled models can give rise to identical optimal solutions of the models'**  
 439 **respective (annual aggregated) decision variables, and hence a full quantity convergence. The necessary shadow price**  
 440 **convergence is shown in the detailed derivation of the harmonization conditions (h1-h7) in Appendix D.**

441

442 The analytical derivation workflow, as shown in Fig. 2, is described in detail as follows. First, we apply simplifying assumptions  
 443 to reduce the complexity of the uncoupled models (before the key step in blue in Fig. 2). Assumptions have to be made to justify  
 444 reducing the scope of the REMIND model, such that for the purpose of the analysis, it is on equal footing as DIETER. We  
 445 achieve this by reducing the global REMIND model to single-sector (the power sector), single-year, and single-region. To  
 446 reduce the REMIND model from a macroeconomic-energy model to a power-sector-only model, we make similar assumptions  
 447 as before when formulating the uncoupled REMIND power sector (see Sect. 3.1). To reduce the REMIND model further to a  
 448 single year, we assume that the models only contain constraints in the power sector that are not intertemporal, i.e. ignoring the  
 449 brown-field and near-term constraints for now. Since for each iteration of the REMIND model under “Nash mode”, inter-  
 450 regional trading happens between the iterations, the single-iteration optimization model is already for a single region, and  
 451 therefore does not require simplification. After these simplifying steps, in this part of the derivation, we can treat REMIND’s  
 452 power sector as “separate” from the rest of the model, and treat the dynamics of a single year in REMIND as independent from  
 453 the dynamics of other years. Later, the numerical results of the convergence can confirm to a large degree the validity of these  
 454 assumptions, especially in the green-field temporal ranges, i.e. where the intertemporal brown-field constraints have little  
 455 influence on the dynamics. Note that with the inclusion of these intertemporal constraints in the derivation, the mapping  
 456 becomes more complicated, especially for the near-term range, i.e. before 2035. So in practice, this derivation of the coupling

457 interface is only an approximation to what is needed for a full convergence of DIETER and REMIND, since it deliberately  
 458 ignores such constraints. See also Sec. 6.1.

459 After the necessary simplification assumptions, we construct the Lagrangians for the simplified model REMIND and for  
 460 DIETER (after the blue block in Fig. 2) (Gan et al., 2013). For a single-year reduced REMIND power sector model, the  
 461 Lagrangian is:

$$462 \quad \mathcal{L}_y = \underbrace{\sum_s (c_{y,s} P_{y,s} + o_{y,s} G_{y,s})}_{\text{REMIND objective function}} + \underbrace{\lambda_y \left[ d_y - \sum_s G_{y,s} (1 - \alpha_{y,s}) \right]}_{\text{annual electricity balance equation constraint}} + \underbrace{\sum_s \mu_{y,s} (G_{y,s} - 8760 * \phi_{y,s} P_{y,s})}_{\text{maximum generation from capacity constraint}}. \quad (3)$$

463 We would like to map it to the single-year DIETER Lagrangian  $\underline{\mathcal{L}}$ :

$$464 \quad \underline{\mathcal{L}} = \underbrace{\sum_s \left[ \underline{c}_s \underline{P}_s + \underline{o}_s \sum_h (\underline{G}_{h,s} + \underline{\Gamma}_{h,vre}) \right]}_{\text{DIETER objective function}} + \underbrace{\sum_h \lambda_h \left( \underline{d}_h - \sum_s \underline{G}_{h,s} \right)}_{\text{hourly electricity balance equation constraint}} + \underbrace{\sum_{h,dis} \underline{\mu}_{h,dis} (\underline{G}_{h,dis} - \underline{P}_{dis})}_{\text{maximum dispatchable generation from capacity constraint}} \\ 465 \quad + \underbrace{\sum_{h,vre} \underline{\mu}_{h,vre} (\underline{G}_{h,vre} + \underline{\Gamma}_{h,vre} - \underline{\phi}_{h,vre} \underline{P}_{vre})}_{\text{maximum renewable generation from capacity and weather constraint}}. \quad (4)$$

466 The algebraic derivation of mapping the two Lagrangians term-by-term is presented in Appendix D. From this algebraic  
 467 mapping, we can derive seven harmonization conditions (h1-h7) required for a full convergence. Conditions (h1-h7) are the  
 468 subsequent basis for most of the information exchanged at the coupling interface. Among them, conditions (h3, h5-7) (purple  
 469 blocks in Fig. 2) indicate conditions which contain endogenous information that must come from the previous iteration of  
 470 DIETER that is passed on to REMIND, such as markup and capacity factors. Conditions (h1-2, h4) (yellow blocks) indicate  
 471 conditions which contain information that come from the previous iteration of REMIND and are passed on to DIETER. For  
 472 schematics of the coupled iterations, see Appendix E.

473 This Lagrangian-mapping-based derivation can theoretically show that our approach (in its most simple form) necessarily leads  
 474 to model convergence, and has the advantage of being mathematically straight-forward and rigorous. The necessary information  
 475 from the power sector dynamics is all contained in the list of conditions derived from such a mapping. If the coupling contains  
 476 less information, a convergence is not possible; at the same time, for a model convergence, one does not need to pass on any  
 477 additional information beyond what is contained in this list of conditions. The list of information derived here is therefore  
 478 complete and exhaustive for a coupled convergence.

### 479 3.2.2 List of convergence conditions

480 The convergence conditions (h1-h7), which are derived in detail in Appendix D following the procedure in Sect. 3.2.1, are  
 481 summarized here:

482 **h1)** annual fixed costs are harmonized:  $c_{y,s} = \underline{c}_{y,s}$ ,

483 **h2)** annual variable costs are harmonized:  $o_{y,s} = \underline{o}_{y,s}$ .

484 **h3)** annual average market values for each generation type  $s$  are harmonized via markups from DIETER. We let  $\eta_{y,s}(i-1)$   
 485 denote the markup for technology  $s$  in year  $y$  in the last iteration DIETER, i.e. the difference between market value and  
 486 annual average price of electricity:

$$487 \quad \eta_{y,s} = \frac{\sum_s \lambda_{y,h} \underline{G}_{y,h,s}}{\sum_h \underline{G}_{y,h,s}} - \frac{\sum_h \lambda_{y,h} \underline{d}_{y,h}}{\sum_h \underline{d}_{y,h}}. \quad (5)$$

488 This is the heart of our coupling approach, using markups as the “price signals”. Intuitively, the markups represent the  
 489 market value differences between REMIND and DIETER. The harmonization of market values is implemented by

490 iteratively adjusting the market value for each generator type in REMIND to be the same as that in DIETER. As long as  
 491 the market values (or per-unit-generation revenues) and costs are harmonized, the economic structures of the power  
 492 market are identical and the models can converge.

493 Using markup Eq. (5), we modify the original objective function  $Z$  in the coupled version of REMIND by subtracting the  
 494 product of markups and generations summed over all technologies and all years:

495 
$$Z' = Z - \sum_{y,s} \eta_{y,s}(i-1)G_{y,s}(1 - \alpha_{y,s}), \quad (6)$$

496 where  $Z'$  is the modified REMIND objective function in the coupled version,  $i$  is the iteration index of the iterative soft-  
 497 coupling.

498 **h4)** annual power demands are harmonized:  $\sum_h \underline{d}_{y,h} = d_y$  ,

499 **h5)** annual average prices of electricity are harmonized:

500 
$$\lambda_y = \frac{\sum_h \lambda_{y,h}(i-1) \underline{d}_{y,h}(i-1)}{\sum_h \underline{d}_{y,h}(i-1)}, \quad (7)$$

501 where  $(i-1)$  indicates that the endogenous results are from the last iteration. This is shown in Appendix D to be a direct  
 502 consequence of (h3) and (h4).

503 **h6)** annual average capacity factor for each generation type  $s$  are harmonized:

504 
$$\phi_{y,s} = \sum_h \underline{\phi}_{y,h,s}(i-1) / 8760, \quad (8)$$

505 where  $\underline{\phi}_{y,h,s}(i-1) = \frac{\underline{G}_{y,h,s}(i-1)}{P_{y,s}(i-1)}$  is the hourly capacity factor in DIETER, determined by endogenous hourly generation  
 506 and annual capacities in the last iteration.

507 **h7)** annual curtailment are harmonized:

508 
$$G_{y,vre} \alpha_{y,vre} = \sum_h \underline{G}_{y,h,vre}(i-1). \quad (9)$$

509 In mapping the Lagrangians (Eqs. (3-4)), except the objective function, the rest of the parametrization contains endogenous  
 510 shadow prices and endogenous quantities. Since endogenous values can only be known ex post, this imposes a strict requirement  
 511 on the coupling that it must be iterative, with the endogenous part of the parameterization coming from previous iteration  
 512 optimization results – usually from the other model. The mapping of the endogenous information requires careful argument in  
 513 each case (i.e. the derivation of (h3)-(h7)). In the case of the balance equation constraint Lagrangian term (corresponding to  
 514 (c1)), the shadow prices of the constraint in current-iteration REMIND model are exogenously corrected by a set of technology-  
 515 specific “markups” (see Sect. 3.1 introduction), such that the new “corrected” market value in REMIND is manipulated to  
 516 match the market value of the previous iteration of DIETER. This is the heart of our coupling approach, using markups as the  
 517 “price signals”. In the case of the constraint on maximum generation from capacity (corresponding to (c4)), the endogenous  
 518 shadow prices in the current iteration REMIND can be shown to be automatically mapped to the those in the previous iteration  
 519 of DIETER, given that the annual average capacity factors in the constraints are harmonized (h6-h7).

520 In actual implementation, most of the above mappings are modified for numerical stability (Sect. 3.3.2, Appendix H).

### 521 3.2.3 Theoretical tools for validating convergence

522 Here we first state the convergence criteria, which are mathematical relations which are being satisfied under model  
 523 convergence. Then we also discuss equilibrium conditions of the coupled models which alongside the convergence criteria can  
 524 be used to check numeric results to validate and assess the convergence outcome.

525 Under a theoretical full convergence of the coupled model,  
526     v1) annual average electricity prices,  
527     v2) capacities,  
528     v3) (post- or pre-curtailment) generations,  
529 all should be identical at the end of the coupling in both models. These are the most important criteria by which we validate full  
530 model convergence. Technically, electricity price convergence (v1) (i.e. convergence condition (h5)) can be derived from (h3)-  
531 (h4). Nevertheless, we check this ex post, together with quantity convergence (v2-v3). In actual coupled model runs, following  
532 only the convergence conditions (h1-h7), the convergence criteria (v1-v3) might not be exactly fulfilled. Therefore in practice,  
533 in order to validate the degree of numerical convergence, the alignment between REMIND and DIETER generation shares is set  
534 to be within a few percentage points before coupled runs terminate.  
535 Besides using convergence criteria (v1-v3), we also use a type of equilibrium condition – the so-called “zero-profit rules”  
536 (ZPRs) to validate the numerical model convergence. ZPRs are mathematical relations which state that under market  
537 equilibrium, prices are equal to the costs for electricity. This is not always the case, especially in the situation where there are  
538 extra constraints in the model which distort this equality. ZPRs contain model parameters and decision variables at market  
539 equilibrium, and they can be derived from the KKT conditions of the model (Appendix F). ZPRs are therefore reliable tools in  
540 ascertaining the sources of market values or the price of electricity of the power sector, because according to the ZPRs, one can  
541 always decompose the prices into the cost components, i.e. so-called leveled costs of electricity (LCOE). The decomposition  
542 of prices into cost components is important, because the prices of electricity in the power market are overdetermined by the  
543 energy mix, so it is possible that two different power mixes correspond to the same electricity price. In numerical results, a  
544 slight mismatch of energy mix at the end of the coupling is unavoidable, so alongside comparing the prices, it is often helpful to  
545 compare the makeup of the LCOE across the models, such that they also appear harmonized at the end of the iterative  
546 convergence. Overall, ZPRs is a helpful tool for visualizing and understanding the power market dynamics, both from the point  
547 of view of each generator type as well as from the point of view of the entire electricity system. It is worth noting, that the zero-  
548 profit rules, which are mathematical conditions derived from an idealized modeling of the power sector as fully competitive, are  
549 only an approximation to the real-world markets, where firm profits exist. ZPRs in its technical definition simply means that at  
550 model equilibrium, cost equals revenue. Given that the profits are defined as the difference between revenue and cost, the profits  
551 are zero in this situation. The name “zero-profit rule” therefore should not be overinterpreted beyond their technical contents,  
552 and one should be aware of their theoretical origin and assumptions under which they are valid.  
553 The ZPRs of the coupled model can be derived based on: 1), the uncoupled models; 2), the modification made to the model due  
554 to the coupling interface (h1-h7); 3), any additional modifications made to the model during our numerical implementation. In  
555 the last category, for a complete numerical implementation of the coupling, we add one additional capacity constraint (c7) and  
556 (c8) for each model. The first capacity constraint (c7) is created in REMIND to circumvent the issue of extremely high markup  
557 from peaker gas plants in the scarcity hour of the year in the DIETER model, which otherwise causes instability during the  
558 iterative coupling. The second constraint (c8) is a simple brown-field constraint implemented in DIETER to address the fact that  
559 DIETER is a green-field model, which is otherwise ignorant about standing-capacities in the real world. For simplicity, (c7) and  
560 (c8) are not included in the convergence condition derivations in Sect. 3.2.1. The derivation of the ZPRs outlined by the above  
561 three steps have been carried out in: Appendix F (uncoupled models), Appendix G (coupled REMIND only including coupling  
562 interface, coupled DIETER including constraint (c8)), and Appendix H (coupled REMIND, including constraint (c7)).  
563 In summary, the ZPRs for both coupled models are as follows:  
564     a) Coupled REMIND:

565 i) Technology-specific ZPR:

$$\begin{aligned}
 & \frac{\sum_y (c_{y,s} P_{y,s} + o_{y,s} G_{y,s})}{\sum_y G_{y,s}} + \frac{\sum_y (c_{y,s} P_{y,s} + o_{y,s} G_{y,s}) \alpha_{y,s}}{\sum_y G_{y,s} (1 - \alpha_{y,s})} \\
 & = - \frac{\sum_y (\omega_{y,s} - \sigma_{y,s} + \gamma_{y,s} + \nu_{y,s}) P_{y,s}}{\sum_y G_{y,s} (1 - \alpha_{y,s})} + \frac{\sum_y (\lambda_y + \eta'_{y,s}) G_{y,s} (1 - \alpha_{y,s})}{\sum_y G_{y,s} (1 - \alpha_{y,s})} \\
 & \quad \text{Capacity shadow price}'_s \quad \text{Market value}'_s
 \end{aligned} \tag{10}$$

568 ii) System ZPR:

$$\begin{aligned}
 & \frac{\sum_{y,s} (c_{y,s} P_{y,s} + o_{y,s} G_{y,s})}{\sum_{y,s} G_{y,s}} + \frac{\sum_{y,s} (c_{y,s} P_{y,s} + o_{y,s} G_{y,s}) \alpha_{y,s}}{\sum_{y,s} G_{y,s} (1 - \alpha_{y,s})} \\
 & = - \frac{\sum_{y,s} (\omega_{y,s} - \sigma_{y,s} + \gamma_{y,s} + \nu_{y,s}) P_{y,s}}{\sum_{y,s} G_{y,s} (1 - \alpha_{y,s})} + \frac{\sum_{y,s} (\lambda_y + \eta'_{y,s}) G_{y,s} (1 - \alpha_{y,s})}{\sum_{y,s} G_{y,s} (1 - \alpha_{y,s})} \\
 & \quad \text{Capacity shadow price}'_{\text{system}} \quad \text{Electricity price}'_{\text{system}}
 \end{aligned} \tag{11}$$

571 b) Coupled DIETER:

572 i) Technology-specific ZPR:

$$\frac{\underline{c}_s P_s + \underline{o}_s \sum_h (\underline{G}_{h,s} + \underline{\Gamma}_{h,vre})}{\sum_h \underline{G}_{h,s}} = - \frac{(\underline{\omega}_s + \underline{\varsigma}_s) P_s}{\sum_h \underline{G}_{h,s}} + \frac{\sum_h \underline{\lambda}_h \underline{G}_{h,s}}{\sum_h \underline{G}_{h,s}}. \tag{12}$$

574 ii) System ZPR:

$$\frac{\sum_s [\underline{c}_s P_s + \underline{o}_s \sum_h (\underline{G}_{h,s} + \underline{\Gamma}_{h,vre})]}{\sum_{h,s} \underline{G}_{h,s}} = - \frac{\sum_s (\underline{\omega}_s + \underline{\varsigma}_s) P_s}{\sum_{h,s} \underline{G}_{h,s}} + \frac{\sum_h \underline{\lambda}_h \underline{d}_h}{\sum_h \underline{d}_h} \text{Annual average electricity price}_{\text{system}}. \tag{13}$$

576 “Prime” sign indicates the term has been modified from the uncoupled versions due to implementation in the coupling.  $\nu$  and  $\varsigma$  577 are capacity shadow prices introduced from the additional constraints (c7-c8) (Appendix G-H). It is worth noting that constraints 578 (c7-c8) introduced due to coupling can impact the Lagrangians of the two models which we used to derive convergence 579 conditions and criteria. However, in actual coupled runs, evidently there is only a moderate distortion due to these extra 580 constraints. Condition (c8) even helps with convergence, because it puts most of the brown-field and near-term constraints 581 which REMIND sees also into DIETER (see Sect. 6.1).

582 Due to the fact that several sources of shadow prices cannot be incorporated during the derivation for convergence (Sect. 3.2.1), 583 in numerical experiments of coupled run it is appropriate to compare the following two types of prices across the two models for 584 price convergence:

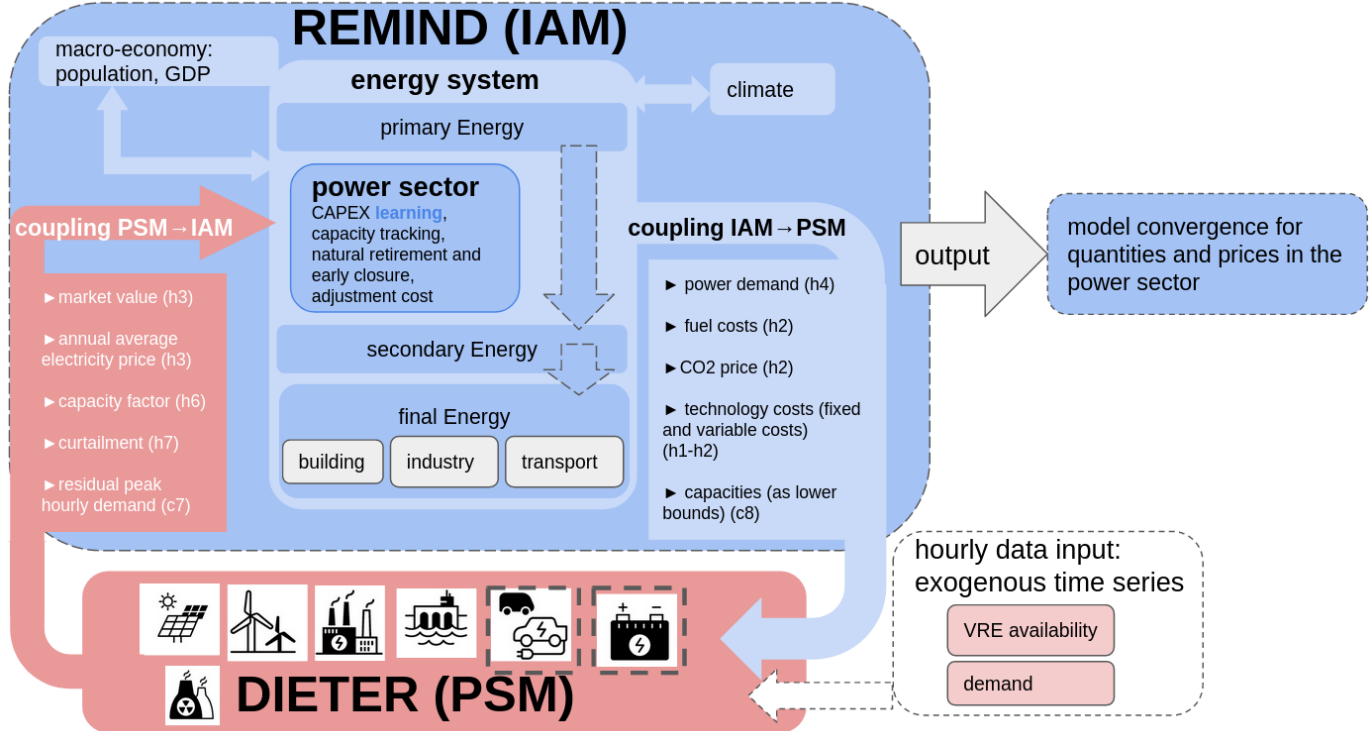
585 1) Electricity price convergence, not including any capacity shadow prices;

586 2) Sum of electricity prices and all respective capacity shadow prices converge.

587 Under the simplified analysis of convergence (discounting brown-field constraints, scarcity prices, etc), price convergence in 1) 588 is predicted by theory (see also convergence condition (h5)). However, it is only under the most idealized situation. 589 Convergence in 2) on the other hand includes all the prices, which should match if LCOEs match across the system. We use the 590 first type to check price convergence over iteration, and use the second type only in the context of checking the system ZPRs 591 across the models because of the theoretical relations between full prices and LCOEs.

592 **3.3 Implementation via interface: exchange of variables**

593 In this section we list parameters and endogenous variables that are exchanged between REMIND and DIETER. This already  
 594 satisfies most convergence conditions, while the remaining condition (h5) is checked in Sect. 4 as part of the convergence  
 595 criteria (v1-v3). An overview of the model coupling and the flow of information under convergence conditions is shown in Fig.  
 596 3.



597

598 **Figure 3: The schematics of the REMIND-DIETER iterative soft-coupling. The power sector module of IAM REMIND,**  
 599 **which is between the layer of primary to secondary energy transformation, is hard-coupled with other modules inside**  
 600 **REMIND such as macro-economy, industry and transport. In PSM DIETER, the power market with generators of**  
 601 **various types is modeled with hourly resolution, with options for storage and flexible demand. The information**  
 602 **exchanged between the models (block arrows) are determined via the convergence conditions (h1-h7) derived before**  
 603 **(Sect. 3.2.1). In order to improve performance and facilitate convergence, additional constraints (c7) and (c8) are**  
 604 **included in the coupling interface. The coupling interface for REMIND → DIETER is programmed as a part of modified**  
 605 **DIETER code, and vice versa. Both interfaces are written in GAMS. For a single-region, the scheduling of coupled**  
 606 **iterations is illustrated in Fig. E1 in Appendix E. 16 DIETER optimization problems are solved for each representative**  
 607 **year of REMIND in parallel, scheduled after each internal REMIND “Nash” iteration (see Sect. 2.1 for a description of**  
 608 **the iterative “Nash” algorithm).**

609

610 During the coupling, the following exchanges of parameters and variables take place iteratively in both directions via the  
 611 interface.

612 **3.3.1 REMIND to DIETER**

613 The following information flow from REMIND to DIETER.

614 1. Technology fixed costs (convergence condition (h1)):

615 a. Annualized capital investment cost: It is calculated from endogenously determined overnight investment cost, plant  
 616 lifetime, and the endogenously determined interest rate. The overnight investment cost is determined from floor cost,  
 617 learning rate and the endogenous global accumulated deployment. Note that investment costs decrease according to  
 618 endogenous learning rate. Interest rate is about 5% on average but is endogenous and time dependent in REMIND;  
 619 b. Annualized operation and maintenance (O&M) fixed costs (OMF): They are a fixed share of the capital costs;  
 620 c. Adjustment cost: It is technology-specific and is proportional to the capital investment cost. See Appendix I for its  
 621 implementation.

622 2. Technology variable costs (convergence condition (h2)):

623 a. Primary energy fuel costs: They are endogenously determined as the shadow prices of the primary fuel balance  
 624 equations in REMIND. Import prices, domestic prices of extraction, amount of regional reserve, and the amount of fuel  
 625 demand can all influence the fuel cost. The relevant fuel costs include coal, gas, biomass and uranium. The fuel costs  
 626 can have interannual intertemporal oscillatory components which can cause instability during iteration if coupled  
 627 directly. We mitigate this by conducting a linear fit to the time series before passing them to DIETER;  
 628 b. Conversion efficiency of each generation technology;  
 629 c. O&M variable costs (OMV);  
 630 d. CO2 emission cost: Exogenous or endogenous CO2 price from REMIND multiplied by the carbon content of a type of  
 631 fossil fuel and divided by the conversion efficiency of a generation technology gives the CO2 cost of 1MWh of  
 632 generation. Note that in REMIND, biomass is considered to contain zero carbon emission when combusted.;  
 633 e. Grid cost: In REMIND the stylized grid capacity equation is proportional to the amount of pre-curtailment VRE  
 634 generation. So effectively the grid cost is a variable cost. Note that in future work, grid costs can be modeled in more  
 635 detail either in DIETER or in another PSM. Here, we use the parameterized grid costs which are implemented in  
 636 default REMIND as an approximation to the necessary grid cost.

637 3. Power demand (convergence condition (h4)). REMIND informs DIETER of the total power demand  $d_y$  of a representative  
 638 year  $y$ . In the next iteration of DIETER, the exogenous time series for the hourly demand from a historical year (2019) is  
 639 scaled up to demand of the last iteration REMIND,  $d_y(i-1)$ , such that the annual total power demand in DIETER is equal  
 640 to that of REMIND for each coupled year:  $\underline{d}_h = \underline{d}_{2019,h} * \frac{d_y(i-1)}{\sum_h \underline{d}_{2019,h}}$ .

641 4. Pre-investment capacities  $P_{y-4y/2,s}/(1 - ER)$  as an additional brown-field constraint (see constraint (c8) in Appendix G).  
 642  $ER$  is the endogenous early retirement rate in REMIND.

643 5. Total regional renewable resources for wind, solar and hydro (constraint (c2)), such that DIETER capacities are constrained  
 644 by the same total available resources as in REMIND.

645 6. Annual average theoretical capacity factors of VREs and hydroelectric in REMIND (convergence condition (h6)). We note  
 646 the pre-curtailment utilization rates of VRE capacity as “theoretical capacity factors”, as these can be achieved in theory if  
 647 there is no curtailment. They are usually determined by meteorological factors such as wind and solar potential, as well as  
 648 the efficiency of the turbines or solar photovoltaic modules. In contrast, the post-curtailment utilization rate of VRE are “real  
 649 capacity factors”, as these are the real utilization rates after optimal endogenous dispatch. The time series of theoretical  
 650 utilization rate of VRE generations of one historical year in DIETER are scaled up such that the annual average theoretical  
 651 capacity factors in DIETER equals the exogenous parameters in REMIND:

652 
$$\underline{\phi}_{h,vre}(y) = \min \left( 0.99, \underline{\phi}_{h,vre}(y=2019) * \frac{\phi_{vre}}{\sum_h \underline{\phi}_{h,vre}(y=2019)} \right).$$

653 In DIETER, to be realistic, the rescaled hourly capacity factor for solar and wind has an upper bound at 99%. The slight  
654 mismatch of the capacity factors due to this additional upper bound is negligible

### 655 3.3.2 DIETER to REMIND

656 The following information is passed from last-iteration DIETER to REMIND:

657 1. Market values  $\underline{MV}'_{y,s}$  and the annual average electricity price  $\underline{J}'_y$  (convergence condition (h3)), where  $\underline{MV}'_{y,s}$  is the annual  
658 average market value without the surplus scarcity hour price, and  $\underline{J}'_y$  is the annual average electricity price without the  
659 surplus scarcity hour price.

660 2. Peak hourly residual power demand  $\underline{d}_{residual}$  as a fraction of total annual demand  $\sum_h \underline{d}_h$  (constraint (c7)). This produces the  
661 peak residual demand in REMIND  $d_{residual,y}$  that is proportional to the last-iteration DIETER peak to total demand ratio  
662  $\frac{\underline{d}_{residual}(y,i-1)}{\sum_h \underline{d}_h(y,i-1)}$ , and the in-iteration total annual demand  $d_y(i)$ :

$$663 d_{residual,y}(i) = \frac{\underline{d}_{residual}(y,i-1)}{\sum_h \underline{d}_h(y,i-1)} * d_y(i),$$

664 where  $\underline{d}_{residual}$  was defined in Appendix H (Eq. (H1)).

665 3. Annual capacity factors of dispatchable plants  $\underline{\phi}_{dis} = \frac{\sum_h \underline{G}_{h,dis}}{P_{dis} * 8760}$  (convergence condition (h6)).

666 4. Annual solar and wind curtailment ratio: curtailment as a fraction to total annual post-curtailment generation  $\frac{\sum_h \underline{\Gamma}_{h,vre}}{\sum_h \underline{G}_{h,vre}}$   
667 (convergence condition (h7)).

668 For the information flowing from DIETER to REMIND, we use an innovative method of multiplicative “prefactors”, which can  
669 stabilize the coupling and increase the speed towards model convergence. The prefactors are automatic linear stabilizers of the  
670 current-iteration variables in REMIND. They depend on current-iteration endogenous variables in REMIND, and are multiplied  
671 usually with the last-iteration endogenous DIETER results that are exogenously passed to REMIND. This allows some degree of  
672 endogeneity in these exchanged variables, and their values can be adjusted according to the updated dynamics in the current  
673 REMIND iteration, such as interregional trading or price elasticity of demand, under which the exogenous last-iteration  
674 DIETER optimality can be used as an approximate starting point but do not necessarily hold exactly.

675 The prefactors usually depend on the differences between generation shares in the two models: e.g. the prefactor for markup is a  
676 linear function of the difference between the current-iteration REMIND endogenous generation share and last-iteration DIETER  
677 generation share. We illustrate the mechanism of prefactors using markup for solar as an example: A lower market value for  
678 solar is consistent with a higher solar share, according to the well-known self-cannibalization effect of decreasing VRE market  
679 value as the VRE share increases (Hirth, 2018). Therefore, we can introduce an automatic stabilization measure through a  
680 negative feedback loop: If the REMIND endogenous share is larger than in the last DIETER iteration, in which case the in-  
681 iteration market value should be lower than the last-iteration DIETER market value, the multiplicative prefactor for market  
682 value should be so constructed such that it is smaller than one. This lowers the market value for solar, and decreases the in-  
683 iteration REMIND markup  $\eta_{y,s}(i)$ , hence preventing over-incentivizing the solar generation using the old market value based on  
684 the last-iteration energy mix. Overall, this produces a stabilizing effect on the system by making the markup as a price signal  
685 responsive to endogenous quantity change. We use prefactors ubiquitously when passing variables from DIETER to REMIND,  
686 such that during the iteration REMIND can adjust more smoothly and easily. We discuss the implementation of these prefactors  
687 in detail in Appendix H.2.

688 **4 Numerical convergence under “proof-of-concept” baseline scenario**

689 In this section, we check the convergence behavior for prices and quantities (capacity and generation) in coupled model runs  
690 using the convergence validation criteria from the last section. Comparing the numerical results with the theoretical prediction,  
691 we can validate that REMIND-DIETER soft-coupling indeed produces almost full convergence.

692 Throughout this section, we only use one scenario – a “proof-of-concept” baseline scenario. Under the “proof-of-concept”  
693 scenario of the coupled run, we disable storage (i.e. batteries and hydrogen) and flexible demand (i.e. electrolyzers) in both  
694 models, as this allows us to use the theoretically derived convergence criteria from Sect. 3, which would become overly  
695 complex in a model with storage and flexible demand. The coupled run is under a baseline scenario, i.e. there is no additional  
696 climate policy implementation. Since this is a configuration created only for comparing to the theoretical prediction, it is not  
697 meant to be a policy-relevant configuration. In more policy-relevant coupled runs, we turn on storage and flexible demand (see  
698 Sect. 5). For schematics and computational runtimes of the coupled iterations, see Appendix E.

699 For the coupled runs, we define a baseline scenario for single-region Germany under SSP2 assumptions, corresponding to the  
700 “middle-of-the-road” scenario (for a definition of the SSPs, see Koch and Leimbach, 2022). Specifically, this means that  
701 REMIND runs for all global regions in parallel, but DIETER only runs for Germany. Only information in the German power  
702 sector is exchanged for the two models. We use a low CO<sub>2</sub> price to represent “no additional policy”, which is 30\$/tCO<sub>2</sub> in 2020  
703 and 37\$/tCO<sub>2</sub> for years beyond 2020. According to the 2011 Nuclear Energy Act of Germany, remaining nuclear capacities are  
704 set to early retire in REMIND within the time period until 2022. We assume hydroelectric generation in Germany to come from  
705 run-of-the-river. In DIETER, we cap dispatchable generation’s annual capacity factors at 80% for non-nuclear power plants, and  
706 85% for nuclear power plants, so the dispatch results are in line with real-world power sectors. This constraint only adjusts the  
707 capacity factor constraint (c4), which would pose no additional distortion to our mathematical analysis.

708 Due to the particular implementation of offshore wind in REMIND, DIETER wind offshore capacities are fixed to that of  
709 REMIND to avoid too much distortion. Since in our scenarios, offshore wind capacity in Germany is relatively small compared  
710 to other generators, this fixing presents only a minor distortion to the coupling. Hydroelectric generation in REMIND is  
711 assumed to have an average annual capacity factor of around 25%. This capacity factor is implemented as a bound in DIETER.  
712 For simplicity, instead of a time series profile for hydroelectric generation, we allow the hourly capacity factor to be no higher  
713 than 90%, meaning hydro is close to being dispatchable in all our scenarios. In the German context, hydro usually means run-of-  
714 the-river, which has a variable output. Nevertheless, we find the 90% maximum hourly capacity factor a reasonable assumption  
715 to make, since in our runs we do not yet consider pumped hydro as a technology in this study, so a more dispatchable quality of  
716 hydro can be assumed. Results presented in this section belong to the same coupled run under the “proof-of-concept” scenario.

717 **4.1 Electricity price convergence**

718 According to theoretical convergence criteria (under simplifying assumptions, Sect. 3.2.1-3), at numerical convergence, the  
719 electricity price of REMIND should be equal to the price of DIETER. However, REMIND is interannual intertemporal, whereas  
720 DIETER is only year-long, so we compare the differences over time, as well as the interannual average of the price differences  
721 (Fig. 4).

722

723



725  
 726 **Figure 4: Annual average electricity price convergence behavior of a coupled run for Germany under a “proof-of-**  
 727 **concept” baseline scenario. (a): the difference between the annual electricity price time series of REMIND and the**  
 728 **annual average electricity price time series in DIETER as a function of coupled iteration. (b): the interannual average of**  
 729 **the differences in (a) as a share of REMIND price. Due to the interannual intertemporal nature of REMIND, in (a) the**  
 730 **price difference can appear to have oscillatory components, obscuring the visual assessment of convergence. As a result,**  
 731 **we show the trend of price convergence over iterations more clearly in panel (b) by taking the temporal average of the**  
 732 **price differences. The REMIND price in both plots is a running average of three neighboring time periods to visually**  
 733 **smooth out oscillations.**

734  
 735 In Fig. 4a, the price difference oscillates from period to period. As the coupling starts, the REMIND price is much higher than  
 736 DIETER, especially in the earlier years. After around the 10th iteration, the difference in early years starts to reverse: DIETER’s  
 737 price becomes higher than REMIND. Around 2040-2060, REMIND has a higher average price than DIETER, due to the VRE  
 738 market values being higher than their LCOE. This is discussed later in Sect. 4.3.2.

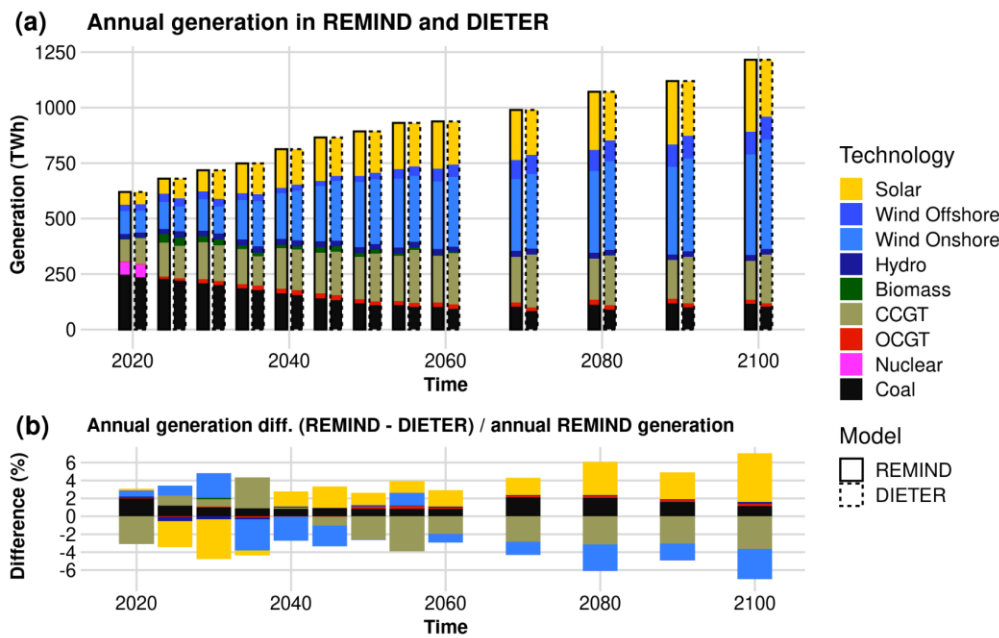
739 In Fig. 4b, we calculate the difference between two time series – the time-averaged power prices in the two models. We observe  
 740 the difference between them decreases over the iterations, showing a clear converging trend, and stabilizes at around 3% of the  
 741 REMIND price. There are two observations regarding the price convergence of the coupled run. First, the convergence happens  
 742 rather quickly within 10 iterations. Second, the converged value of the price difference is not exactly 0, but slightly above 0, at a  
 743 few percent of the full price (a few \$/MWh). Under ideal convergence conditions, according to (v1), the two prices should be  
 744 equal at full convergence for every coupled year. However, in practice, the average prices do not perfectly match, as there are  
 745 several sources of distortions from capacity shadow prices. The capacity shadow prices come from many sources in both  
 746 models: extra constraints such as (c7-c8) which are not part of the analysis leading to (v1), constraints that are in REMIND but  
 747 not in DIETER (c5-c6), and exogenous wind offshore capacity in DIETER. Some of these capacity shadow prices in both  
 748 models can be more or less consistent with each other (such as standing capacity constraint in DIETER and brown-field

749 constraints in REMIND), but others are not and can distort two models in different ways, causing some degrees of misalignment  
 750 in prices. As discussed before, prices can be overdetermined by the energy mix (Sect. 3.2.3). Therefore, some of the capacity  
 751 shadow prices – even though not aligned between the two models – can nevertheless cancel each other (especially averaged over  
 752 time), potentially causing the price differences to be moderate. To examine exactly how well the prices at the end of the  
 753 coupling match, we need to check the cost decomposition of prices. This is discussed later in Sect. 4.3.

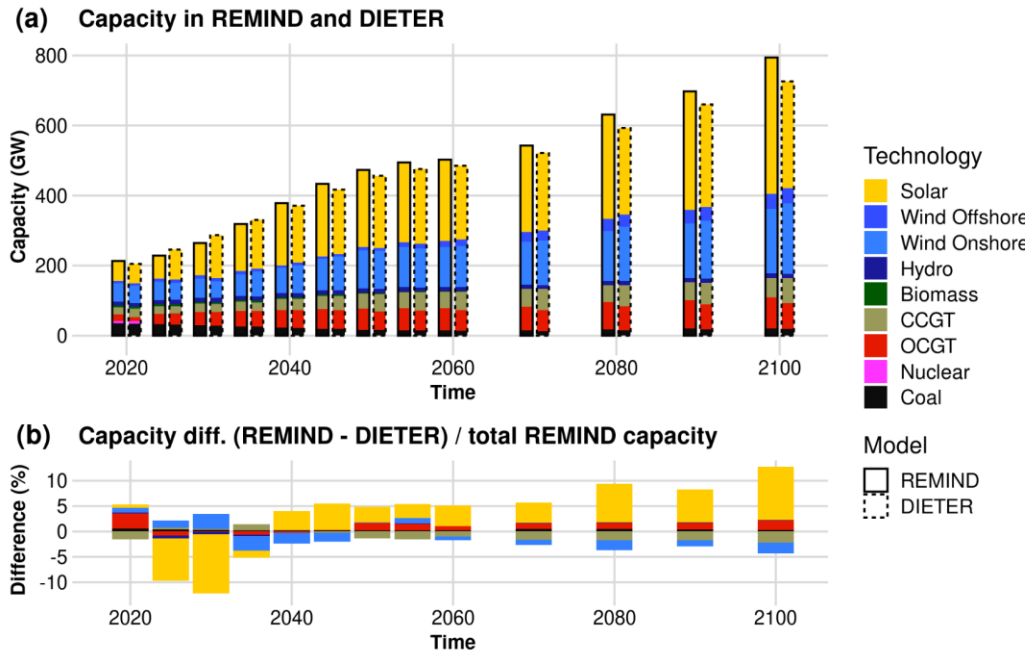
754 Also note that Fig. 4b presents a time-averaged price comparison, and on average the difference between the prices in the two  
 755 models is small at the end of the coupling. However, when one compares the maximal deviation for any single year at the end of  
 756 the coupling, it can be as high as 10\$/MWh, e.g. around 2050 (Fig. 4a). This is much larger than the 3% averaged deviation in  
 757 Fig. 4b. However, compared to default REMIND prices (which we cannot show due to limited space), we are fairly confident  
 758 that the oscillation of coupled REMIND results from internal dynamics that are also visible in the default uncoupled version. So  
 759 a time-averaged treatment is adequate in displaying total price convergence here.

## 760 4.2 Quantity convergence

761 Besides price convergence, the capacity and generation decision variables must also converge within a certain tolerance at the  
 762 end of the coupling. This is reflected in the generation mix (Fig. 5) and the capacity mix (Fig. 6) at the end of the coupled run.  
 763 Due to the existence of several sources of mismatch between the two models already mentioned in the last section, which is  
 764 already manifested in the mismatch in electricity prices of the two models, a certain degree of mismatch in quantities is also to  
 765 be expected. Nevertheless, the agreement between the two endogenous sets of decision variables is satisfactory. For this coupled  
 766 run, the differences of the generation share of any single technology between the two models are smaller than 4.4% for each  
 767 year until 2100. Figure (5b) highlights some subtle model differences in generation. For example, after 2040, REMIND favors  
 768 solar and coal, whereas DIETER tends to have more combined cycle gas turbines (CCGT) and wind onshore. Due to the low  
 769 capacity factor of OCGT and solar compared to the capacity factors of the other generators, the capacity mix differences  
 770 between models are amplified for these two technologies (Fig. 6). But overall, the generation mixes and the capacity portfolios  
 771 at the end of coupled run are generally similar.



773 **Figure 5: Annual electricity generation convergence at the final iteration of a coupled run for Germany under the**  
 774 **“proof-of-concept” baseline scenario. (a) Side-by-side comparison of the two generation portfolios at the end of the**  
 775 **coupled run. (b) The difference between the generation mix in the two models as a share of total REMIND generation.**



776  
 777 **Figure 6: Capacity convergence at the final iteration of a coupled run for Germany under the “proof-of-concept”**  
 778 **baseline scenario. (a) Side-by-side comparison of the two models’ capacity mix at the end of the coupled run. (b) The**  
 779 **capacity difference between the two models as a share of total REMIND capacity.**

780  
 781 For periods that are policy relevant in the short- to medium-term (i.e. before 2070), the convergence for quantities is generally  
 782 slightly worse in the near-term, i.e. in the 2020s and 2030s, likely due to the capacity bounds mismatch in the near-term (such as  
 783 the capacity bounds (c5-c6) in REMIND not being completely replicated by standing capacity constraint (c8) in DIETER). If  
 784 DIETER does not contain identical bounds as REMIND, then its endogenous decision will have more of a green-field rationale  
 785 than REMIND does, the latter of which is more constrained in the near-term. In case an improvement of near-term convergence  
 786 is desired, these bounds could be implemented more carefully, and more technology-specific. Due to the limited scope, we only  
 787 apply a generic standing capacity constraint (c8) in DIETER to represent the basket of various constraints. The convergence of  
 788 quantities is also not perfect in the green-field periods, such as after 2040, where both models are less constrained by near-term  
 789 dynamics. The reason for this is likely due to the fact that in DIETER, hydroelectric generation is not economically competitive  
 790 against other cheaper forms of generation such as solar and wind. But in REMIND it is economically competitive, likely due to  
 791 the long life-time of the plants. Semi-exogenous wind offshore capacitates in both models could also play a role. This is  
 792 discussed in more detail in Section 6.1.

#### 793 **4.3 Zero-profit rules for the coupled model**

794 As our analytical discussion showed before in Sect. 3.2.3, model equilibria in the form of ZPRs are useful in validating  
 795 convergence in a more detailed way by decomposing prices into cost components as well as any perturbation from capacity  
 796 shadow prices. In this section, we first compare the system LCOE, price and capacity shadow prices of the two models for ZPRs  
 797 on the system level, then we show the technology-specific ZPRs. Using this validating step, we can visually ascertain that the

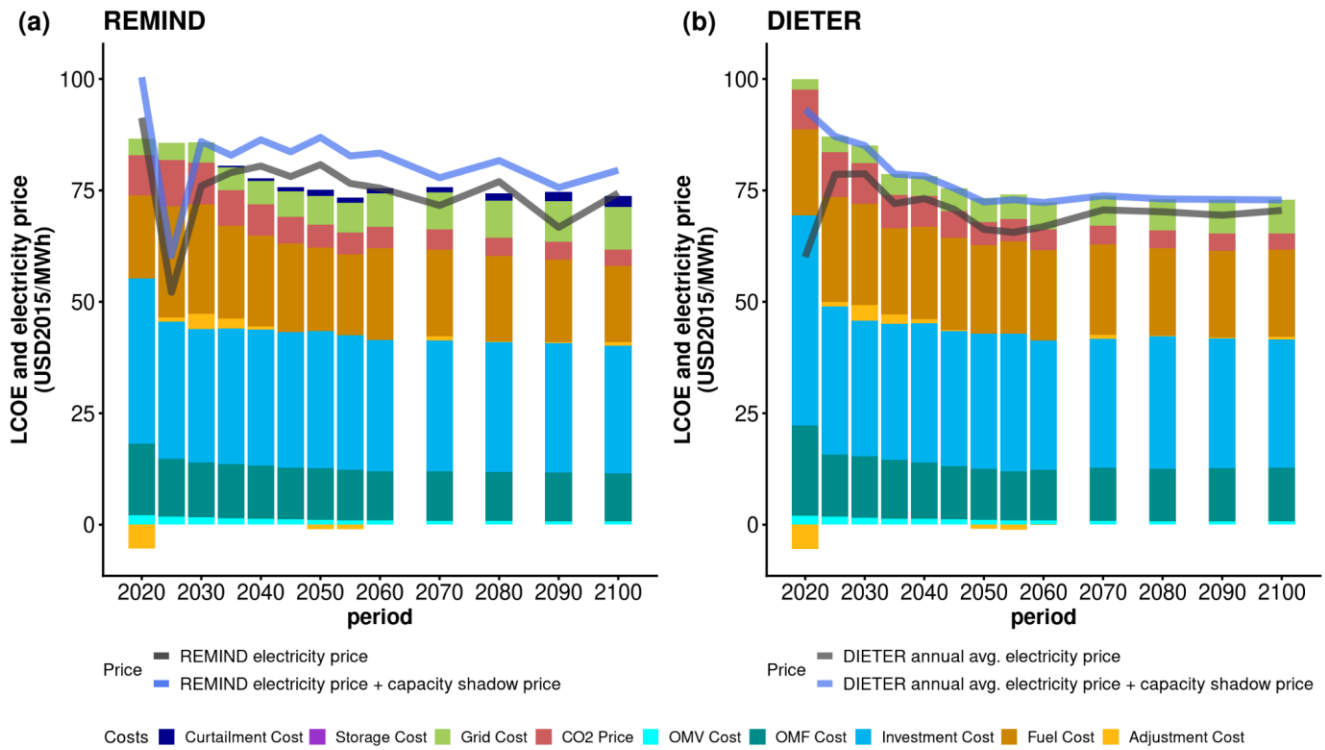
798 cost components and prices/market values in the two models are remarkably similar on the system level as well as on the  
799 technological level, demonstrating that the underlying principle behind the coupled convergence holds to a good degree.

800 **4.3.1 System-level zero-profit rule**

801 At the convergence of the soft-coupled model, we expect ZPRs to be satisfied for the two systems individually (Eq. (11) for  
802 REMIND and Eq. (13) for DIETER), i.e. each price times series also matches the LCOE time series to a good degree, barring  
803 distortions from the capacity shadow prices. This is to say, under full convergence, the time series of system LCOE, and the sum  
804 of the time series of the electricity prices and time series for capacity shadow prices for both models should overlap one another  
805 within numerical tolerance. The costs and prices at the last iteration of the coupled run are summarized in Fig. 7. The electricity  
806 prices derived from the shadow prices of the balance equations are shown in dark grey: (a), REMIND electricity price  $\lambda_y$ , (b)  
807 DIETER annual average electricity price  $J_y = \frac{\sum_h \lambda_{y,h} d_{y,h}}{\sum_h d_{y,h}}$ . Adding all the sources of capacity shadow prices, we obtain the blue  
808 lines: (a) REMIND capacity constraints (c5-c7), (b) DIETER capacity constraint (c8). All capacity shadow prices have been  
809 converted to per energy unit via capacity factors. (Note: Fig. 4 shows the difference between the black lines, without considering  
810 the capacity shadow prices. See Sect. 3.2.3.)

811 From Fig. 7, we can conclude that the ZPR for DIETER is satisfied to very good accuracy for every year (the blue line – the  
812 sum of electricity price and capacity shadow price has exactly the same value as the sum of LCOE bars). For REMIND, the ZPR  
813 is satisfied year-on-year to a lesser degree, but on average to a good degree given the interannual fluctuations. The prices in  
814 coupled REMIND become very erratic for the early years (2020-2025), likely due to the interaction between the historical or  
815 near-term bounds in REMIND and the exchanged information from DIETER for those years. The LCOEs component structures  
816 match well across the models for most years, which serves as additional visual support on price convergence shown in Fig. 4,  
817 i.e. the cost structures behind the prices are harmonized as well at the end of coupling. The origins of the differences between  
818 LCOEs and prices, as well as the degree with which capacity shadow prices account for them, can be found when one examines  
819 the LCOE and market values of specific technologies, which are analyzed next.

820

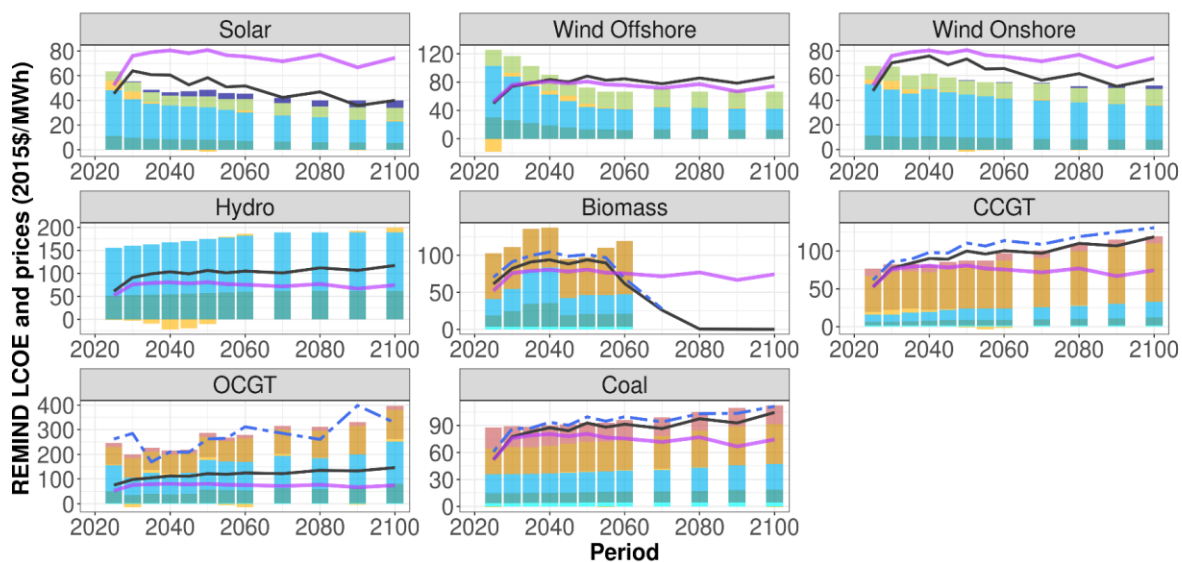


821  
822 **Figure 7: Cost components of the system LCOEs (bars), electricity prices (grey lines) and the sum of electricity prices**  
823 and capacity shadow prices for (a) REMIND and (b) DIETER under “proof-of-concept” baseline scenario. Visually the  
824 ZPRs for both models are satisfied within numerical tolerance. The intertemporal structure of the LCOE breakdown is  
825 very similar for most of the coupled periods. For DIETER, a small remaining difference exists between the price (grey  
826 line) and the LCOE (bars), which can be entirely explained by the capacity shadow price due to the standing capacity  
827 constraint. The REMIND price time series is a rolling average of 3 time periods. The large negative adjustment costs in  
828 2020 are due to coal and nuclear phase-out.

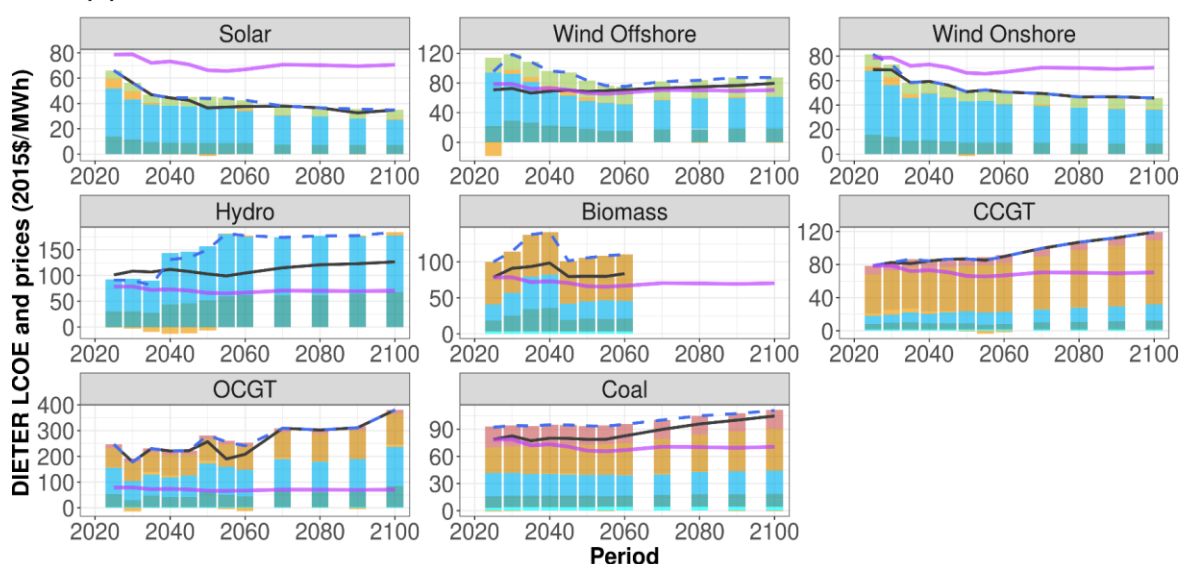
#### 829 4.3.2 Technology-specific zero-profit rule

830 After validating ZPRs on the system level, we further dive into each technology and check the ZPRs for each technology in both  
831 models at the last iteration of the coupled run (Fig. 8).

**(a) REMIND**



**(b) DIETER**



— Storage Cost ■ Grid Cost ■ CO2 Price ■ OMV Cost ■ OMF Cost ■ Investment Cost ■ Fuel Cost ■ Adjustment Cost

832 **Figure 8: Technology-specific costs and market values for (a) REMIND and (b) DIETER under “proof-of-concept”**  
833 **scenario. Cost components of the technology LCOE are plotted in stacked bars. Market values are shown in solid black**  
834 **lines. The sum of market values and all sources of capacity shadow prices are shown in dashed lines: for DIETER (two-**  
835 **dash blue lines), they contain mostly the standing capacity shadow price, and to a small extent the capacity shadow**  
836 **prices of the resource constraint; for REMIND (dashed blue lines), they contain mostly the peak demand capacity**  
837 **shadow price, and small capacity shadow prices due to brown-field and resource constraints. Electricity prices are**  
838 **shown in purple solid lines as references. Due to large positive shadow prices in 2020 due to fixings to the historical**  
839 **capacities, only periods beyond 2020 are shown. REMIND market values and capacity shadow prices are a rolling**  
840 **average of 3 time periods.**

832

833

834

835

836

837

838

839

840

841

842

843 In Fig. 8(b), DIETER LCOE and market values for the eight types of generators are shown. As expected from the ZPR, the  
844 LCOE always matches the sum of the market value and capacity shadow prices for each technology, and for each year (Eq.  
845 (12)). The difference between the dashed and solid lines are largely the generation capacity shadow prices. It is worth noting  
846 that at the end of convergence, the sizes of the shadow prices are in general small for the main generator types, e.g. solar, wind  
847 onshore, CCGT and OCGT. This indicates the fact that for these technologies for most periods, the optimal DIETER generation  
848 mix is close to that of a green-field model. That is, DIETER hardly faces any exogenous constraints (except resource constraints  
849 that are aligned with those of REMIND) and can make fully endogenous investment and dispatch decisions based on cost  
850 information alone. On the whole, DIETER at the coupled convergence experiences only a small amount of distortion from the  
851 brown-field model REMIND, especially concerning the “model suboptimal” real-world standing capacities from biomass, hydro  
852 and coal.

853 In Fig. 8(a), we show the REMIND LCOE and market values for the same generation technologies. Due to the intertemporal  
854 nature of REMIND, the sum of market value and capacity shadow price for each technology, and for each year matches the  
855 LCOE generally slightly less well than DIETER. This means for REMIND the ZPR (Eq. (10)) for each generator type is also  
856 satisfied to a good degree for main generator types, e.g. solar, wind onshore, coal, CCGT and OCGT. The mismatch in biomass  
857 and hydro might come from the shadow price from historical capacities.

858 Since the differences between market values and costs are accounted for by capacity shadow price to a large degree, it is worth  
859 interpreting physically the sources of these “hidden” costs/revenues. For REMIND, the capacity shadow prices consist of those  
860 in (c2), (c5), (c6), as well as the “peak residual demand constraint” from DIETER (c7). Constraint (c7) is created to circumvent  
861 high markups especially from peaker gas plants (Appendix H.1). Because peaker gas plants generate power mostly only at hours  
862 with high prices (especially scarcity hour price), and therefore have very high market values compared to annual average  
863 electricity price. The high market values of OCGT – usually more than 5 times the average annual electricity prices – acts as a  
864 large incentive in the next iteration REMIND, and leads to overinvestment in capacities. Over iterations, this causes oscillations  
865 in the quantities and prices in the coupled model and prevents model convergence. To circumvent the issue of high markup, we  
866 implement (c7) as an equivalent peak residual demand constraint. As can be shown mathematically (Appendix H), (c7)  
867 generates essentially the scarcity hour price, and it is very easy to validate this for OCGT in Fig. 8(a). The capacity shadow  
868 price derived from this peak residual demand constraint, when translated to energy terms and added to the market value,  
869 correctly recovers the LCOE for OCGT, recovering the original ZPR (Appendix H.1.2). This indicates that under multiscale  
870 model coupling, an extra constraint is an effective way to circumvent potential issues of numerical divergence due to the large  
871 impact from short-term dynamics, such as the large market value of peaker gas plants.

872 For DIETER, the two sources of capacity shadow price are the total renewable potential limit (constraint (c2) in Sect. 3.1), and  
873 the standing capacity constraint from REMIND (constraint (c8) in Sect. 3.2.3). For the first type, the resulting capacity shadow  
874 price is a hidden “positive cost” from the perspective of the power user. Since endogenously DIETER would like to invest more,  
875 but is limited by the natural resources available. An example for this first type is hydroelectric power between 2020 and 2035,  
876 due to the limited resource (run-of-the-river) in Germany. It is worth noting that from the generator’s perspective, the capacity  
877 shadow price from resource constraint can be interpreted as an extra resource rent. The second type of capacity constraint  
878 originates from the standing capacity, the latter is received by DIETER from REMIND as a lower bound. This constraint usually  
879 results in a hidden “negative cost” from the perspective of a power user, i.e. a part of the cost (LCOE) does not get passed on to  
880 the electricity price, so the users get part of the capacity “for free”. (This can also be interpreted as subsidies for generators to  
881 sustain these unprofitable capacities.) This is because based on greenfield cost optimization, DIETER endogenously would  
882 invest less in certain technologies. However, since the standing capacities account for the existing generation assets in the real

883 world, which can be model suboptimal, the overall costs are above a greenfield equilibrium and above the prices the user pays.  
884 We find examples of such a capacity shadow price manifested in biomass, coal and hydroelectric, all of which are part of the  
885 existing German power capacity mix, but evidently not all of them for any given period are “green-field optimal” based on pure  
886 cost consideration in DIETER. Interestingly, after 2035, the sign of the capacity shadow price for hydroelectric generators  
887 reverses. This is likely due to the continuous decline of the VRE costs after 2035 tips the power sector into a regime where  
888 hydroelectric becomes less economically competitive in DIETER, at least compared to REMIND. As a result, the standing  
889 constraint from REMIND starts to be binding on the capacity from below, relieving the resource constraint binding from above.  
890 For DIETER, the capacity shadow price from standing capacities also indicates the degree of disagreement between DIETER  
891 and REMIND. For most future years, REMIND standing capacity constraints are not binding in DIETER for solar, wind  
892 onshore, CCGT and OCGT, indicating good agreement between the models. The small amount of shadow prices near 2060 for  
893 OCGT and solar in Fig. 8(b) are likely due to the time step size change in REMIND which causes a small jump in the interest  
894 rates near these years.

895 Lastly, in Fig. 4 before we observe a slightly higher average electricity price in REMIND than in DIETER, especially in the  
896 intermediate years. This could be due to fixed offshore wind capacities, which are never economical to be invested  
897 endogenously in the parameterization used here. This generates a high capacity shadow price until around 2045-2060, visible in  
898 both DIETER and REMIND.

## 899 **5 Scenario results under baseline and policy scenarios**

900 In this section, we present baseline and policy scenario results for Germany, using a more realistic configuration of the coupled  
901 model with electricity storage and flexible electrolyzer demand for green hydrogen production which is then used outside the  
902 power sector (e.g. in industry or heavy trucks). We show results for a baseline scenario and a net-zero by 2045 climate policy  
903 scenario. Note that due to REMIND’s global scope, under the net-zero scenario we also assume a larger climate policy  
904 background of 1.5C goal for end-of-century temperature rise globally (corresponding to a 500Gt of CO<sub>2</sub> emission budget until  
905 2100), and a larger regional goal of EU-wide net-zero emission. Both scenarios consider nuclear phaseout law in Germany.

906 In Sect. 5.1, we present long-term power sector development. In Sect. 5.2, we present short-term power sector hourly dispatch  
907 and price results. In the following, we broadly describe how these additional features are implemented:

908 1. Storage: We use a simple storage implementation where DIETER makes endogenous investment into two kinds of storage  
909 technologies:  
910 1) lithium-ion utility-scale batteries;  
911 2) onsite green hydrogen production via flexible electrolyzers, storage and combustion for power production.

912 The principle of the coupling remains mostly unchanged. REMIND receives the price markups from generation technologies  
913 as in the case before without storage. However, for simplicity, the capacities of storage are not part of endogenous  
914 investment in REMIND. In REMIND, the energy loss due to storage conversion efficiency is taken as a fraction of total  
915 demand from DIETER as a parameter, and stabilized with a prefactor for each type of renewable generation (similar to the  
916 case of curtailment rate in Sect. 3.3.2, 4). Our battery cost development is given in Supplemental Material S1-2.

917 The reason we only allow DIETER to endogenously invest in storage technologies, is that the additional intertemporal  
918 optimization offered in REMIND is relatively less important than that for the investment of generation technologies. In  
919 REMIND, intertemporality mainly accounts for two aspects in the real-world: 1) implementing adjustment cost and 2)  
920 tracking of standing capacity. The adjustment costs simulate system inertia to rapid capacity addition or removal. In the case  
921 of battery and other storage technologies, the ramp up of deployment faces relatively fewer inertia compared to wind and

922 solar. Compared to generation technologies such as wind and solar, the storage technologies tend to have lower total  
 923 capacities, meaning their ramp up rate is usually lower. Also, their deployment is mostly constrained by their higher cost.  
 924 For utility storage technologies, they are mostly not yet deployed at scale, which means there is very little existing capacity,  
 925 the investment for storage in REMIND is mostly green-field, rendering it unnecessary to give DIETER a standing capacity  
 926 of them.

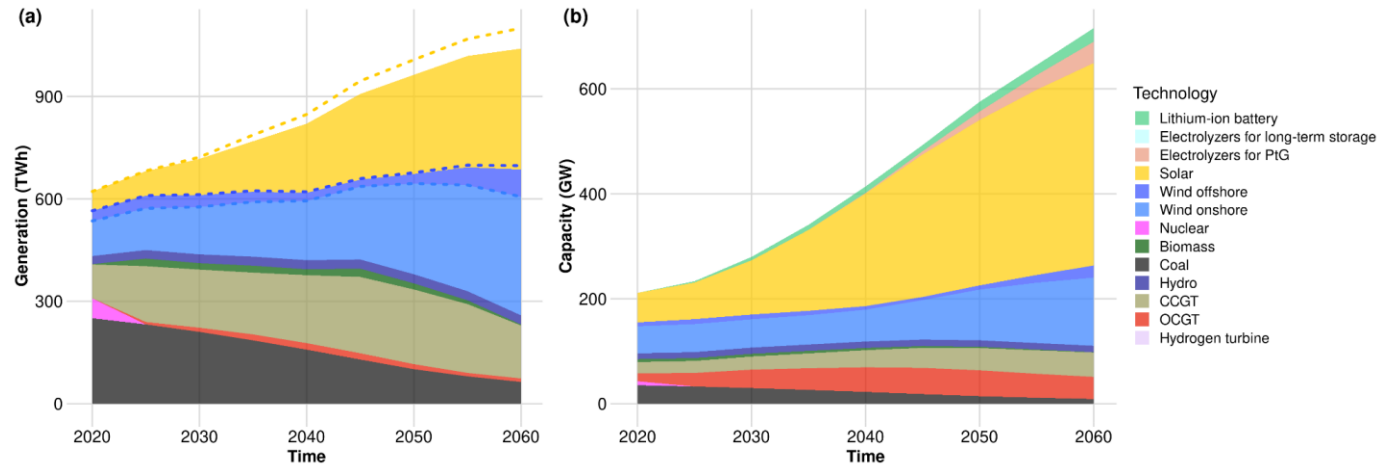
927 2. Flexible demand: As a simple representation of flexible demand, we choose to implement a common Power-to-Gas (PtG)  
 928 technology, namely the so-called “green hydrogen” electrolysis. We split the total power demand required to produce green  
 929 hydrogen from REMIND from the total power demand  $d_y(i-1)$  (Sect. 3.3.1, 3) – both demands are endogenous in  
 930 REMIND. We implement the electrolysis demand as completely flexible in DIETER, i.e. there is no ramping cost or  
 931 constraint. Thereby flexibilizing part of endogenous total power demand  $d_y(i-1)$  in REMIND. As a result, the cost  
 932 minimization in DIETER automatically allocates the flexible demand to hours where electricity costs are low due to the  
 933 existence of low-cost VRE. The economic value of flexible demand can be quantified by the capture price. The annual  
 934 capture price of demand-side technology  $s_d$  is the annual average price of the hours when the flexible demand consumes  
 935 electricity, weighted by the hourly flexible power demand by electrolyzers: 
$$\underline{CP}_{s_d} = \frac{\sum_{h,s_d} d_{h,s_d} \lambda_h}{\sum_{h,s_d} d_{h,s_d}}$$
.

936 This concept is equivalent to the market value for a variable or dispatchable generator, but here for a flexible or inflexible  
 937 demand source. Similar to before, we implement a stabilization measure using a prefactor (Appendix H.2, 5).

### 938 5.1. Long-term development

939 This section presents scenario results of the coupled model with a long-term view on capacity and generation, using either the  
 940 proof-of-concept scenario or more realistic configurations.

#### 941 5.1.1 Baseline scenario



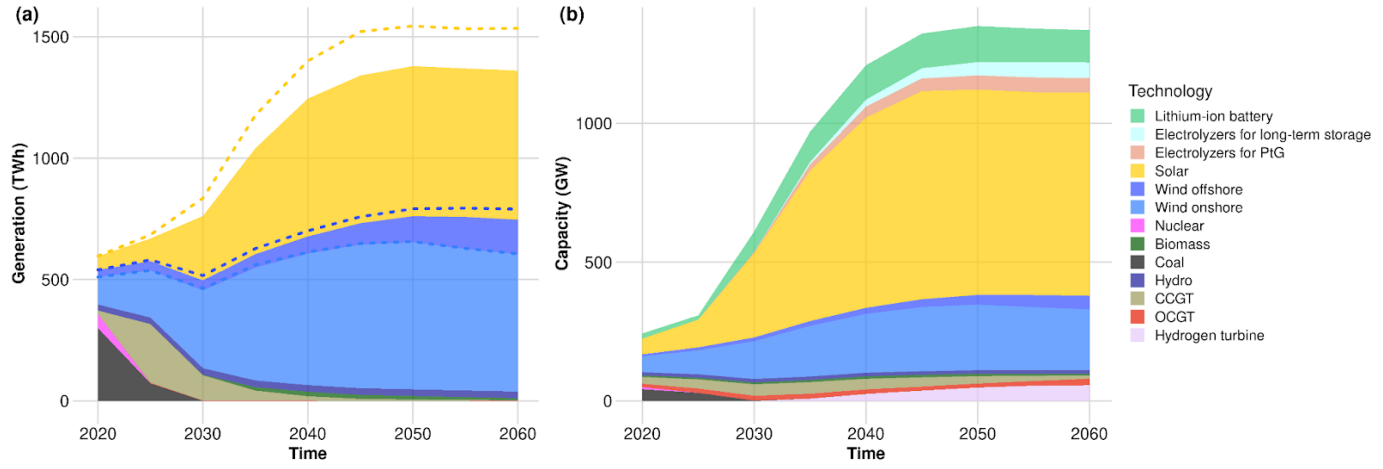
942 **Figure 9: DIETER-REMIND converged results of the long-term (a) generation and (b) capacity expansion for**  
 943 **Germany's power sector in the baseline scenario, assuming a constant 37\$/tCO<sub>2</sub> CO<sub>2</sub> price. Dashed lines represent**  
 944 **generation before storage loss and curtailment. Storage generation is not visualized in (a).**

945 In Fig. 9(a), under baseline scenario, and with available storage and flexible demand, we observe a more than 35% increase of  
 946 the total power demand from 2020 to 2045, and more than 65% by 2080. This is due to an increase in end-use electrification.  
 947 The increased electrification comes from a moderate growth in electricity use in the building sector and a more significant

950 growth in EV fleet. In the building sector, the final energy share of electricity is projected to increase from 28% in 2020 to 39%  
 951 in 2045. The final energy share of electricity in the transport sector is 22% by 2045, up from 2% in 2020. Note that even under  
 952 no additional climate policies, based on only the increase in EVs shares in new-cars sales in many world markets today, we  
 953 expect higher power usage from EVs in the future. Within the energy mix, we see a slow decline in coal generation over time,  
 954 which is replaced by CCGT generation and a significant increase of VRE. VRE share reaches above 50% by 2045, but slightly  
 955 less than half of the energy mix still contains coal and gas power. In terms of capacity expansion (Fig. 9(b)), due to both lower  
 956 generation cost and higher power demand, solar capacity expands by almost 5 times from today until 2045. However, the  
 957 moderate VRE shares mean that the requirement on battery capacity is not high, namely only 12GW of batteries by 2045. Due  
 958 to the low CO<sub>2</sub> price, long-term electricity storage through hydrogen does not appear to be economically competitive and is not  
 959 invested under the baseline.

960 By comparing the above baseline scenario (with storage and flexible demand) (Fig. 9) with the “proof-of-concept” baseline  
 961 scenario (without storage or flexible demand) before (Fig. 5 and 6), it is clear that while battery storage and partial demand  
 962 flexibility play a role after 2040 in increasing the VRE share in Fig. 9, in the near term, the scenarios with and without available  
 963 storage and demand flexibility look very similar under no additional climate policies. However, due to technological learning  
 964 effect, even absent additional CO<sub>2</sub> price policy, the energy mix here has a relatively high VRE share (>60%) after 2050  
 965 compared to the basic case without storage and demand-side flexibilization. However, due to the low CO<sub>2</sub> price there is still a  
 966 significant share of dispatchable technologies such as CCGT and OCGT, which is more economical than the implementation of  
 967 long-term power storage via electrolysis and hydrogen turbines.

### 968 5.1.2 Net-zero policy scenario



969  
 970 **Figure 10: DIETER-REMIND results of the long-term generation and capacity expansion for Germany's power sector**  
 971 **in the “net-zero 2045” scenario. CO<sub>2</sub> price is endogenously determined based on the climate goal. It is 115\$/tCO<sub>2</sub> for**  
 972 **2030, 292\$/tCO<sub>2</sub> for 2035, 464\$/tCO<sub>2</sub> for 2040, and 636\$/tCO<sub>2</sub> for 2045. Dashed lines represent pre-curtailment**  
 973 **generation. Storage generation is not visualized in (a).**

974  
 975 In Fig. 10, under stringent climate policy (economic-wide carbon neutrality in 2045), with available storage and partially  
 976 flexibilized demand (for hydrogen production used in other sectors), the total power demand more than doubles, and the power  
 977 mix is dramatically transformed. Compared to both the baseline case without storage and demand-side flexibilization (Fig. 5 and  
 978 6) and the baseline scenario with storage and flexible demand (Fig. 9), a very high VRE share in the generation mix is reached

979 already by 2040 (>94%). This is mostly due to an earlier investment in VRE to drive down the cost, combined with the  
980 increased deployment of both short- and long-term storage and flexibilization of part of the demand. Capacities for storage  
981 increase significantly: lithium-ion batteries from 18GW in 2020 to 125GW in 2045, and 37 GW of hydrogen electrolysis and  
982 hydrogen turbine capacity (with ~40TWh of H2 storage capacity). Despite high storage capacities, due to high VRE share,  
983 curtailment and storage loss still increases quite significantly with time, especially for solar PV. But note that in a coupled run  
984 where interregional transmission expansion is possible connecting Germany and the rest of Europe, this loss can be reduced (see  
985 Sec. 6.3). In terms of capacity expansion (Fig. 10(b)), gas power plants are mostly replaced, as hydrogen turbines fill the role of  
986 peaking dispatchable plants that guarantee supply for peak demand hours. The CCGT gas turbines are equipped with CCS.  
987 Under the stringent climate policy scenario, dramatic changes in the end-use sectors will be underway in the form of direct  
988 electrification and substitution of fossil gas with hydrogen. In the building sector, the final energy share of electricity is  
989 projected to increase from 28% in 2020 to 66% in 2045. In transport, the final energy share of electricity is 56% by 2045. In the  
990 industry sector, the share of electricity increases from 25% to 63%. By 2045 there is also a notable increase in the use of green  
991 hydrogen produced from 45GW flexible electrolyzers (at about 42% average annual capacity factor), amounting to 0.5EJ (3.5  
992 million tons) per year in the final energy, which is primarily used in industry. For a comparison with other published Germany  
993 net-zero scenarios results, see Supplemental material S4.

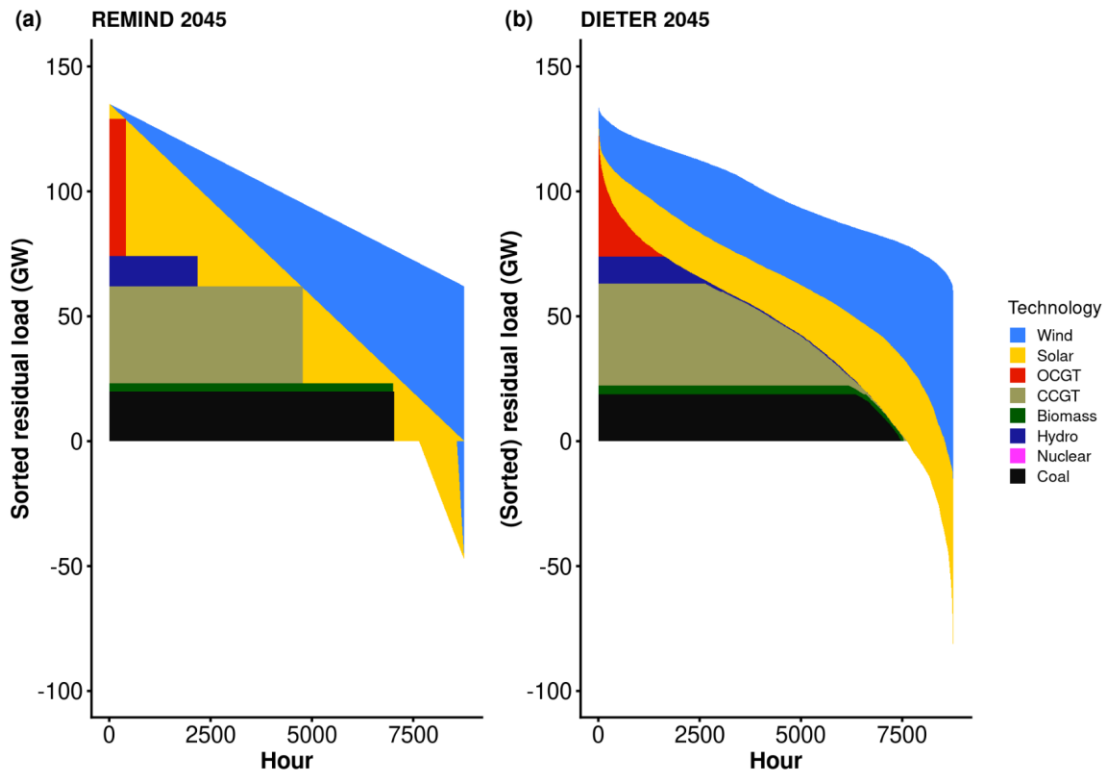
## 994 **5.2. Short-term dispatch**

995 In this section, results of hourly resolution are shown and discussed for a selected model year. We use established methods such  
996 as residual load duration curves (RLDCs) to visualize the hourly dispatch result, as well as show the hourly generation and  
997 dispatch time series for some typical days in summer and winter.

### 998 **5.2.1 Residual load duration curve model comparison**

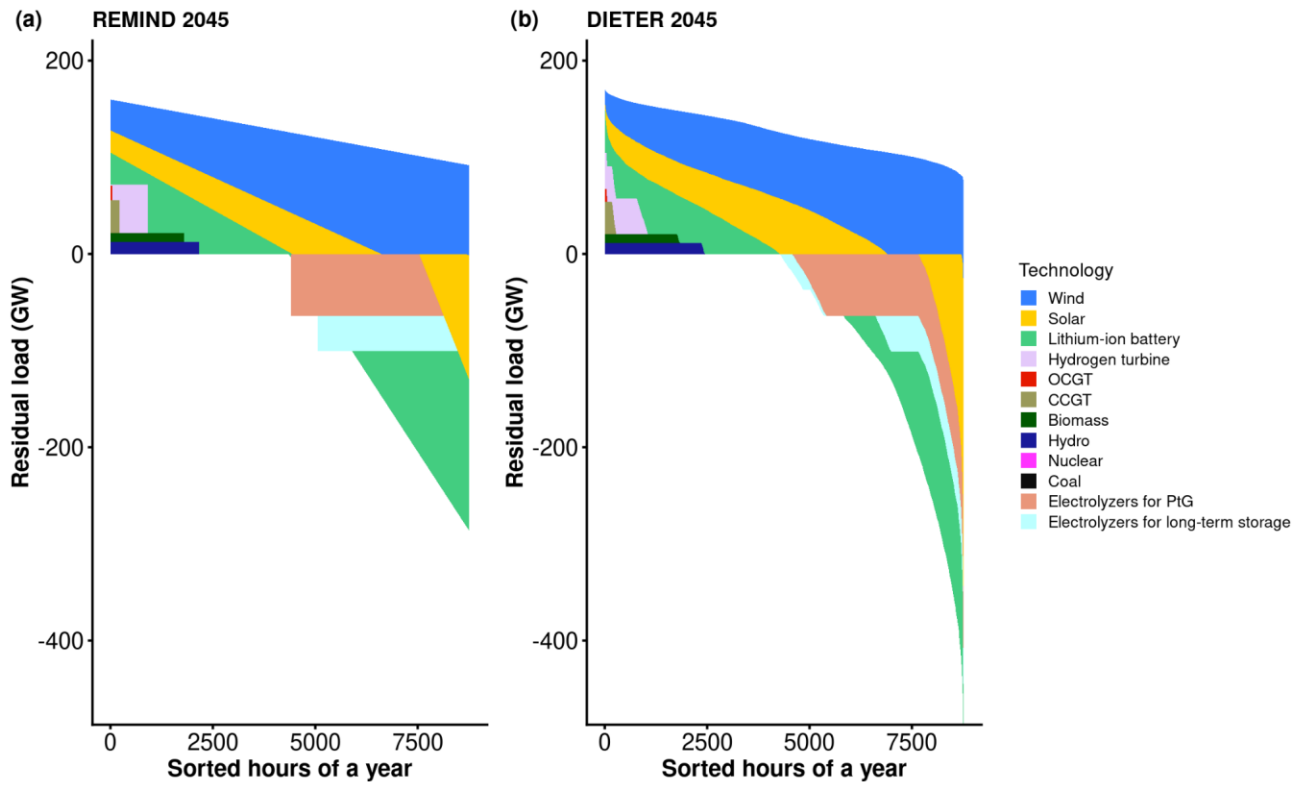
999 RLDCs can be used to visualize the dispatch of energy system models. Each subsequent curve is calculated by subtracting the  
1000 generation of a technology from the hourly residual demand curve, and then sorting the remaining demand in descending order.  
1001 On the left-side of RLDC graphs one can easily check the amount of residual demand not met by variable wind and solar  
1002 production. The top-most line in RLDC graph is the load duration curve for inflexible demand (excluding the demand from  
1003 flexible electrolysis for hydrogen production used in other sectors).

1004 In a baseline configuration without flexibilized demand or storage, despite lacking the explicit hourly dispatch, via bidirectional  
1005 soft-linkage, REMIND could achieve a final dispatch result that replicates DIETER to a satisfactory degree (Fig. 11). This is a  
1006 combined effect of a convergence of capacities (Sect. 4.2) and full-load hours at the end of the coupled run. In the peak residual  
1007 demand hour (the leftmost point in the RLDC), the DIETER-coupled REMIND accounts for the requirement of dispatchable  
1008 capacities via the constraint (c7), and the composition of the mix is replicated from DIETER and correctly guarantees that the  
1009 peak hourly demand is met.



1010  
1011 **Figure 11: Side-by-side RLDC comparison between (a) REMIND and (b) DIETER for the simple configuration under**  
1012 **the baseline scenario without storage or flexible demand. The DIETER RLDC (panel (b)) is constructed by subtracting**  
1013 **hourly generation from hourly load and sorting, with dispatchable generation technologies plotted in order of their**  
1014 **annual average capacity factors. VREs are arranged such that the generation with higher curtailment rate (i.e., solar, in**  
1015 **this case) is on the inside of the graph. To construct the REMIND RLDC (panel (a)), the dispatchable generations are**  
1016 **sorted by their capacity factors and stacked from the bottom. The rectangles depicting dispatchable generation are made**  
1017 **up by the width equal to the full-load-hour and the height equal to the capacity. The top-most lines on either side are**  
1018 **load-duration curves (sorted hourly demand, which is entirely inflexible under this setup). For the purpose of better**  
1019 **visualizations, solar and wind RLDCs are tilted at an angle for REMIND and plotted in the same order as the DIETER**  
1020 **RLDC. For simplicity, in REMIND wind and solar RLDC share the same top pivot point in peak residual demand hour.**

1021  
1022 In net-zero policy with storage and flexible electrolysis demand, comparing dispatch results under both scenarios (Fig. 11 and  
1023 12) for model year 2045, it can be observed that under a stringent emission constraint, the system allocates a significant amount  
1024 of short-term storage to replace the dispatchable generation such as coal and CCGT. Long-term storage such as hydrogen  
1025 electrolysis combined with hydrogen turbines further reduce the capacity factor of remaining OCGT and CCGT. Besides  
1026 storage, there is also a significant amount of deployment of flexible electrolysis demand for producing hydrogen (PtG), which is  
1027 not used in the power sector, but in industry or heavy-duty transport. The use of PtG technologies leverages cheap variable wind  
1028 and solar energy to achieve the goal of sector coupling. By way of storage and PtG, a significant share of the curtailment can be  
1029 utilized (more than 70%), either by shifting the supply to times of low VRE production via storage, or by producing hydrogen  
1030 using surpluses which can be used in other sectors.



1032

1033 **Figure 12: Side-by-side comparison between (a) REMIND and (b) DIETER RLDCs for net-zero by 2045 scenario with**  
 1034 **storage and flexibilized demand for Germany. The storage loading and discharging in DIETER RLDC (panel (b)) is**  
 1035 **constructed by subtracting hourly loading or discharging from hourly inflexible load and sorting. The REMIND RLDC**  
 1036 **(panel (a)) is constructed similar to Fig. 11. The top-most lines on either side are load-duration curves for inflexible**  
 1037 **demand. For better visual comparison, in REMIND solar RLDC starts at 80% of the peak residual demand.**

1038 **5.2.2 Hourly dispatch and power consumptions for typical days in summer and winter**

1039 To more directly inspect the results of the hourly dispatch under various scenarios, we visualize the hourly generation and  
 1040 demand for typical days. Due to the climate in Germany, solar potential is particularly low during winter months. Therefore it is  
 1041 important to observe the periods in both summer and winter.

1042 From the optimal hourly dispatch results of typical days from the coupled model, we observe that compared to baseline (Fig.  
 1043 13a-b), in 2045 for a net-zero year (Fig. 13c-d), there is a significant amount of surplus solar generation in the summer during  
 1044 the day, and some amount of surplus wind generation in the winter during nights and days. Under a net-zero scenario, the  
 1045 generation from fossil fuel plants in the baseline is replaced by battery dispatch (especially in summer) and hydrogen turbines  
 1046 (especially in winter), and the peaker plants, which under baseline are turned on in the summer evening, are partially replaced by  
 1047 solar over-capacity and batteries. A significant share of renewable surplus energy is used for the production of green hydrogen –  
 1048 hydrogen made from zero-carbon electricity. Due to the complete flexibility of electrolyzers, the capture price of hydrogen  
 1049 production is only around  $\frac{1}{3}$  of the average price of electricity (Supplemental Material S2 and Fig. S1 in Supplemental  
 1050 Material).

1051 In winter, hydrogen turbines serve as a baseload for the few days when wind generation is insufficient to meet the demand. To  
 1052 ensure supply during longer winter periods of “renewable droughts” with little wind and solar output, e.g., over a 2-3-day period  
 1053 (hour 540-600 in Fig. 13d), long-term duration storage with hydrogen electrolysis and hydrogen turbines, as well as some  
 1054 dispatchable generation (such as CCGT with CCS and integrated biomass gasification combined cycle) play a major role.

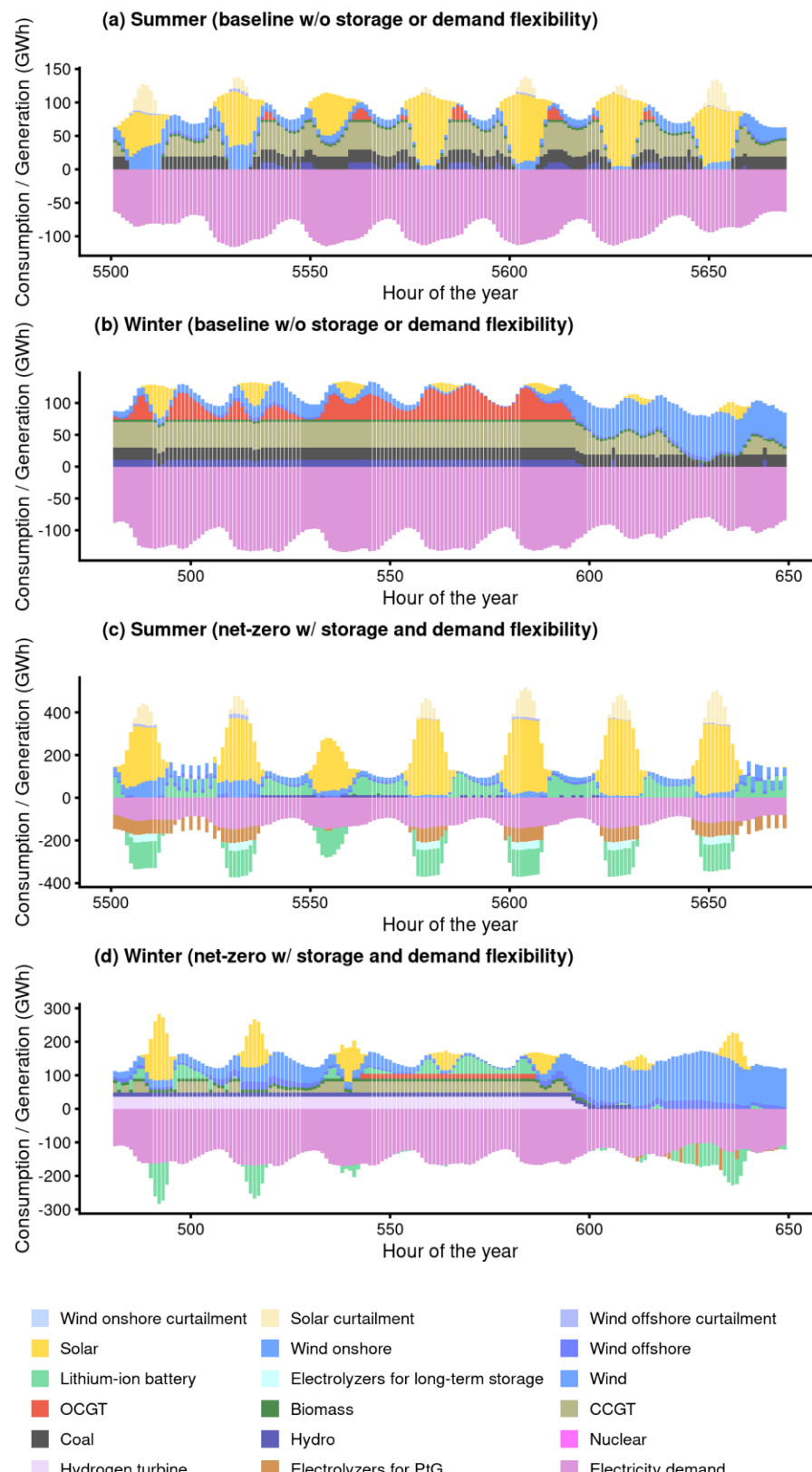


**Figure 13: Comparison of hourly generation (positive) and consumption/storage loading (negative) for a few consecutive typical days in two seasons in Germany in 2045. (a) Summer, under “proof-of-concept” baseline scenario, no storage or flexible demand; (b) Winter, under “proof-of-concept” baseline scenario, no storage or flexible demand; (c) Summer,**

1060 **net-zero scenario, with storage and flexible demand; (d) Winter, net-zero scenario, with storage and flexible demand.**  
1061 **Due to the fact that modern electrolyzers are very flexible, no ramping costs are applied to them in the models, and**  
1062 **therefore some switching behavior between PtG electrolyzers turning on and off can be seen, but it is a minor artifact.**

## 1063 **6 Discussion**

1064 In this section, we discuss the reasons for remaining differences between the coupled models, as well as the assumptions and  
1065 limitations of the soft-coupling.

### 1066 **6.1 Remaining discrepancies**

1067 In all our test runs, at the end of the coupling, it is always the case that the two models cannot be perfectly harmonized, and  
1068 there is a slight residual difference in the convergence results (Section 4). The reason is two-fold.

1069 The first reason is “legacy mismatch”, i.e. a mismatch in brown-field standing capacity constraints in the two models. The  
1070 coupling method we develop here is mostly based on price information for achieving convergence. Therefore, capacity  
1071 constraints that are present in the standalone long-term model but not in the standalone hourly dispatch model need to be  
1072 transferred. These standing capacities are hard to evaluate purely based on economic terms, as they are ultimately a result of  
1073 real-world actions and policies, which might not align with the simplified economic incentives in techno-economic energy  
1074 models. Therefore, the only way this information can be transferred from the “brown-field” model to the “green-field” model is  
1075 by implementing a lower capacity bound in the latter. However, this bound nevertheless might not capture all the shadow prices  
1076 caused by the standing capacities in REMIND. This is ultimately due to the specific generic form of the constraint we  
1077 implemented, i.e. we pass on the pre-investment capacities as a lower bound regardless of technology types. In general, hidden  
1078 “legacy revenues”, which are manifested as the shadow prices of economically less competitive generators in DIETER, such as  
1079 biomass, coal, hydroelectric (solid line lower than bars in Fig. 8), provide incentives for brown-field models to deploy them over  
1080 long-term, but does not provide enough economic case for the green-field model. This results in an observed phenomenon in the  
1081 coupled run, that if these “legacy” capacities and their impact on the costs have not been fully transferred to the green-field  
1082 model, the prices of the green-field model tend to be lower than the coupled brown-field models, causing distortion to the  
1083 convergence of quantities. The effect of legacy mismatch and illustrative test run results are discussed in more detail in  
1084 Supplemental Material S3.

1085 The second reason for the discrepancies at the end of the coupling is that there are actual mismatches in the Lagrangian  
1086 harmonization itself, which can originate from multiple sources. It could due to intertemporal constraints and dynamics (such as  
1087 adjustment costs and brown-field constraints) not linearly reducible to single-year dynamics, resulting in misalignment between  
1088 multi-period REMIND and single-year DIETER. It could be also due to slight numerical inaccuracies of the interest rate  
1089 estimate, which is not explicit in REMIND, but are derived from endogenous and intertemporal consumption. Lastly, there  
1090 could be a mismatch due to a linear fitting of REMIND endogenous time series of fuel costs (biomass, oil, coal, uranium) before  
1091 passing this information to DIETER which might a small amount of mismatch for fuel costs between REMIND and DIETER.

### 1092 **6.2 Limitation of the coupling methodology**

1093 There are limitations to our proposed methodology, both in terms of converging two multiscale power sector models, as well as  
1094 other potential applications of model convergence. Firstly, in terms of the problem presented here – a multiscale power sector  
1095 model coupling, the method derived here is only necessary for a full convergence, but may not be sufficient, i.e. a full  
1096 convergence is not guaranteed. A number of additional factors could prevent a full convergence. One is the “legacy mismatch”

1097 and misalignment in Lagrangian mappings mentioned above in Sect. 6.1. Another factor is the role prefactors play (Sect. 3.3.2,  
1098 Appendix H.2). The prefactors help stabilize the coupling by turning exogenous values obtained from last-iteration DIETER to  
1099 endogenous values in REMIND, such that they can be adjusted to be in line with the optimal mix of current iteration. However,  
1100 they usually contain some small positive or negative parameters that are determined heuristically (e.g.  $b_{y,s}$  in Eq. (H13)). These  
1101 heuristic parameters usually come from rough estimates based on relations between variables in the system and generation  
1102 shares, e.g. how much market value of solar generation will decrease when solar generation share increases by a certain  
1103 percentage. In practice, while the prefactors help stabilize the run and improve convergence speed, choosing the wrong prefactor  
1104 parameters can lead to divergence or instability. Second, another limitation when it comes to modeling power market multiscale  
1105 coupling, is the number of products in the market. In the formulation here, both models describe the general equilibrium of a  
1106 competitive market with one type of homogenous goods, i.e. electricity. However, if we introduce heat as a by-product, such as  
1107 from a combined heat and power plant, then there are two types of goods: heat and electricity. The feasibility of coupling  
1108 models with more than one type of goods/market is not yet explored. Thirdly, there are multiple iterative processes that are  
1109 internal to REMIND, which happen concurrent with the DIETER-REMIND coupled convergence. Among these processes,  
1110 DIETER and the REMIND “Nash” algorithms (for inter-regional trading) both run between the internal REMIND “Nash”  
1111 iterations, which means they are external to the REMIND single-region optimization problems and therefore are soft-linked.  
1112 Nevertheless, in our runs, we observe the power sector convergence to be rather swift and smooth, and happen in parallel to  
1113 other iterative processes, such as the “Nash” algorithm and the CO2 price path algorithm (for climate policy runs). However, a  
1114 systematic monitoring of the multiple internal convergence processes in REMIND during the REMIND-DIETER convergence  
1115 processes under other model setups and configurations is still to be more thoroughly researched.

1116 More generally, the approach developed here – the Lagrangian mapping method for converging two multiscale optimization  
1117 problems – could be useful for a general modeling of market equilibrium of multiple time resolutions. In this study, the  
1118 resolution in the coupled problems is specifically only meant for temporal resolution. However, mathematically speaking,  
1119 coupling models of different spatial resolutions (or both temporal and spatial resolutions) should be very similar. At least in  
1120 theory, the soft-coupling approach developed here should be applicable to increasing the resolution in any arbitrary  
1121 independent/orthogonal dimension of the problem of finding equilibrium market dynamics. In theory, it is also possible to build  
1122 a multi-layer coupled problem architecture, where at each level the low-resolution variables can be disaggregated into finer  
1123 resolution along some dimensions. However, further research is needed to explore the feasibility and convergence performance  
1124 of such schemes.

### 1125 **6.3 Limitation of coupled results**

1126 Since the nature of this study is a proof-of-concept, the scenario results presented should be primarily interpreted as such.  
1127 Nevertheless, it may be useful to enumerate a list of limitation for a more accurate interpretation of the results:

- 1128 1) The power-sector is only coupled for one single global region, i.e. information exchange only occurs for the variables  
1129 of one region – Germany, while all other regions contain the low-resolution version of the power sector of uncoupled  
1130 REMIND. The former coupled one-region result is based on a time series of VRE production today in a world of low to  
1131 medium VRE share and very limited power grid expansion (in 2019). The latter results of the uncoupled regions  
1132 however are parametrized based on results from detailed PSM under a more optimistic assumption of transmission  
1133 build-out, which allows VRE pooling from an expanded EU-wide power grid to smooth out regional weather variations  
1134 (Pietzcker et al., 2017). Note that in standalone REMIND, while by default there are no annual electricity import and  
1135 export imbalances between countries and regions, transmission during the year is implicitly assumed, especially for the

1136 EU region. Comparing the capacity and generation mixes of the coupled and uncoupled runs (Appendix J), we find that  
1137 in the uncoupled case, there are slightly more solar and wind capacities and generations, and much less gas generation  
1138 in the long term. EU-wide transmission expansion would pool both supply and demand variability, thus reducing the  
1139 need for dispatchable capacity for meeting the peak demand.

1140 2) Due to the scope of this study, we implemented a limited set of options on storage and sector coupling technologies in  
1141 this study, and neglected the additional supply-side details for the German power market (such as the reserve market).  
1142 Many potentially significant technological options consisting of pumped hydro storage, compressed-air energy storage,  
1143 vehicle-to-grid, and flexible heat-pumps are not explicitly modeled.

1144 3) Ramping costs for dispatchable generators are not considered, although the effect should be small (Schill et al., 2017).

1145 4) In terms of power transmission and trading inside Germany, we assume a very simple “copperplate” spatial resolution,  
1146 not explicitly modeling transmission bottlenecks inside the region. Currently, the grid capacity equation is parametrized  
1147 to be proportional to pre-curtailment variable renewable generation, and the parametrization is rather optimistic based  
1148 on PSM studies conducted in Pietzcker et al., 2017. As hinted in a recent work by Frysztacki et al., 2022, lower level of  
1149 spatial detail results in an underestimation of constraints present in a real electric system, leading to an underestimation  
1150 of system cost.

1151 5) Near-term events: we have not modeled the current gas and energy crisis in Europe, which is likely to imply an  
1152 overestimation of near-term gas availability in the power sector. Relatedly, we are likely to have overestimated the  
1153 early retirement of coal power plants, which are capped at maximum 9% per year of current capacity early retirement  
1154 rate in REMIND if it is uneconomical relative to cheaper sources of generation. We have included the COVID shock to  
1155 the GDP projection.

1156 6) Only one weather year (2019) is used for the DIETER input data. From the perspective of sufficient power supply  
1157 under all weather conditions with few blackout events, this could introduce an underestimation of the need for reserve  
1158 capacity, storage and demand-side flexibility.

1159 7) Climate impacts under various scenarios on building sector power demand is not included in current version of  
1160 REMIND or its energy demand model for building sector “EDGE-B” (Levesque et al., 2018). Climate extremes such as  
1161 heat waves are not included in either model due to the fact that annual degree days are used which are the results of  
1162 temporal averaging. Representative weather years which maintain the temperature extremes and can represent long-  
1163 term trends are also not used. However, the demand projection does change in a minor way based on SSP scenarios due  
1164 to their different population projections.

1165 8) “Perfect foresight” is assumed under REMIND’s intertemporal optimization over several decades, therefore also  
1166 assumed under the coupled model. There exist many discussions related to the differences between the “ideal world”  
1167 depicted in IAM and energy system modeling on the one hand and “imperfect” but realistic real-world decision making  
1168 and political economy on the other (Ellenbeck and Lilliestam, 2019; Geels et al., 2016; Keppo et al., 2021; Staub-  
1169 Kaminski et al., 2014; Pahle et al., 2022). Considering perfect foresight models such as REMIND dominate IPCC  
1170 model results, it is especially important to understand the differences between the approaches with perfect foresight and  
1171 those without (the so-called “myopic models”). Such work has been carried out in studies such as Fuso Nerini et al.,  
1172 2017; Sitarz et al., 2023. If myopia is introduced in the model, the climate policy exemplified by carbon prices still  
1173 follows an increasing expectation for more and more stringent climate policies, but the trajectory can be less smooth,  
1174 and in the near-term looks more “flat”, hence inducing lock-in effects which slows the transition in the near-term.  
1175 These additional lock-in effects are not modelled in our work here.

1176 9) The resulting power mix is largely due to limited options within the available energy portfolio due to Germany's  
1177 energy policy and natural resources, e.g. the political decision of nuclear and coal capacity phase-out, as well as limited  
1178 hydro and offshore wind potential. In future research, we would like to apply the same method to all global regions.

1179 **6.4 Potential computational barriers under soft-coupling**

1180 Even though via soft-coupling IAM can obtain hourly resolution with only a moderate computational cost increase, it  
1181 nevertheless increases the complexity of the whole problem, increasing the solver time of the IAM, especially before  
1182 convergence is reached under the iteration with a PSM. With additional complexity of endogenous climate policies,  
1183 computational time can be long for scenarios under climate constraint (see Appendix E). This can be potentially overcome by  
1184 several measures, which can be the topics for future research:

- 1185 1) Optimize for computational costs in individual models. Individual IAM and PSM are usually developed incrementally,  
1186 which results over time in less overall computational efficiency. However, because individually the models are not too  
1187 costly to run, there are less incentive to manage computational cost when they are run as standalone models. However,  
1188 when coupled, the computational cost may become a barrier. One of the easiest ways to reduce coupled run time is to  
1189 reduce run times of the individual coupled models. Because the soft-coupling takes many iterations, a small reduction  
1190 in computational time in either model will multiply to give a large reduction in iteratively soft-coupled runs.
- 1191 2) Other internal iterations of the IAM (if they exist) can be optimized. For example, in REMIND, most of the iterations  
1192 (usually 30-50 iterations) in the coupled runs are dedicated to converging inter-regional trade between the 21 regions in  
1193 the model, because DIETER iteration converges usually quite fast (5-10 iterations). By making the algorithm for the  
1194 convergence of inter-regional trade faster, we can reduce total coupled iterations, therefore reducing overall  
1195 computational cost. Less computational time can also be achieved, if DIETER is no longer run together with REMIND  
1196 after DIETER-REMIND iteration convergence is reached, and when trade adjustment (or other internal adjustments in  
1197 REMIND) is small enough to not have substantial impact on the power sector results. This is especially the case if PSM  
1198 gets more complex and its computational time exceeds far more than single-iteration REMIND time (also see Appendix  
1199 E for a comparison of the contributions to runtime due to REMIND internal iteration and due to PSM).
- 1200 3) Limiting endogenous investments of capacities of certain technologies only in one model. For example, in the case of  
1201 electricity transmission, more than one region (e.g. Germany with neighboring European countries) will need to be  
1202 hard-coupled together in the PSM, which naturally increases computational cost of the PSM. But when the solutions are  
1203 passed to the IAM, the regions can again be parallelized, as long as IAM does not engage in the endogenous investment  
1204 of the transmission capacity. Hence the increased cost of computation due to implementing transmission is only limited  
1205 to PSM. This is also the case if within Germany the spatial resolution is increased.
- 1206 4) Only include essential features in PSM. Some PSMs are quite detailed and complicated for the purpose of studying  
1207 specific technologies and the behavior of many agents or users. To couple to IAM, PSM should consider coarse-  
1208 graining or aggregating some details, while retaining the essence of the dynamics being studied. For example, to  
1209 implement smart EV charging (e.g. vehicle-to-grid), modelers of PSM should create a version for coupling which  
1210 aggregates the many time series of charging and discharging of EVs to only one or two time series.

1211 Faster solvers and faster supercomputers will also contribute to improving the computational efficiency of the coupled model.

1212 **7 Conclusion and Outlook**

1213 In this study, we develop a new method of soft-coupling an IAM with a coarse temporal resolution and a PSM with an hourly  
1214 temporal resolution. Our coupling method can be shown both mathematically and in practice to produce a convergence of the  
1215 two systems to a sufficient degree. This method allows the incorporation of the temporal details of variable renewable  
1216 generation explicitly in large-scope IAM modeling frameworks, and increases the accuracy of power sector dynamics in long  
1217 term models. Furthermore, it allows a more explicit modeling of the power sector and sector-coupling, a vision of the energy  
1218 transition where end-use demand sectors such as building, industry and transport make economic use of the generation from  
1219 variable sources by

- 1220 1) directly using the power at the time of production for inflexible form of demand,
- 1221 2) shifting time of power supply via battery and other power storage technology,
- 1222 3) transforming it to another energy carrier or product ahead of time of consumption and at times of surplus wind and  
1223 solar production (e.g. PtG), without conversion back to electricity.

1224 The fully coupled framework allows a more explicit modeling of economic competition of these options under high shares of  
1225 variable renewables, finding more accurate optimal paths under long-term climate scenarios towards a net-zero power sector and  
1226 the wider economy globally. In future research we plan to expand the study in the direction of demand-side management and  
1227 flexibilization, and later possibly in the direction of heat storage.

1228 Coupling DIETER to the global model REMIND for the single region Germany, this study serves as a proof-of-concept. Our  
1229 main innovation is two-fold: we derive convergence theoretically, and show almost full convergence numerically. Theoretically,  
1230 we derive the coupling methodology by mapping the KKT Lagrangians of the simplified versions of the two models. One key  
1231 aspect of the mapping consists of iterative adjustment of the market value (i.e. the annual average revenue of one energy unit of  
1232 generation) or the capture price (i.e. the annual average price of one energy unit of consumption) in the low-resolution IAM  
1233 such that they take on the values as those in the high-resolution PSM. By finding the set of mathematical coupling conditions  
1234 necessary for an iterative convergence as defined by the convergence of both quantities and prices, we could then design the  
1235 coupling interface accordingly, such that at the end of the coupling a joint optimal result can be found.

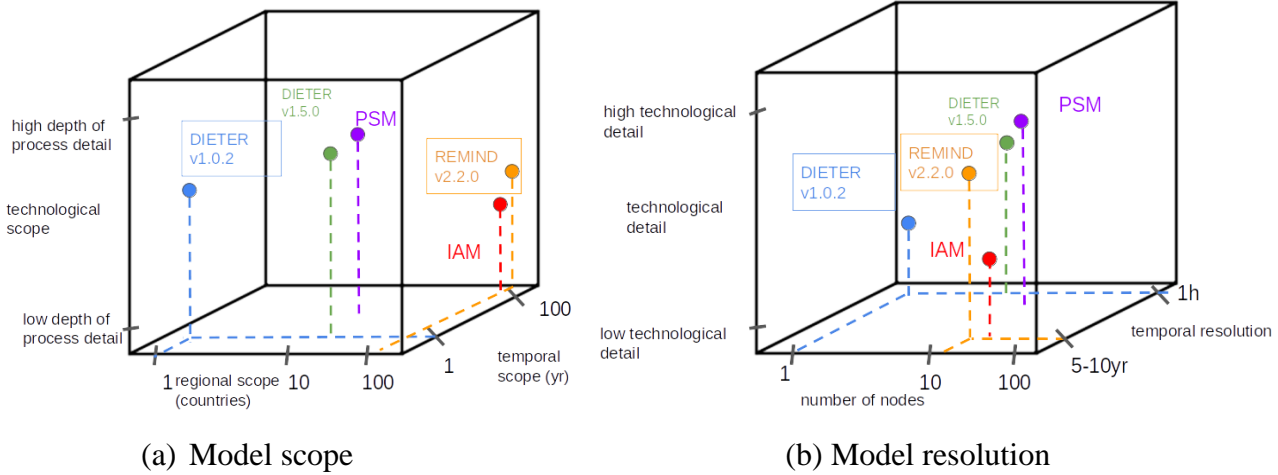
1236 Numerically, we compare the converged results of the two models by examining the long-term power mix (both capacity and  
1237 generation quantities), prices of electricity, as well as generation dispatch (via RLDC), and find good agreement between the  
1238 two models at the end of coupled convergence despite some slight mismatches. For a “proof-of-concept” baseline scenario  
1239 under simple configuration without storage or flexible demand, we could achieve an energy mix with 4.4% tolerance for any  
1240 technology’s absolute share difference in each time step. For a climate policy scenario under a more realistic configuration with  
1241 storage and flexible demand, we could achieve 6-7% tolerance. The cost breakdown and prices of power generations for both  
1242 models are found to be very similar at the end of the iterative process, providing additional evidence that the quantity  
1243 harmonization follows the underlying principle of the price and cost harmonization. The remaining differences can be partially  
1244 explained by the lack of full harmonization of the brown-field and near-term capacity constraints, as well as potential  
1245 mismatches due to numerical techniques aimed at enhancing performance and stability. Using the coupling methodology, we  
1246 provide scenarios for power sector transition under a stringent German climate goal. Under this scenario, we observe a least-cost  
1247 pathway consisting of an almost complete transformation to a wind- and solar-based power system. The results indicate an  
1248 increasing role of storage and dispatchable capacity in a deep decarb scenario, consistent with the findings of previous PSM  
1249 studies, but which is now transferred to the long-term models via soft-coupling.

1250 For future works, besides expanding the research program on sector coupling into a direction containing a broader technological  
1251 portfolio, we also aim to apply this framework to other world regions of interest in the REMIND model. Another important

1252 aspect would be to represent the variability-smoothing effect of transmission grids by using the same coupling framework to  
1253 couple REMIND to other power sector models with more explicit modeling of transmission bottlenecks and expansion for two  
1254 or more regions.

1255 **Appendices**

1256 **Appendix A: Comparison of model scope and specification**



1257

1258 (a) Model scope

(b) Model resolution

1259 **Figure A1: Comparison of resolution and scope for REMIND and a typical IAM, as well as two versions of DIETER**  
1260 (**v1.0.2 is used in this study**) and a typical PSM.

	Model name and version	REMIND v3.0.0 (dev)	DIETER v1.0.2
	model type	IAM	PSM
Scope and resolution	spatial scope	entire globe	single region (Germany)
	intertemporal scope of “perfect foresight”	2005-2100 (in actual model it is 2005-2150)	any year-long period
	temporal resolution	5- or 10-year time-step	hourly (all consecutive hours)
	regional resolution	single EU region	single EU region
	sectoral scope	all energy sectors (transport, building, industry), industrial processes, air pollution, land-use sector, etc	power sector
	available climate policy options	CO2 price, early-phase nuclear and coal phase out (for Germany), EU-ETS	CO2 price
Power sector dynamics	endogenous hourly dispatch	no	yes
	differentiated market value for various technologies	no	yes
	price elasticity of demand	yes	no
	capital cost of technology	endogenous via learning curve (Leimbach et al., 2010)	exogenous
	vintage tracking of existing capital stock	yes	no
	transmission assumption	copper plate within region	copper plate within region
Model code and data specification	programming language	GAMS	GAMS
	input data openness	partially open data	fully open data (for Germany)
	source code openness	open	open
	solver	CONOPT	CPLEX

1261

Table A1: Comparison between the coupled models REMIND and DIETER.

1262

1263

Because IAMs usually start out with certain assumptions for the development of macroeconomic metrics such as for GDP and population, which in turn determine the corresponding energy service levels to a larger degree prior to optimizing the energy system mix to meet demand, they are also frequently referred to as “top-down” energy system models. PSMs usually start out

1266 modeling the fine spatiotemporal detail of the real-world power systems, expanding the capacity installation of power  
1267 generating plants, grid transmission and storage at minimum cost. Such models are also known as “unit commitment models”  
1268 for electrical power production (Padhy, 2004). Later in model development PSMs usually expand to include other energy  
1269 services such as heating and transportation which are electrified. In this way PSMs are also often referred to as “bottom-up”  
1270 models. Reviews and intercomparison of IAMs have been carried out recently where various IAMs are analyzed and  
1271 harmonized (Weyant, 2017; Butnar et al., 2019; Keppo et al., 2021; Wilson et al., 2021; Giarola et al., 2021).  
1272 For methodological reasons, we have to set the length of the model time horizon to be until 2150, which is longer than the valid  
1273 model time horizon until 2100. This is because without the extra years after 2100, the model has much less time to utilize the  
1274 capacities installed in the few decades before 2100, making it more difficult to justify the installation of new capacity  
1275 economically. This is manifested in a model artifact, where in the last few model periods investment in capacities decrease in  
1276 general. By extending the time horizon, this “boundary” effect is pushed further to the future, so the artifact only appears after  
1277 2100. Therefore the meaningful model results for REMIND are only between 2005-2100, even though years until 2150 are also  
1278 modeled and coupled.

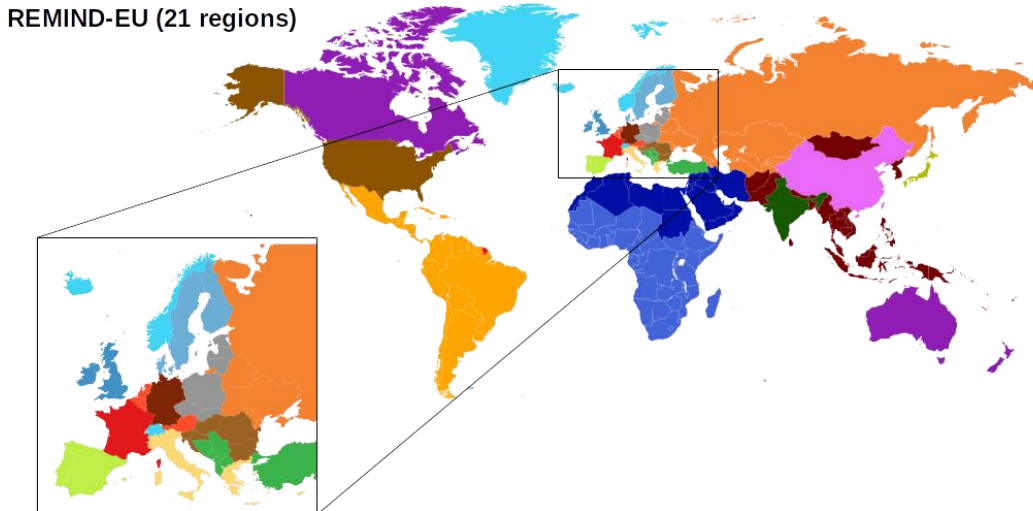
1279 Reviews and intercomparison of typical scopes and resolutions of PSMs can be found in Supplemental Material S5. Comparison  
1280 of more PSMs can be found in Ringkjøb et al. 2018 and Prina et al. 2020.

1281 Both models have open published source code. Partially thanks to the PSM community’s advocacy of “open models”, which  
1282 encompasses all steps from input data, model source code to numerical solvers (openmod - Open Energy Modelling Initiative,  
1283 2022), many research institutions also responded to their calls to openly publish their models. For example, the IAM used in this  
1284 study – REMIND, has for two years opened its source code on popular hosting site GitHub.

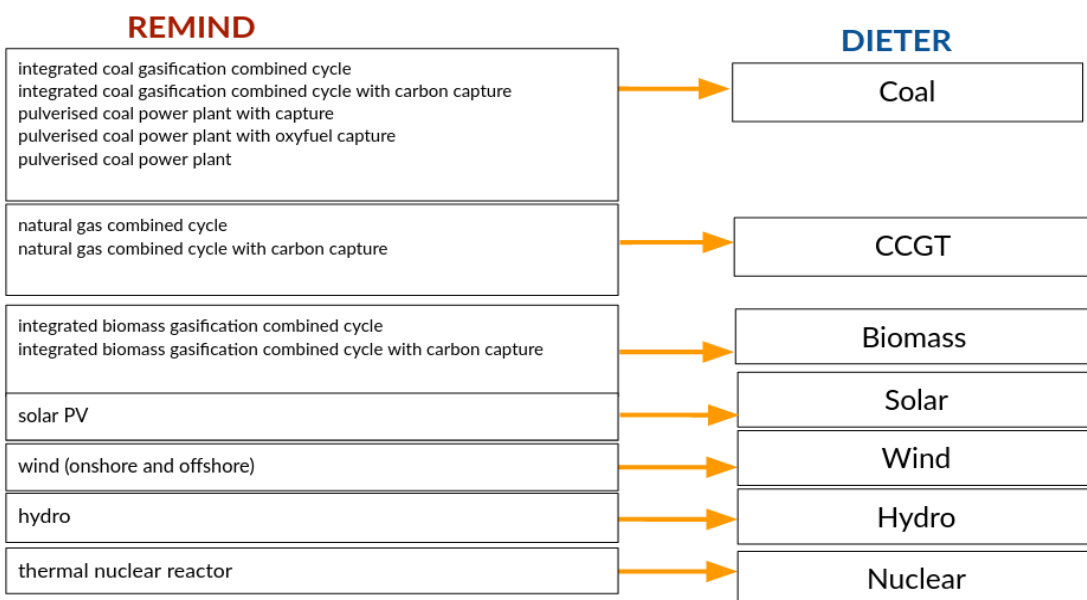
1285

## 1286 **Appendix B: Model coupling scope**

1287 While REMIND and DIETER can both model a European-wide system with spatial subdivision (see Fig. B1 for REMIND  
1288 regional division), the soft-coupling currently is only applied to Germany, in line with the proof-of-concept nature of this study.  
1289 The coupling is from 2020 to 2150 for every defined REMIND period. All common and available REMIND generating  
1290 technologies are enabled for the coupling, as shown in Fig. B2. The information for the species of technologies in REMIND are  
1291 upscaled and coupled to DIETER, whereas information from DIETER is then downscaled during the feedback loop that  
1292 completes the coupled iteration.



1293  
1294 **Figure B1: REMIND regional resolution used in this study (21 global regions, including detailed differentiations of EU**  
1295 **regions). The spatial resolution of REMIND is flexible and depends on the resolution of the input data. Regional**  
1296 **mapping is from the REMIND-EU model (Rodrigues et al., 2022).**



1298  
1299 **Figure B2: Mapping of coupled technologies between REMIND and DIETER.**

1300 **Appendix C: REMIND's interannual intertemporal objective function for single-region**

1301 Single-region interannual intertemporal welfare is an aggregated utility, which in turn is a logarithm function of consumption. In  
1302 REMIND, the total welfare of a region is maximized and is equal to

$$1303 W_{reg} = \sum_{y=2005}^{2150} \frac{1}{(1 + \varrho_{reg})^{y-2005}} * \Delta y * V_{y,reg} * \ln \left( \frac{\chi_{y,reg}}{\Gamma_{y,reg}} \right),$$

1304 where regional consumption is  $\chi_{y,reg}$  at model time  $y$ , and the weight of the consumption determined by the pure rate of time  
1305 preference  $\varrho_{reg}$  and population  $V_{y,reg}$ . The consumption  $\chi_{y,reg}$  at time  $y$  is in turn equal to the difference between regional

1306 income (gross domestic product) minus export (which is not available for consumption) and saving (i.e. investments), subtracted  
 1307 by the cost of the energy system (including the power sector) and other costs in the economy. For simplicity we do not discuss  
 1308 several other expenditures such as capital investment for energy service, other energy related expenditures such as R&D and  
 1309 innovation, taxes, cost of pollution and land-use change.

1310 **Appendix D: Deriving the soft-coupling convergence conditions**

1311 In Sect. 3.2.1, we sketch the derivation procedure and offer a short summary of the analytical results. Here we describe the  
 1312 derivation procedure of the coupled convergence framework in detail.

1313 Using the Lagrangian multiplier method, based on the objective functions (Eqs. (1-2)) and constraints (c1-c6) in Sect. 3.1 we  
 1314 can construct the KKT Lagrangians (Karush, 1939; Kuhn and Tucker, 1951; Gan et al., 2013):

1315 REMIND:

$$\begin{aligned}
 1317 \quad \mathcal{L} = & \underbrace{\sum_{y,s} (c_{y,s} P_{y,s} + o_{y,s} G_{y,s})}_{\text{REMIND objective function}} + \underbrace{\sum_y \lambda_y \left[ d_y - \sum_s G_{y,s} (1 - \alpha_{y,s}) \right]}_{\text{annual electricity balance equation constraint}} + \underbrace{\sum_{y,s} \omega_{y,s} (P_{y,s} - \psi_s)}_{\text{resource constraint}} + \underbrace{\sum_{y,s} \xi_{y,s} (-G_{y,s})}_{\text{positive generation constraint}} \\
 1318 \quad & + \underbrace{\sum_{y,s} \mu_{y,s} (G_{y,s} - 8760 * \phi_{y,s} P_{y,s})}_{\text{maximum generation from capacity constraint}} + \underbrace{\sum_{y \leq 2020, s} \sigma_{y,s} (p_{y,s} - P_{y,s})}_{\text{standing capacity constraint}} + \underbrace{\sum_{y=2025, s} \gamma_{y,s} (P_{y,s} - P_{y-\Delta y, s} - q_{y,s})}_{\text{near-term ramp-up capacity constraint}}, \quad (D1)
 \end{aligned}$$

1316 DIETER:

$$\begin{aligned}
 1319 \quad \underline{\mathcal{L}} = & \underbrace{\sum_s \left[ \underline{c}_s \underline{P}_s + \underline{o}_s \sum_h (\underline{G}_{h,s} + \underline{\Gamma}_{h,vre}) \right]}_{\text{DIETER objective function}} + \underbrace{\sum_h \underline{\lambda}_h \left( \underline{d}_h - \sum_s \underline{G}_{h,s} \right)}_{\text{hourly electricity balance equation constraint}} + \underbrace{\sum_s \underline{\omega}_s (\underline{P}_s - \underline{\psi}_s)}_{\text{resource constraint}} + \underbrace{\sum_{h,s} \underline{\xi}_{h,s} (-\underline{G}_{h,s})}_{\text{positive generation constraint}} \\
 1320 \quad & + \underbrace{\sum_{h,dis} \underline{\mu}_{h,dis} (\underline{G}_{h,dis} - \underline{P}_{dis})}_{\text{maximum dispatchable generation from capacity constraint}} + \underbrace{\sum_{h,vre} \underline{\mu}_{h,vre} (\underline{G}_{h,vre} + \underline{\Gamma}_{h,vre} - \underline{\phi}_{h,vre} \underline{P}_{vre})}_{\text{maximum renewable generation from capacity and weather constraint}}. \quad (D2)
 \end{aligned}$$

1321 Comparing Lagrangians  $\mathcal{L}$  and  $\underline{\mathcal{L}}$ , there are notable similarities between the terms. But first, we can reduce the complexity by  
 1322 noticing that there are terms containing capacity shadow prices that are either trivial or already harmonized: resource constraint  
 1323 shadow prices  $\omega$  are already identical for both models by design (constraint (c2) in Sect. 3.1); positive generation constraint  
 1324 shadow price  $\xi$  is 0 due to KKT conditions for both models (constraint (c3)). These constraint terms can be safely excluded from  
 1325 the subsequent mapping. We then note the important fact that REMIND Lagrangian is a sum over multiple years, whereas  
 1326 DIETER Lagrangian is for each year. To make a direct comparison and therefore mapping possible, we assume that the brown-  
 1327 field and near-term constraints are not binding. After this simplifying assumption, we realize that REMIND becomes linearly  
 1328 independent in terms of the temporal slices, because by now the only yet-to-be-harmonized constraints left in the standalone  
 1329 models are (c1) and (c4), which are both constraints for each year and do not result in temporal correlations. Note that this  
 1330 simplifying assumption is assumed to be valid only for the derivation in this section. Later in actual simulations, we see that  
 1331 these bounds generate shadow prices which are not necessarily small, impacting the degree of convergence especially in earlier  
 1332 years. These constraints are also temporally localized in early periods, exerting little impact on later, more “green-field” years.  
 1333 In fact, when including brown-field constraint into DIETER (c8), the model convergence is improved (Sec. 6.1).  
 1334 After the aforementioned simplifications, we can construct a single-year REMIND Lagrangian  $\mathcal{L}_y$ :

$$1335 \quad \mathcal{L}_y = \underbrace{\sum_s (c_{y,s} P_{y,s} + o_{y,s} G_{y,s})}_{\text{REMIND objective function}} + \underbrace{\lambda_y \left[ d_y - \sum_s G_{y,s} (1 - \alpha_{y,s}) \right]}_{\text{annual electricity balance equation constraint}} + \underbrace{\sum_s \mu_{y,s} (G_{y,s} - 8760 * \phi_{y,s} P_{y,s})}_{\text{maximum generation from capacity constraint}}, \quad (D3)$$

1336 and map it to the single-year DIETER Lagrangian  $\underline{\mathcal{L}}$ :

$$\begin{aligned}
 1337 \quad \underline{\mathcal{L}} = & \underbrace{\sum_s [c_s \underline{P}_s + o_s \sum_h (\underline{G}_{h,s} + \underline{\Gamma}_{h,vre})]}_{\text{DIETER objective function}} + \underbrace{\sum_h \lambda_h (\underline{d}_h - \sum_s \underline{G}_{h,s})}_{\text{hourly electricity balance equation constraint}} + \underbrace{\sum_{h,dis} \mu_{h,dis} (\underline{G}_{h,dis} - \underline{P}_{dis})}_{\text{maximum dispatchable generation from capacity constraint}} \\
 1338 \quad & + \underbrace{\sum_{h,vre} \mu_{h,vre} (\underline{G}_{h,vre} + \underline{\Gamma}_{h,vre} - \underline{\phi}_{h,vre} \underline{P}_{vre})}_{\text{maximum renewable generation from capacity and weather constraint}}.
 \end{aligned} \tag{D4}$$

1339 These are the same as Eqs. (3)-(4).

1340 Comparing  $\mathcal{L}_y$  and  $\underline{\mathcal{L}}$ , we can map them by matching the following four terms in the Lagrangians individually:

- 1341 A) annual total power sector costs:  $Z_y = \sum_s (c_{y,s} P_{y,s} + o_{y,s} G_{y,s})$  and  $\underline{Z} = \sum_s [c_{y,s} \underline{P}_{y,s} + o_{y,s} \sum_h (\underline{G}_{y,h,s} + \underline{\Gamma}_{y,h,vre})]$ ,
- 1342 B) annual revenue of usable (post-curtailment) generation for each generator  $s$ :  $\lambda_y G_{y,s} (1 - \alpha_{y,s})$  and  $\sum_h \lambda_{y,h} \underline{G}_{y,h,s}$ ,
- 1343 C) annual payment made by the consumers:  $\lambda_y d_y$  and  $\sum_h \lambda_{y,h} \underline{d}_{y,h}$ ,
- 1344 D) maximum generation from capacity constraint term for each generator  $s$ :  $\mu_{y,s} (G_{y,s} - 8760 * \phi_{y,s} P_{y,s})$  and

1345  $\sum_h \mu_{y,h,s} (\underline{G}_{y,h,s} + \underline{\Gamma}_{y,h,s} - \underline{\phi}_{y,h,s} \underline{P}_{y,s})$  (we write the two terms for VRE and dispatchable into one term for DIETER here

1346 for simplicity, i.e.  $\underline{\Gamma}_{y,h,dis} = 0$  and  $\underline{\phi}_{y,h,dis} = 1$  for dispatchables).

1347 The following conditions (h1-h7) can be derived from the harmonization of terms (A)-(D). Each term is harmonized by  
1348 matching the values in front of decision variables at the aggregated levels, namely capacities and annual generations.

1349 Term A) can be mapped if:

1350 **h1)** annual fixed costs are harmonized for each generator species  $s$ :  $c_{y,s} = \underline{c}_{y,s}$ ,

1351 **h2)** annual variable costs are harmonized for each generator species  $s$ :  $o_{y,s} = \underline{o}_{y,s}$ .

1352 Term B) can be mapped if:

1353 **h3)** for each generator species  $s$ , the annual average revenue per unit generation, i.e. the market value, is harmonized by  
1354 exogenously manipulating the market value in REMIND to be the same as the last-iteration annual average market value in  
1355 DIETER. We achieve this by adding a correction term, thereby modifying REMIND original objective function  $Z$  to  $Z'$ :

$$1356 \quad Z' = Z - \sum_{y,s} \eta_{y,s} (i-1) G_{y,s} (1 - \alpha_{y,s}),$$

1357 where  $\eta_{y,s} (i-1)$  is the markup for technology  $s$  in DIETER in the last iteration  $i-1$ ,  $i$  is the index of the iteration of the  
1358 iterative soft-coupling.  $Z'$  is the modified REMIND objective function in the coupled version.

1359 The detailed derivation is as follows.

1360 Lagrangian term B for the models have the physical meanings of total annual revenue of usable (post-curtailment)  
1361 generation. (Annual revenue is equal to the product of usable generation and annual market value.) We denote total annual  
1362 revenue from technology  $s$  as  $\theta_{y,s}$  for REMIND and  $\underline{\theta}_{y,s}$  for DIETER. Then for REMIND the revenue (term B) is

$$1363 \quad \theta_{y,s} = \lambda_y G_{y,s} (1 - \alpha_{y,s}), \tag{D5}$$

1364 and for DIETER

$$1365 \quad \underline{\theta}_{y,s} = \sum_h \lambda_{y,h} \underline{G}_{y,h,s}. \tag{D6}$$

1366 To harmonize terms  $\theta_{y,s}$  and  $\underline{\theta}_{y,s}$ , our goal is to create a one-to-one mapping of the values in front of the decision variable  
1367 annual aggregated post-curtailment generation of technology  $s$ , which is  $G_{y,s} (1 - \alpha_{y,s})$  for REMIND and  $\sum_h \underline{G}_{y,h,s}$  for  
1368 DIETER, the latter is namely a direct sum of the hourly generations. However, we notice for DIETER revenue  $\underline{\theta}_{y,s}$  is a  
1369 weighted sum of the hourly generation, and the direct sum cannot be separated in a straight-forward way. So first we have  
1370 to rewrite  $\underline{\theta}_{y,s}$  (Eq. (D6)) by first dividing then multiplying by the aggregated annual generation:

$$1373 \quad \underline{\theta}_{y,s} = \frac{\sum_h \underline{\lambda}_{y,h} \underline{G}_{y,h,s}}{\sum_h \underline{G}_{y,h,s}} \sum_h \underline{G}_{y,h,s}. \quad (D7)$$

1371 We notice that the multiplicative term in front of the DIETER annual aggregated generation  $\sum_h \underline{G}_{y,h,s}$  is  $\frac{\sum_h \underline{\lambda}_{y,h} \underline{G}_{y,h,s}}{\sum_h \underline{G}_{y,h,s}}$ , which  
1372 is nothing other than the market value of generation technology  $s$  (see also Eq. (F24)).

1374 We now take a look at revenue  $\underline{\theta}_{y,s}$  on the REMIND side, which is equal to  $\lambda_y G_{y,s} (1 - \alpha_{y,s})$  (Eq. (D5)). To map (D5) to  
1375 the DIETER revenue term  $\underline{\theta}_{y,s}$  (Eq. (D7)) in terms of the aggregated decision variable  $G_{y,s} (1 - \alpha_{y,s})$  and  $\sum_h \underline{G}_{y,h,s}$ , we  
1376 essentially would like the multiplicative term in front of the generation variable in  $\underline{\theta}_{y,s}$ , which is  $\lambda_y$ , to be also  $\frac{\sum_h \underline{\lambda}_{y,h} \underline{G}_{y,h,s}}{\sum_h \underline{G}_{y,h,s}}$   
1377 like in DIETER. This means the DIETER-corrected revenue in REMIND *should* be

$$1382 \quad \underline{\theta}'_{y,s} = \frac{\sum_h \underline{\lambda}_{y,h} \underline{G}_{y,h,s}}{\sum_h \underline{G}_{y,h,s}} G_{y,s} (1 - \alpha_{y,s}). \quad (D8)$$

1388 To harmonize  $\underline{\theta}_{y,s}$  and  $\underline{\theta}'_{y,s}$ , we can simply add a linear correction term to compensate for the difference between them.

1379 Noticing in Eq. (D5), the multiplicative term in front of the REMIND generation variable  $G_{y,s} (1 - \alpha_{y,s})$  is  $\lambda_y$ , which can  
1380 be interpreted as the REMIND market value, we realize essentially for a linear correction term, we should add the market  
1381 value difference  $\Delta MV_{y,s}$  between the two models

$$1383 \quad \Delta MV_{y,s} = \underline{MV}_s - MV_s = \frac{\sum_h \underline{\lambda}_{y,h} \underline{G}_{y,h,s}}{\sum_h \underline{G}_{y,h,s}} - \lambda_y, \quad (D9)$$

1384 to the multiplicative term  $\lambda_y$  in  $\underline{\theta}_{y,s}$ , so  $\lambda_y$  is canceled. Note that in Eq. (D9), as discussed before, the DIETER market  
1385 value is dependent on technology index  $s$ , whereas the REMIND one does not.

1386 After adding the linear correction term, the modified revenue in REMIND  $\underline{\theta}'_{y,s}$  after harmonization is:

$$1387 \quad \underline{\theta}'_{y,s} = \underline{\theta}_{y,s} + \Delta MV_{y,s} G_{y,s} (1 - \alpha_{y,s}) = (\Delta MV_{y,s} + \lambda_y) G_{y,s} (1 - \alpha_{y,s}), \quad (D10)$$

1388 plugging in (D9),

$$1389 \quad \underline{\theta}'_{y,s} = \left( \frac{\sum_h \underline{\lambda}_{y,h} \underline{G}_{y,h,s}}{\sum_h \underline{G}_{y,h,s}} - \lambda_y + \lambda_y \right) G_{y,s} (1 - \alpha_{y,s}) = \frac{\sum_h \underline{\lambda}_{y,h} \underline{G}_{y,h,s}}{\sum_h \underline{G}_{y,h,s}} G_{y,s} (1 - \alpha_{y,s}), \quad (D11)$$

1390 which is as desired in (D8).

1391 In practice, in the case of annual shadow price  $\lambda_y$  in REMIND, we find that the coupling behaves more stable numerically,  
1392 if we use the annual average electricity price of DIETER instead of the last-iteration electricity price of REMIND  $\lambda_y$  in  
1393 (D9). The equivalence between the two prices is expressed later in (h5). We can use this substitution, since as we show  
1394 later that (h5) can be derived from market value harmonization (h3) and demand harmonization (h4). With this  
1395 substitution, the correction term which we call  $\underline{\eta}_{y,s}$  is in fact:

$$1396 \quad \underline{\eta}_{y,s} = \underline{MV}_s - \underline{J} = \frac{\sum_h \underline{\lambda}_{y,h} \underline{G}_{y,h,s}}{\sum_h \underline{G}_{y,h,s}} - \frac{\sum_h \underline{\lambda}_{y,h} \underline{d}_{y,h}}{\sum_h \underline{d}_{y,h}}, \quad (D12)$$

1397 where  $\underline{J} = \frac{\sum_h \underline{\lambda}_{y,h} \underline{d}_{y,h}}{\sum_h \underline{d}_{y,h}}$  is the annual average electricity price in DIETER. We calculate (D12) using the last iteration  
1398 DIETER solutions. Note that compared to the earlier (D9), we have simply replaced the second term REMIND annual  
1399 price with DIETER annual price.

1400 It is not hard to recognize  $\underline{\eta}_{y,s}$  as the “markup” for technology  $s$  in DIETER, where markup as defined before is the  
1401 difference between the market value of a technology  $\underline{MV}_s$  and the load-weighted annual average electricity price  $\underline{J}$  (see  
1402 Sect. 3.1 introduction).

1403 Now we have concluded the derivation for the markup term  $\underline{\eta}_{y,s}$  in (h3).

1404 Although the multiplicative terms in front of decision variables in the two models can be harmonized via the correction  
 1405 term (D12), we notice that it contains endogenous values, i.e. hourly generation  $\underline{G}_{y,h,s}$  and hourly shadow price  $\underline{\lambda}_{y,h}$  in  
 1406 DIETER. Since any endogenous value can only be known ex post, this means the Lagrangian mapping relies on  
 1407 endogenous values from the last iteration, i.e.

$$1408 \underline{\eta}_{y,s}(i-1) = \underline{M}_{y,s}(i-1) - \underline{J}(i-1) = \frac{\sum_h \underline{\lambda}_{y,h}(i-1) \underline{G}_{y,h,s}(i-1)}{\sum_h \underline{G}_{y,h,s}(i-1)} - \frac{\sum_h \underline{\lambda}_{y,h}(i-1) \underline{d}_{y,h}(i-1)}{\sum_h \underline{d}_{y,h}(i-1)}.$$

1409 Now, using the markup term  $\underline{\eta}_{y,s}$ , we define the linear correction term for the revenue in REMIND  $\theta_{y,s}$  as

$$1410 \Delta\theta_{y,s} = \underline{\eta}_{y,s}(i-1) G_{y,s}(1 - \alpha_{y,s}).$$

1411 The physical meaning of  $\Delta\theta_{y,s}$  is the revenue difference in the two models for technology  $s$ , given that the post-  
 1412 curtailment generations are expressed in terms of REMIND variables.

1413 The coupled REMIND has a modified objective function  $Z'$  based on a linear correction. The correction term  $\Delta\theta_{y,s}$  need to  
 1414 be summed over  $s$  and  $y$  and subtracted – due to the negative sign in front of term B, from the REMIND objective function  
 1415  $Z$ , since the objective term as a part of the Lagrangian can be directly manipulated:

$$1416 Z' = Z - M = Z - \sum_{y,s} \Delta\theta_{y,s} = Z - \sum_{y,s} \underline{\eta}_{y,s}(i-1) G_{y,s}(1 - \alpha_{y,s}),$$

1417 where we call the total system revenue differences  $M$ , again, these are revenues where the post-curtailment generations are  
 1418 expressed in terms of REMIND variables (and not DIETER variables).

1419 Now we have concluded the derivation for the convergence condition (h3).

1420 Depending on the starting point of the REMIND power system, and due to the internal iterative changes of REMIND  
 1421 results due to the adjustments in trade between regions during the “Nash” algorithm, coupled convergence usually can only  
 1422 be achieved over multiple iterations. Therefore the derived markup equation (Eq. (D12)) in general can be only expected to  
 1423 reflect the actual market value differences approximately in the two models. This is the reason that in the iterative  
 1424 algorithm after the first iteration, we add  $M(i) - M(i-1)$  to the objective function  $Z$ , as the quantities and prices  
 1425 gradually converge between the two models. As convergence is approached, the total revenue difference between iteration  
 1426  $M(i) - M(i-1)$  should go to zero. This is confirmed by the numerical experiments (not shown).

1427 Term C) can be mapped if:

1428 **h4)** annual power demand in the two models are harmonized:  $d_y = \sum_h \underline{d}_{y,h}$  ,

1429 **h5)** annual average price of electricity is mapped to each other  $\lambda_y = \frac{\sum_h \underline{\lambda}_{y,h} \underline{d}_{y,h}}{\sum_h \underline{d}_{y,h}}$  (dividing term (C) by (h4)). Because

1430 electricity price is by definition equal to total annual system revenue divided by total annual demand, (h5) can be shown to  
 1431 hold true, given technology-specific revenues are harmonized in (h3) and demand are harmonized in (h4). (If technology-  
 1432 specific revenues are harmonized in (h3), then the system revenues which are technology-specific revenues summed over  
 1433 technologies are also harmonized.) (h5) therefore can be seen as a derived condition from (h3) and (h4).

1434 Term D) can be mapped if:

1435 **h6)** annual average capacity factors are harmonized, i.e.  $\phi_{y,s}$  in REMIND is set to equal to the endogenous last-iteration  
 1436 DIETER result for each generation type  $s$ :

$$1437 \phi_{y,s} = \sum_h \underline{\phi}_{y,h,s} / 8760 ,$$

1438 where  $\underline{\phi}_{y,h,s} = \frac{G_{y,h,s}}{P_{y,s}}$  is the hourly capacity factor in DIETER. Without explicit manipulation of the shadow prices  $\mu_{y,s}$  and  
 1439  $\underline{\mu}_{y,h,s}$ , we show the following claim is true, i.e. by above capacity factor harmonization, the terms containing endogenous  
 1440 shadow prices will be automatically mapped. Showing this requires careful mathematical argument, which we make in  
 1441 detail in the case of dispatchable, and later argue the case is similar for renewable.

1442 For dispatchable generators the argument is as follows. (For simplicity we use the generic index  $s$ .)

1443 We first rewrite REMIND term D by plugging in the harmonization condition  $\phi_{y,s} = \sum_h \underline{\phi}_{y,h,s} / 8760$ :

$$1444 \mu_{y,s} (G_{y,s} - 8760 * \phi_{y,s} P_{y,s}) = \sum_y \mu_{y,s} \left( G_{y,s} - \sum_h \underline{\phi}_{y,h,s} P_{y,s} \right),$$

1445 and it should be mapped to the term  $\sum_y \underline{\mu}_{y,h,s} \left( \underline{G}_{y,h,s} - P_{y,s} \right)$  in DIETER.

1446 Splitting the two terms, these four terms need to be harmonized:

$$1447 \mu_{y,s} G_{y,s} \quad \text{and} \quad \sum_h \underline{\mu}_{y,h,s} \underline{G}_{y,h,s} \quad (D13)$$

$$1448 \mu_{y,s} \sum_h \underline{\phi}_{y,h,s} P_{y,s} \quad \text{and} \quad \sum_h \underline{\mu}_{y,h,s} P_{y,s} \quad (D14)$$

1449 for all  $y, s$ .

1450 To show the mappings (D13)-(D14) are automatically satisfied given (h6), we first consider two simplified power sector  
 1451 toy problems, Q1 and Q2, with only dispatchable technologies. Both problems have identical objective functions  $\tilde{Z} =$   
 1452  $\sum_s (\tilde{c}_s \tilde{P}_s + \tilde{o}_s \tilde{G}_s)$ , and the fixed and variable cost parameters  $\tilde{c}_s$  and  $\tilde{o}_s$  are identical. Both problems have identical hourly  
 1453 balance equation constraint, but with two different kinds of maximum generation constraint, Q1 has an inequality  
 1454 constraint for each hour, Q2 has an aggregated annual equality constraint:

$$1455 \text{Q1: } \min Z, \text{ s.t. } \tilde{G}_{h,s} \leq \tilde{P}_s \perp \tilde{\mu}_{h,s}, \tilde{d}_h = \sum_s \tilde{G}_{h,s} \perp \tilde{\lambda}_h$$

$$1456 \text{Q2: } \min Z, \text{ s.t. } \sum_h \tilde{G}_{h,s} = 8760 * \tilde{\phi}_s \tilde{P}_s \perp \tilde{\mu}'_s, \tilde{d}_h = \sum_s \tilde{G}_{h,s} \perp \tilde{\lambda}'_h$$

1457 Then the Lagrangians are:

$$1458 \tilde{\mathcal{L}}_1 = \underbrace{\sum_s \left( \tilde{c}_s \tilde{P}_s + \tilde{o}_s \sum_h \tilde{G}_{h,s} \right)}_{\text{objective function}} + \underbrace{\sum_h \tilde{\lambda}_h \left( \tilde{d}_h - \sum_s \tilde{G}_{h,s} \right)}_{\text{hourly electricity balance equation constraint}} + \underbrace{\sum_{h,s} \tilde{\mu}_{h,s} \left( \tilde{G}_{h,s} - \tilde{P}_s \right)}_{\text{maximum generation from capacity constraint}}$$

$$1459 \tilde{\mathcal{L}}_2 = \underbrace{\sum_s \left( \tilde{c}_s \tilde{P}_s + \tilde{o}_s \sum_h \tilde{G}_{h,s} \right)}_{\text{objective function}} + \underbrace{\sum_h \tilde{\lambda}'_h \left( \tilde{d}_h - \sum_s \tilde{G}_{h,s} \right)}_{\text{hourly electricity balance equation constraint}} + \underbrace{\sum_s \tilde{\mu}'_s \left( \sum_h \tilde{G}_{h,s} - 8760 \tilde{\phi}_s \tilde{P}_s \right)}_{\text{maximum generation from capacity constraint}}.$$

1460 The relevant KKT conditions:

1461 Stationarity condition for Q1:

$$1462 \frac{\partial \tilde{\mathcal{L}}_1}{\partial \tilde{P}_s} = \tilde{c}_s - \sum_h \tilde{\mu}_{h,s} = 0 \quad (D15)$$

1463 Stationarity condition for Q2:

$$1464 \frac{\partial \tilde{\mathcal{L}}_2}{\partial \tilde{P}_s} = \tilde{c}_s - 8760 \tilde{\phi}_s \tilde{\mu}'_s = 0 \quad (D16)$$

1465 Since the fixed cost  $\tilde{c}_s$  are equal for the two models, from Eqs. (D15)-(D16) we can derive the relation between the two  
 1466 shadow prices:

$$1467 8760 * \tilde{\phi}_s \tilde{\mu}'_s = \sum_h \tilde{\mu}_{h,s}. \quad (D17)$$

1468 Note that for the toy models, the identical balance equation constraints do not contain capacity  $P$ , which is why the balance  
 1469 equation constraints do not influence the stationary conditions for  $P$  (Eqs. (D15)-(D16)).

1470 We now show (D14) is automatically mapped given capacity factor harmonization (h6). We first write the equality  
 1471 condition for the REMIND-DIETER case, analogous to the toy model result (D17),

$$1472 8760 * \phi_{y,s} \mu_{y,s} = \sum_h \underline{\mu}_{y,h,s} \quad . \quad (D18)$$

1473 Note that we can apply the toy model case to the REMIND-DIETER coupling case in rather straight-forward way, because  
 1474 in the case of REMIND-DIETER, the objective function terms have been already harmonized by (h1)-(h2), and the balance  
 1475 equation constraint terms do not contain  $P$ , so they have no bearing on the generation-capacity constraint term, just like in  
 1476 the case of the toy models.

1477 Plugging (h6)  $\phi_{y,s} = \sum_h \underline{\phi}_{y,h,s} (i - 1) / 8760$  into (D18), we have derived the equality for the parameter mapping required  
 1478 in (D14), i.e.,

$$1479 \mu_{y,s} \sum_h \underline{\phi}_{y,h,s} (i - 1) = \sum_h \underline{\mu}_{y,h,s} .$$

1480 To show (D13), we first use hourly capacity factor from DIETER,

$$1481 \underline{G}_{y,h,s} = \underline{\phi}_{y,h,s} \underline{P}_{y,s} , \quad (D19)$$

1482 as well as the primal feasibility condition from REMIND  $G_{y,s} = 8760 * \phi_{y,s} P_{y,s}$  (Eq. (F9)), to rewrite both sides of the  
 1483 mapping in (D13) in capacity terms. For REMIND, plugging in (F9),

$$1484 \mu_{y,s} G_{y,s} = \mu_{y,s} * 8760 * \phi_{y,s} P_{y,s} , \quad (D20)$$

1485 and for DIETER, plugging in (D19),

$$1486 \sum_h \underline{\mu}_{y,h,s} \underline{G}_{y,h,s} = \sum_h \underline{\mu}_{y,h,s} \underline{\phi}_{y,h,s} \underline{P}_{y,s} . \quad (D21)$$

1487 Take the complementary slackness condition of DIETER  $\underline{\mu}_{h,s} (\underline{G}_{h,s} - \underline{P}_s) = 0$  (Eq. (F16)), insert (D19) on the left-hand-  
 1488 side, we obtain

$$1489 \underline{\mu}_{h,s} (\underline{G}_{h,s} - \underline{P}_s) = \underline{\mu}_{h,s} (\underline{\phi}_{y,h,s} \underline{P}_{y,s} - \underline{P}_s) = 0 .$$

1490 Rearranging, we get

$$1491 \underline{\mu}_{y,h,s} \underline{\phi}_{y,h,s} \underline{P}_s = \underline{\mu}_{y,h,s} \underline{P}_s , \quad (D22)$$

1492 for each hour  $h$ .

1493 Plug (D22) and then (D18) into the right-hand-side of (D21), to obtain

$$1494 \sum_h \underline{\mu}_{y,h,s} \underline{G}_{y,h,s} = \sum_h \underline{\mu}_{y,h,s} \underline{P}_{y,s} = 8760 * \phi_{y,s} \mu_{y,s} \underline{P}_{y,s} . \quad (D23)$$

1495 Compare (D20) with (D23), they now have identical parameters in front of the capacity variable  $P_{y,s}$  and  $\underline{P}_{y,s}$ , as desired.

1496 We concluded the proof that by exogenously setting the annual capacity factor of REMIND to that of the last iteration  
 1497 DIETER, we automatically harmonize the generation-capacity constraint term of the Lagrangian, in the case of  
 1498 dispatchable generators.

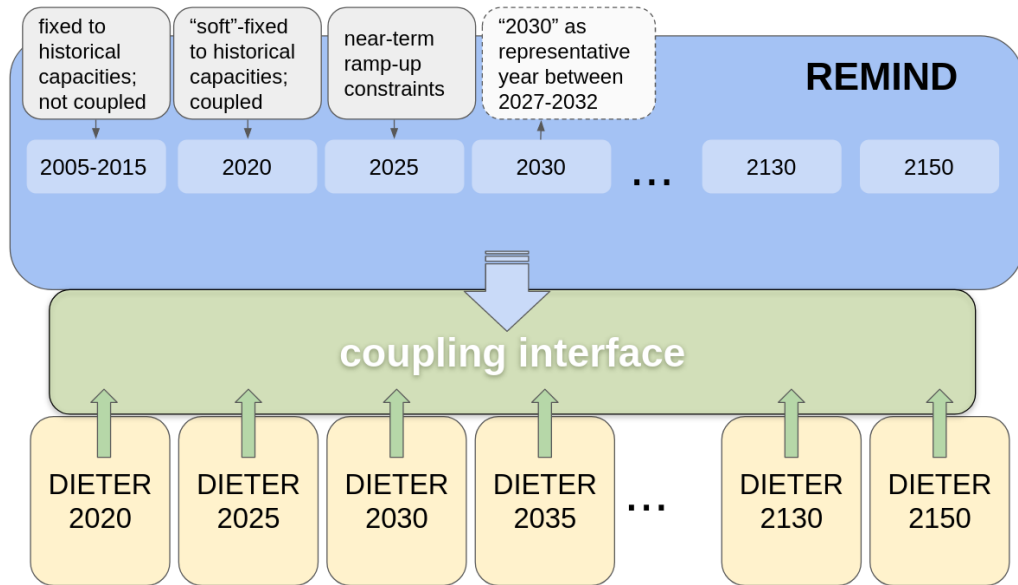
1499 **h7)** for VRE, annual curtailment rates are harmonized  $G_{y,vre} \alpha_{y,vre} = \sum_h \underline{I}_{y,h,vre}$ , i.e. by exogenously setting curtailment rate  
 1500 in REMIND  $\alpha_{y,vre} = \sum_h \underline{I}_{y,h,vre} (i - 1) / G_{y,vre}$ , taking the endogenously determined curtailed power  $\underline{I}_{y,h,vre}$  from the last  
 1501 iteration DIETER. This in general also harmonizes terms other than term D, as it harmonizes the definition for generation  
 1502 variable in DIETER which is post-curtailment and REMIND definition for generation variable which is pre-curtailment.  
 1503 For VREs the derivation is conceptually similar to the above case for dispatchable in (h6), since we can define a real  
 1504 capacity factor (post-curtailment) similar to the capacity factor for the dispatchable generators above,  
 1505  $\underline{\phi}_{y,h,vre} = \underline{G}_{y,h,vre} / \underline{P}_{vre}$ .

1506 Due to the limitations of this paper, we will not present the derivation here. A detailed derivation is available upon request.

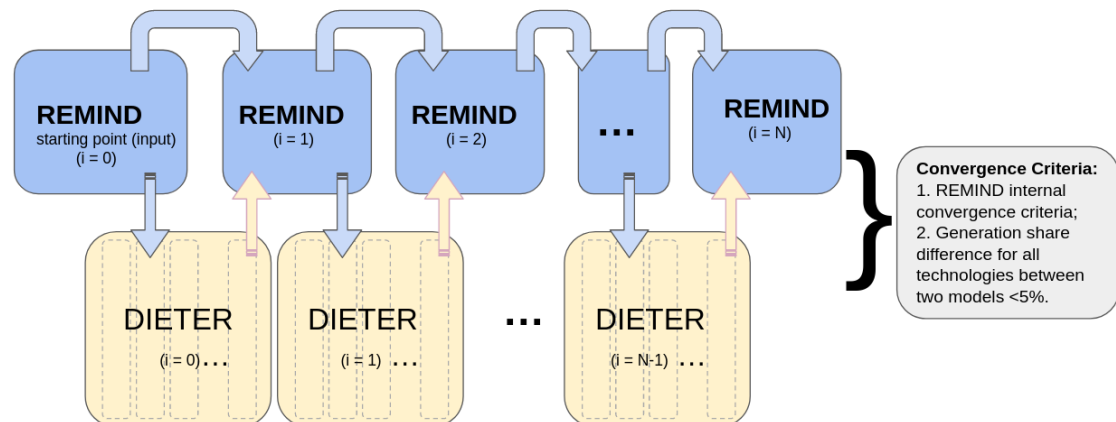
1507 **Appendix E: Coupling iteration schematics**

1508 Coupled region: Germany

1509 Coupled REMIND time horizon: 2020-2150 (2010-2015 are not coupled since they are historical years and have mostly hard-  
1510 fixed quantities)



1511  
1512 (a) Graphic illustration of the bi-directional coupling in the temporal dimension.



1513

1514 (b) Graphic illustration of the bi-directional coupling in the iteration dimension.

1515 Figure E1: A graphic description of the model iterative coupling. (a) The temporal slices of REMIND which are mapped  
1516 to multiple parallel year-long DIETER problems are illustrated here. The convergence conditions are iteratively mapped  
1517 at the interface. (b) Every  $i$ -th iteration of REMIND takes the  $(i-1)$ -th iteration of REMIND as a starting point for  
1518 optimization, and the endogenous output of the  $(i-1)$ -th DIETER as exogenous input parameters. When the convergence  
1519 conditions are met, i.e. REMIND satisfies its internal convergence condition, and the coupled models differ in their  
1520 generation share of each technology at most by a certain percentage (e.g. 5% for baseline run without storage), the  
1521 coupled run halts.

1522

1523 Under simple configuration (no storage, no flexible demand), every REMIND run takes around 3 minutes and DIETER run  
1524 takes a few seconds to solve. Under more detailed configurations (with storage and flexible demand) and climate policies, every

1525 REMIND run takes around 4 minutes and a DIETER run takes a few minutes to solve. The entire REMIND-DIETER coupled  
 1526 run for a single region Germany under simple configuration is around 3~4 hours. It is around 6~10 hours for the more detailed  
 1527 configurations under climate policies.

1528 **Appendix F: Derivation of the equilibrium conditions for uncoupled REMIND and DIETER**

1529 In this appendix, we discuss the equilibrium conditions of the uncoupled models, resulting in a rigorous formulation of the so-  
 1530 called “zero-profit rules” (ZPRs). We first construct the Lagrangians and compute KKT conditions, then derive the ZPRs for the  
 1531 standalone versions of REMIND reduced power-sector model and DIETER model.

1532 Using the objective functions and constraints in Sect. 3.1, we can construct Lagrangians for the two standalone models. Using  
 1533 the KKT conditions derived from the Lagrangians, we can show that if the historical and resource constraint are non-binding,  
 1534 i.e. shadow prices  $\omega$ ,  $\sigma$  and  $\gamma$  are zero, then each generator would have recovered their fixed, variable cost and curtailment cost  
 1535 through their total market revenue, i.e. each producer of electricity gets “zero profit”, given that the profits are defined as the  
 1536 difference between revenue and cost. When the capacity constraints exist and are binding, we arrive at a modified version of the  
 1537 original ZPR, which describes the relation between cost, revenue and the capacity shadow prices.

1538 Here we first construct the Lagrangians and derive the KKT conditions from them (Sect. F.1) for both models. Then both  
 1539 models’ ZPRs are derived, two for each model, namely, the technology-specific ZPR and the system ZPR (Sect. F.2).

1540 **F.1 Lagrangians and KKT conditions**

1541 The Lagrangians of the uncoupled model have been constructed in Appendix D (Eqs. (D1)-(D2)). From the KKT conditions for  
 1542 minimization, we can ascertain the following first-order conditions at stationarity for each model.

1543 For REMIND,

1544 1) Stationary conditions:

$$1545 \frac{\partial \mathcal{L}}{\partial P_{y,s}} = 0 \Rightarrow c_{y,s} + \omega_{y,s} - 8760 * \mu_{y,s} \phi_{y,s} - \sigma_{y,s} + \gamma_{y,s} = 0, \quad (F1)$$

$$1546 \frac{\partial \mathcal{L}}{\partial G_{y,s}} = 0 \Rightarrow o_{y,s} - \lambda_y (1 - \alpha_{y,s}) - \xi_{y,s} + \mu_{y,s} = 0. \quad (F2)$$

1547 2) Complementary slackness:

$$1548 \omega_{y,s} (P_{y,s} - \psi_s) = 0, \quad (F3)$$

$$1549 \xi_{y,s} G_{y,s} = 0, \quad (F4)$$

$$1550 \mu_{y,s} (G_{y,s} - 8760 * \phi_{y,s} P_{y,s}) = 0, \quad (F5)$$

$$1551 \sigma_{y,s} (p_{y,s} - P_{y,s}) = 0, \quad (y \leq 2020), \quad (F6)$$

$$1552 \gamma_{y,s} (P_{y,s} - P_{y-\Delta y,s} - q_{y,s}) = 0, \quad (y = 2025). \quad (F7)$$

1553 3) Primal feasibility:

$$1554 d_y - \sum_s G_{y,s} (1 - \alpha_{y,s}) = 0, \quad (F8)$$

$$1555 G_{y,s} - 8760 * \phi_{y,s} P_{y,s} = 0, \quad (F9)$$

1556 4) Dual feasibility:

$$1557 \xi_{y,s} \geq 0, \omega_{y,s} \geq 0, \sigma_{y,s} \geq 0, \gamma_{y,s} \geq 0. \quad (F10)$$

1558 For DIETER,

1559 1) Stationary conditions:

1560  $\frac{\partial \underline{\mathcal{L}}}{\partial \underline{P}_s} = 0 \Rightarrow \underline{\omega}_s + \underline{\omega}_s - \sum_h \underline{\phi}_{h,s} \underline{\mu}_{h,s} = 0 \text{ , } \underline{\phi}_{h,s} = 1 \text{ for dispatchables, } 0 < \underline{\phi}_{h,s} < 1 \text{ for renewables} \quad (\text{F11})$

1561  $\frac{\partial \underline{\mathcal{L}}}{\partial \underline{G}_{h,s}} = 0 \Rightarrow \underline{\omega}_s - \underline{\lambda}_h - \underline{\xi}_{h,s} + \underline{\mu}_{h,s} = 0 \text{ , } \quad (\text{F12})$

1562  $\frac{\partial \underline{\mathcal{L}}}{\partial \underline{G}_{h,vre}} = 0 \Rightarrow \underline{\omega}_{vre} + \underline{\mu}_{h,vre} = 0 \text{ .} \quad (\text{F13})$

1563 2) Complementary slackness:

1564  $\underline{\omega}_s (\underline{P}_s - \underline{\psi}_s) = 0, \quad (\text{F14})$

1565  $\underline{\xi}_{h,s} \underline{G}_{h,s} = 0, \quad (\text{F15})$

1566  $\underline{\mu}_{h,dis} (\underline{G}_{h,dis} - \underline{P}_{dis}) = 0, \quad (\text{F16})$

1567 3) Primal feasibility:

1568  $\underline{d}_h = \sum_s \underline{G}_{h,s}, \quad (\text{F17})$

1569  $\underline{G}_{h,vre} + \underline{I}_{h,vre} = \underline{\phi}_{h,vre} \underline{P}_{vre}, \quad (\text{F18})$

1570 4) Dual feasibility:

1571  $\underline{\omega}_s \geq 0, \underline{\xi}_{h,s} \geq 0, \underline{\mu}_{h,dis} \geq 0. \quad (\text{F19})$

1572 **F.2 Derivation of the zero-profit rules**

1573 **F.2.1 REMIND**

1574 The derivation of ZPRs is very similar to the one in Brown and Reichenberg, 2021. Starting with the total costs for technology  $s$  for all years, and applying various KKT conditions (after “|”),

1576 
$$\sum_y (c_{y,s} \underline{P}_{y,s} + o_{y,s} \underline{G}_{y,s}) \\ = \sum_y \{(-\omega_{y,s} + 8760 * \mu_{y,s} \phi_{y,s} + \sigma_{y,s} - \gamma_{y,s}) \underline{P}_{y,s} + [\lambda_y (1 - \alpha_{y,s}) + \xi_{y,s} - \mu_{y,s}] \underline{G}_{y,s}\} \quad | \text{ (F1), (F2)}$$

1577  $= \sum_y \{(-\omega_{y,s} + 8760 * \mu_{y,s} \phi_{y,s} + \sigma_{y,s} - \gamma_{y,s}) \underline{P}_{y,s} + [\lambda_y (1 - \alpha_{y,s}) - \mu_{y,s}] \underline{G}_{y,s}\} \quad | \text{ (F4)}$

1578  $= \sum_y \{(-\omega_{y,s} + \sigma_{y,s} - \gamma_{y,s}) \underline{P}_{y,s} + \lambda_y \underline{G}_{y,s} (1 - \alpha_{y,s})\} \quad | \text{ (F5)}$

1580 Rearranging, we arrive at the ZPR of multi-year uncoupled REMIND for technology cost-revenue balance:

1581 
$$\sum_y (c_{y,s} \underline{P}_{y,s} + o_{y,s} \underline{G}_{y,s}) = - \sum_y (\omega_{y,s} - \sigma_{y,s} + \gamma_{y,s}) \underline{P}_{y,s} + \sum_y \lambda_y \underline{G}_{y,s} (1 - \alpha_{y,s}). \quad (\text{F20})$$
  

$$\text{Generation costs} \quad \text{Capacity shadow revenues} \quad \text{Generation revenues}$$

1582 Normally, when there are no capacity shadow prices, or when the capacity constraints are not binding, the cost exactly equals revenue. However, when capacity shadow prices are non-zero, i.e. the constraints (c2) and (c5-c6) are binding, the capacity shadow prices act as a distortion to the equality relation between costs and revenues. As an example, the shadow price  $\omega_{y,s}$  from limited generation resources (e.g. hydroelectric power in Germany) would be positive  $\omega_{y,s} > 0$ , when the constraint is binding, and would appear as a “positive cost”, or a “negative revenue” in the modeled power market. We can therefore put it either on the left (cost) or right (revenue) side of the equation. Here we group it together with revenues.

1588 One observes that from the right-hand-side of Eq. (F20), there is no differentiation between the annual market values of variable and dispatchable generations such as gas and solar – they are both equal to the annual electricity price  $\lambda_y$ .

1590 From Eq. (F20), we can derive a ZPR between levelized cost of electricity (LCOE), capacity shadow price and market value (MV), for each generator type. Taking Eq. (F20), we separate the pre-curtailment LCOE from the LCOE due to curtailment,

1592 then divide by total post-curtailment generation  $\sum_y G_{y,s} (1 - \alpha_{y,s})$  for the generator type  $s$ , to obtain the technology-specific  
 1593 ZPR:

$$1597 \frac{\sum_y (c_{y,s} P_{y,s} + o_{y,s} G_{y,s})}{\sum_y G_{y,s}} + \frac{\sum_y (c_{y,s} P_{y,s} + o_{y,s} G_{y,s}) \alpha_{y,s}}{\sum_y G_{y,s} (1 - \alpha_{y,s})} = - \frac{\sum_y (\omega_{y,s} - \sigma_{y,s} + \gamma_{y,s}) P_{y,s}}{\sum_y G_{y,s} (1 - \alpha_{y,s})} + \frac{\sum_y \lambda_y G_{y,s} (1 - \alpha_{y,s})}{\sum_y G_{y,s} (1 - \alpha_{y,s})}. \quad (\text{F21})$$

Pre-curtailment LCOEs      Curtailment LCOEs      Capacity shadow prices      Market Value<sub>s</sub>

1594 The pre-curtailment LCOE is the cost of one unit of generated electricity – regardless whether it is curtailed or being used to  
 1595 meet demand, whereas the curtailment LCOE is the cost of one unit of curtailed electricity. Together they add up to post-  
 1596 curtailment LCOE, i.e. the cost of one unit of usable electricity.

1598 To obtain the ZPR for the whole power system in REMIND, we first sum Eq. (F20) over all generator types  $s$ , and obtain the  
 1599 ZPR for system cost and revenue. Then dividing by total post-curtailment system generation, and split the LCOE into pre-  
 1600 curtailment and curtailment components, we get

$$1601 \frac{\sum_{y,s} (c_{y,s} P_{y,s} + o_{y,s} G_{y,s})}{\sum_{y,s} G_{y,s}} + \frac{\sum_{y,s} (c_{y,s} P_{y,s} + o_{y,s} G_{y,s}) \alpha_{y,s}}{\sum_{y,s} G_{y,s} (1 - \alpha_{y,s})} = - \frac{\sum_{y,s} (\omega_{y,s} - \sigma_{y,s} + \gamma_{y,s}) P_{y,s}}{\sum_{y,s} G_{y,s} (1 - \alpha_{y,s})} + \frac{\sum_{y,s} \lambda_y G_{y,s} (1 - \alpha_{y,s})}{\sum_{y,s} G_{y,s} (1 - \alpha_{y,s})}, \quad (\text{F22})$$

Pre-curtailment LCOE<sub>system</sub>      Curtailment LCOE<sub>system</sub>      Capacity shadow price<sub>system</sub>      Electricity Price<sub>system</sub>

1602 i.e. the LCOE of the system for usable (pre-curtailment) power, which is equal to the sum of the system LCOE for total power  
 1603 generated and the curtailment cost, can be recovered by the average electricity price of the system minus system-wide capacity  
 1604 constraint shadow price per energy unit.

1605 The ZPRs of REMIND hold for the aggregate over multiple years.

1606 From Eqs. (F21)-(F22), we learn that when a market equilibrium can be found, i.e. when the optimization problem can be  
 1607 successfully solved, there is an equality relation between the generation cost and market value for each generator type, and  
 1608 similarly between generation cost and price of electricity for the entire system. Capacity shadow prices due to various extra  
 1609 capacity constraints imposed on the models, distort the equality relation between costs and prices by a linear term, making the  
 1610 prices be either higher or lower than the costs at the market equilibrium.

## 1611 F.2.2 DIETER

1612 Similar to uncoupled REMIND, from KKT conditions, at stationarity, we can obtain the cost-revenue ZPR for a single  
 1613 technology  $s$  for standalone DIETER. We take the total costs for technology  $s$  for all years, and applying various KKT  
 1614 conditions (after “|”),

$$1615 c_s \underline{P}_s + \sum_h [\underline{o}_s (\underline{G}_{h,s} + \underline{I}_{h,vre})] \\ 1616 = (-\underline{\omega}_s + \sum_h \underline{\phi}_{h,s} \underline{\mu}_{h,s}) \underline{P}_s + \sum_h (\underline{\lambda}_h - \underline{\mu}_{h,s} + \underline{\xi}_{h,s}) (\underline{G}_{h,s} + \underline{I}_{h,vre}) \quad | \quad (\text{F11}), (\text{F12}) \\ 1617 = -\underline{\omega}_s \underline{P}_s + \sum_h \underline{\phi}_{h,vre} \underline{\mu}_{h,vre} \underline{P}_{vre} + \sum_h (\underline{\lambda}_h - \underline{\mu}_{h,vre} + \underline{\xi}_{h,vre}) (\underline{G}_{h,vre} + \underline{I}_{h,vre}) + \sum_h \underline{\mu}_{h,dis} \underline{P}_{dis} + \sum_h (\underline{\lambda}_h - \underline{\mu}_{h,dis}) \underline{G}_{h,dis}$$

1618 | split  $\sum_h \underline{\phi}_{h,s} \underline{\mu}_{h,s}$  into  $vre$  and  $dis$ , apply (F15) for dispatchable, i.e.  $\underline{\xi}_{h,dis} \underline{G}_{h,dis} = 0$

$$1619 = -\underline{\omega}_s \underline{P}_s + \sum_h \underline{\phi}_{h,vre} \underline{\mu}_{h,vre} \underline{P}_{vre} + \sum_h (\underline{\lambda}_h - \underline{\mu}_{h,vre} + \underline{\xi}_{h,vre}) (\underline{G}_{h,vre} + \underline{I}_{h,vre}) + \sum_h \underline{\lambda}_h \underline{G}_{h,dis} \quad | \quad (\text{F16})$$

$$1620 = -\underline{\omega}_s \underline{P}_s + \sum_h \underline{\lambda}_h \underline{G}_{h,vre} + \sum_h (\underline{\lambda}_h + \underline{\xi}_{h,vre}) \underline{I}_{h,vre} + \sum_h \underline{\lambda}_h \underline{G}_{h,dis} \quad | \quad (\text{F18}), \text{ apply (F15) for VRE, i.e. } \underline{\xi}_{h,vre} \underline{G}_{h,vre} = 0$$

$$1621 = -\underline{\omega}_s \underline{P}_s + \sum_h \underline{\lambda}_h \underline{G}_{h,vre} + \sum_h \underline{\lambda}_h \underline{G}_{h,dis} \quad | \quad (\text{F12}) \& (\text{F13}) \Rightarrow \underline{\lambda}_h + \underline{\xi}_{h,vre} = 0$$

1622 Rearranging, we arrive at the ZPR of single-year uncoupled DIETER for technology-specific cost-revenue balance:

1623 
$$\underbrace{c_s P_s + o_s \sum_h (G_{h,s} + \Gamma_{h,vre})}_{\text{Annual generation costs}} = - \underbrace{\omega_s P_s}_{\text{Annual capacity shadow revenues}} + \underbrace{\sum_h \lambda_h G_{h,s}}_{\text{Annual generation revenues}}. \quad (\text{F23})$$

1624 Dividing Eq. (F23) by annual aggregated generation of technology  $s$ , we obtain the technology-specific ZPR for DIETER,

1625 
$$\underbrace{\frac{c_s P_s + o_s \sum_h (G_{h,s} + \Gamma_{h,vre})}{\sum_h G_{h,s}}}_{\text{LCOEs}} = - \underbrace{\frac{\omega_s P_s}{\sum_h G_{h,s}}}_{\text{Annual capacity shadow price}_s} + \underbrace{\frac{\sum_h \lambda_h G_{h,s}}{\sum_h G_{h,s}}}_{\text{Market value}_s}. \quad (\text{F24})$$

1626 One observes that from the term of  $\text{Market Value}_s$ , compared to the REMIND case (right-hand-side of Eq. (F21)), DIETER  
1627 has differentiated annual market values of gas and solar generators.

1628 Summing Eq. (F24) over  $s$ , dividing both sides by total annual generation  $\sum_{h,s} G_{h,s}$ , using identity  $\underline{d}_h = \sum_s G_{h,s}$  for  
1629 simplification, we obtain the ZPR for the whole power system in DIETER,

1630 
$$\underbrace{\frac{\sum_s [c_s P_s + o_s \sum_h (G_{h,s} + \Gamma_{h,vre})]}{\sum_{h,s} G_{h,s}}}_{\text{LCOE}_{\text{system}}} = - \underbrace{\frac{\sum_s \omega_s P_s}{\sum_{h,s} G_{h,s}}}_{\text{Annual capacity shadow price}_{\text{system}}} + \underbrace{\frac{\sum_h \lambda_h \underline{d}_h}{\sum_h \underline{d}_h}}_{\text{Annual average electricity price}_{\text{system}}}. \quad (\text{F25})$$

1631 Similar to the case of REMIND, Eqs. (F24)-(F25) show us the equality relations between cost and value (or price) for each  
1632 generator type and for the system hold also for DIETER at its market equilibrium. Compared to REMIND, there are no brown-  
1633 field or near-term capacity shadow price contributions in DIETER in the standalone versions. The DIETER ZPRs hold for one  
1634 year instead of the aggregate of multiple years like in REMIND. For simplicity, even though it is possible to write the LCOE in  
1635 pre-curtailment and curtailment terms, but because for DIETER it is relatively cumbersome to do, we do not do it here.

1636 In summary, at REMIND and DIETER power market equilibriums, each generator exactly recovers its cost of one unit of  
1637 generation through market value, and obtains “zero profit” under a completely competitive market over its modeling time. In the  
1638 aggregate, the entire power sector obtains its cost of one unit of generation through the price of electricity that the consumer  
1639 pays. Both types of relations can be distorted by the existence of capacity shadow prices.

## 1640 Appendix G: Derivation of the equilibrium conditions for the coupled models

1641 Here in this Appendix, we gradually build up the derivation for the ZPRs of the coupled REMIND and DIETER, which will be  
1642 used later for validating numerical results. The derivation consists of three steps:

1643 1) ZPRs for the uncoupled model REMIND and DIETER;  
1644 2) ZPRs for coupled model REMIND and DIETER (simplified version, only considering convergence condition (h1-h7));  
1645 3) ZPRs for coupled model REMIND and DIETER (full version, also considering (c7 and c8)).

1646 Step (1) is entirely derived in Appendix F.

1647 For step (2), based on the uncoupled ZPRs, we recognize that from convergence condition (h1-h7), the only condition which  
1648 impacts the form of the ZPR is (h3), because the markup terms modify the objective function of the (simplified) coupled version  
1649 of REMIND (Eq. (6)). Following similar procedure as in Appendix F, we can derive the technology-specific ZPR for the  
1650 coupled REMIND (simplified version) as follows:

1651 
$$\underbrace{\frac{\sum_y (c_{y,s} P_{y,s} + o_{y,s} G_{y,s})}{\sum_y G_{y,s}}}_{\text{Pre-curtailment LCOEs}} + \underbrace{\frac{\sum_y (c_{y,s} P_{y,s} + o_{y,s} G_{y,s}) \alpha_{y,s}}{\sum_y G_{y,s} (1 - \alpha_{y,s})}}_{\text{Curtailment cost}_s} = - \underbrace{\frac{\sum_y (\omega_{y,s} - \sigma_{y,s} + \gamma_{y,s}) P_{y,s}}{\sum_y G_{y,s} (1 - \alpha_{y,s})}}_{\text{Capacity shadow price}_s} + \underbrace{\frac{\sum_y (\lambda_y + \eta_{y,s}) G_{y,s} (1 - \alpha_{y,s})}{\sum_y G_{y,s} (1 - \alpha_{y,s})}}_{\text{Market Value}_s}. \quad (\text{G1})$$

1652 Compared with the ZPR of the uncoupled version (F24), the only difference is that we replace the market value in the uncoupled  
1653 REMIND  $\lambda_y$  with the DIETER-markup corrected market value  $\lambda_y + \eta_{y,s}$ . DIETER’s ZPR is unchanged at this step.

1654 Step (3) involves two extra capacity constraints, one in each model, the first of which, (c7), is discussed in detail in Appendix H.  
 1655 The implementation of (c7) further modifies Eq. (G1) and results in the ZPRs of the coupled REMIND. The other constraint  
 1656 (c8) will be the focus of discussion here. It only modifies the ZPRs for the coupled DIETER and not for the coupled REMIND.  
 1657 Constraint (c8) is a brown-field capacity constraint implemented in DIETER to address the fact that DIETER is a green-field  
 1658 model, which is otherwise ignorant about standing-capacities in the real world. There are many ways we can implement this  
 1659 standing capacity constraint in DIETER. The most straight-forward way is to implement the “standing capacity” at the  
 1660 beginning of each REMIND period, which REMIND sees before it invests additional capacities, as a lower bound on  
 1661 endogenous capacities in DIETER. This helps put DIETER and REMIND on equal footing before the 5- or 10-year investment  
 1662 period starts, allowing us to compare their investment intentions.

1663 c8) “standing capacity constraint” in DIETER, i.e. DIETER capacities at time  $y$  need to be larger or equal to the REMIND  
 1664 standing capacities at the beginning of the time period:

$$P_s \geq P_{y-\Delta y/2,s} / (1 - ER) \quad \perp \underline{\varsigma}_s ,$$

1666 where the time-step  $\Delta y$  is divided by 2 because the representative year in REMIND is in the middle of the time step,  $ER$  is  
 1667 the endogenous early retirement rate in REMIND.

1668 The reason we implement the standing capacity in this way, is in part because as a proof-of-concept, we want to give DIETER  
 1669 endogenous freedom to invest in all model years, so we use only the pre-investment capacities as “soft” corridors to bound the  
 1670 DIETER capacities from below. If we were to transfer precisely the brown-field and near-term constraints from REMIND to  
 1671 DIETER, it requires a complete list of constraints for each technology, and an identical implementation of all of them in  
 1672 DIETER. This may raise the precision of convergence in some years for some technologies, but in practice it can be more  
 1673 complicated to implement than a generic lower bound for all technologies.

1674 To obtain the ZPRs of coupled DIETER, we simply modify the capacity shadow price term of the uncoupled DIETER ZPRs  
 1675 (Eqs. (F24)-(F25)) by the additional capacity shadow price  $\underline{\varsigma}_s$  from (c8):

$$1676 \underline{\text{Capacity shadowprice}}'_s = \frac{(\underline{\omega}_s + \underline{\varsigma}_s) P_s}{\sum_h \underline{G}_{h,s}}, \quad (G2)$$

$$1677 \underline{\text{Capacity shadowprice}}'_{\text{system}} = \frac{\sum_s (\underline{\omega}_s + \underline{\varsigma}_s) P_s}{\sum_{h,s} \underline{G}_{h,s}}. \quad (G3)$$

## 1678 Appendix H: Additional methods for numerical stability in coupled runs

1679 Here, we introduce the two methods we employed to improve numerical stability of the coupled runs: 1) the dispatchable  
 1680 capacity constraint by peak demand to avoid high markups being exchanged (Sect. H.1); 2), endogenous prefactors for all  
 1681 quantities from last-iteration DIETER to current-iteration REMIND (Sect. H.2).

### 1682 H.1 Dispatchable capacity constraints by peak demand

#### 1683 H.1.1 Description of the capacity constraint and price manipulation in DIETER post-processing

1684 Scarcity hour price can occur in a PSM run, which is the highest hourly price in a year, and it is usually equal to the annuitized  
 1685 fixed cost of Open Cycle Gas Turbine (OCGT) (capital investment cost and fixed O&M costs) (Hirth and Ueckerdt, 2013). In  
 1686 our simulations, the scarcity prices are usually above 50\$/KWh. If we include the scarcity price into the markups, OCGT will  
 1687 receive an annual markup usually more than 5 times higher than the annual average electricity price. The high markup results in  
 1688 OCGT plants receiving too high an incentive in the next iteration REMIND, and the model overshoots (overinvests) in

1689 capacities. Over iterations, this causes oscillations in the quantity and prices in the coupled model. For better numerical stability,  
 1690 instead of passing on the full markups from DIETER, we only pass on the portion of the annual markups unrelated to scarcity  
 1691 hour prices, and replace the exchange of the part of the markup due to scarcity hours from DIETER to REMIND with  
 1692 implementing an additional capacity constraint in REMIND for coupled runs. The two actions can be later shown to be  
 1693 mathematically equivalent. Generators other than OCGT which produce at the scarcity hours also get paid in the hour at this  
 1694 high price. However, because they also produce at other hours with lower prices, their average market values are only  
 1695 moderately impacted by the scarcity hour price, and do not in general lead to instability issues.

1696 Below, we first introduce the aforementioned capacity constraint implemented on the side of REMIND, then discuss the  
 1697 corresponding manipulation of the markups in DIETER. Lastly, we show their mathematical equivalence, and state the modified  
 1698 ZPR of coupled REMIND due to these actions.

1699 The extra capacity constraint states that the sum of all dispatchable capacities needs to be at least as large as the peak residual  
 1700 demand:

1701  $c7) \sum_{dis} P_{y,dis} > d_{y,residual} \perp v_{y,dis},$

1702 where  $d_{y,residual}$  is peak residual demand in REMIND and is semi-endogenous.  $d_{y,residual}$  is a function of the peak hourly  
 1703 residual demand in the last iteration of DIETER  $d_{residual}(y, i - 1)$ . The peak hourly residual demand in DIETER is in turn  
 1704 defined as the maximum hourly amount of inflexible demand not met by wind, solar or hydro generations, and hence must  
 1705 be met by dispatchable generations (under no storage conditions):

1706  $d_{residual} = \max_h (d_h - G_{h,Solar} - G_{h,Wind} - G_{h,Hydro}). \quad (H1)$

1707  $v_{y,dis}$  is the shadow price of the capacity constraint for dispatchable technology  $dis$ .

1708 For the exact implementation of (c7) in coupled run, see Sect. 3.3.2, 2. Under storage implementation, in addition to the  
 1709 variable renewable contribution, the hourly storage discharge is also subtracted from the residual demand.

1710 Simultaneous to implementing this capacity constraint, we remove the surplus scarcity prices in post-processing of DIETER  
 1711 before passing it onto REMIND. In DIETER, we define the scarcity price as the maximum hourly price in a year:

1712  $\underline{\lambda}_{y,h_{scar}} = \max_h (\underline{\lambda}_{y,h}), \quad (H2)$

1713 and the surplus scarcity hour price is the difference between the scarcity price and the second highest price:

1714  $\underline{\lambda}_{y,surplus} = \underline{\lambda}_{y,h_{scar}} - \max(\underline{\lambda}_{y,h|h \neq h_{scar}}) = \max_h (\underline{\lambda}_{y,h}) - \max(\underline{\lambda}_{y,h|h \neq h_{scar}}), \quad (H3)$

1715 where  $h_{scar}$  is the scarcity hour when scarcity price occurs, corresponding to the peak residual demand hour.

1716 Using this, we manipulate the market value and annual average electricity price in DIETER ex post, excluding the surplus  
 1717 scarcity hour price:

1718  $\underline{MV}'_s = \frac{\sum_{h|h \neq h_{scar}} G_{h,s} \underline{\lambda}_h + \sum_{h|h_{scar}} G_{h,s} * \max(\underline{\lambda}_{h|h \neq h_{scar}})}{\sum_{h=1}^{8760} G_{h,s}}, \quad (H4)$

1719  $\underline{J}' = \frac{\sum_{h|h \neq h_{scar}} d_h \underline{\lambda}_h + \sum_{h|h_{scar}} d_h * \max(\underline{\lambda}_{h|h \neq h_{scar}})}{\sum_{h=1}^{8760} d_h}. \quad (H5)$

1720 where  $\underline{MV}'_s$  is the annual average market value without the surplus scarcity hour price, and  $\underline{J}'$  is the annual average electricity  
 1721 price without the surplus scarcity hour price. Thus, the corresponding modified markup term without the surplus scarcity hour  
 1722 price is:

1723  $\underline{\eta}'_s = \underline{MV}'_s - \underline{J}'.$  (H6)

1724 Note that since the above manipulation is done in a post-processing step, the LCOE in DIETER is still fully covered by MV, as  
 1725 the KKT conditions and ZPRs still hold by default in an optimized DIETER model.

1726 With the implementation of (c7), the coupled ZPR (Eq. (G1)) is then further modified to include the new shadow price  $v_{y,s}$  as  
 1727 well as the modified markup  $\underline{\eta}'_{y,s}$  (without surplus scarcity price). (We write from now on  $v_{y,dis}$  simply as  $v_{y,s}$ .) Then,  
 1728 technology-specific ZPR of coupled REMIND is:

$$1729 \frac{\sum_y (c_{y,s} P_{y,s} + o_{y,s} G_{y,s})}{\sum_y G_{y,s}} + \frac{\sum_y (c_{y,s} P_{y,s} + o_{y,s} G_{y,s}) \alpha_{y,s}}{\sum_y G_{y,s} (1 - \alpha_{y,s})} = - \frac{\sum_y (\omega_{y,s} - \sigma_{y,s} + \gamma_{y,s} + v_{y,s}) P_{y,s}}{\sum_y G_{y,s} (1 - \alpha_{y,s})} + \frac{\sum_y (\lambda_y + \underline{\eta}'_{y,s}) G_{y,s} (1 - \alpha_{y,s})}{\sum_y G_{y,s} (1 - \alpha_{y,s})} \quad (H7)$$

1730 System ZPR of coupled REMIND is:

$$1731 \frac{\sum_y (c_{y,s} P_{y,s} + o_{y,s} G_{y,s})}{\sum_y G_{y,s}} + \frac{\sum_y (c_{y,s} P_{y,s} + o_{y,s} G_{y,s}) \alpha_{y,s}}{\sum_y G_{y,s} (1 - \alpha_{y,s})} = - \frac{\sum_y (\omega_{y,s} - \sigma_{y,s} + \gamma_{y,s} + v_{y,s}) P_{y,s}}{\sum_y G_{y,s} (1 - \alpha_{y,s})} + \frac{\sum_y (\lambda_y + \underline{\eta}'_{y,s}) G_{y,s} (1 - \alpha_{y,s})}{\sum_y G_{y,s} (1 - \alpha_{y,s})} \quad (H8)$$

1732 These are the ZPRs of the coupled REMIND for the full version.

### 1733 **H.1.2 Equivalence between surplus scarcity price in DIETER and capacity shadow price due to peak residual demand in 1734 REMIND**

1735 Because of the intuitive relation between the scarcity price and the peak residual demand – i.e., that scarcity price occurs in the  
 1736 hour with peak hourly residual demand due to the pricing power of the peaker gas turbines in the hour where VRE is most  
 1737 scarce, we can draw a quantitative equivalence between the scarcity price contribution to the markup and the capacity constraint  
 1738 shadow price  $v_y$ . This means that the revenue the plant receives in scarcity hour in capacity terms (i.e. capacity credit), can be  
 1739 transformed directly to a revenue in energy terms (i.e. a part of the annual market value). At convergence, for any given year  $y$ ,  
 1740 the negative shadow price,  $-v_{y,dis}$ , when translated into annual generation terms via capacity factor  $\phi_{y,s}$  of dispatchable  
 1741 technology  $s$ , should be equal to the scarcity hour surplus revenue divided by annual generation by  $s$  in DIETER:

$$1742 \frac{-v_{y,dis}}{\phi_{y,dis} * 8760} = \frac{\underline{\lambda}_y \text{surplus } \underline{G}_{h,scar,dis}}{\sum_h \underline{G}_{y,h,dis}}. \quad (H9)$$

1743 In practice, this equivalence is confirmed by numerical results (e.g. Fig. 8 subplot for OCGT).

1744 Using this equivalence, we can show as follows, that at convergence,  $\lambda_y$  should be equal to DIETER power price without  
 1745 surplus scarcity price  $\underline{J}'$  (Eq. (H5)), and  $\lambda_y + \underline{\eta}'_{y,s}$  should be equal to DIETER market value without scarcity price  $\underline{MV}'$  (Eq.  
 1746 (H4)).

1747 At convergence, the annual generations have identical solutions in the two models, i.e.  $\sum_h \underline{G}_{y,h,s} = G_{y,s} (1 - \alpha_{y,s})$ . We plug this  
 1748 and REMIND capacity factor  $\phi_{y,s} = \frac{G_{y,s} (1 - \alpha_{y,s})}{P_{y,s} * 8760}$  into Eq. (H9) to obtain

$$1749 v_y P_{y,s} = \underline{\lambda}_y \text{surplus } \underline{G}_{y,h,scar,s}. \quad (H10)$$

1750 Take Eq. (H7), and only consider REMIND annual revenue by multiplying generation  $\sum_y G_{y,s} (1 - \alpha_{y,s})$  then on the right-  
 1751 hand-side, take both revenue and the capacity shadow revenue contribution from  $v_{y,s}$  for a single year, which is equal to the total  
 1752 single-year REMIND revenue:

$$1753 \Theta_{y,s} = - \frac{v_{y,s} P_{y,s}}{\text{Capacity shadow revenue from c(7)_s}} + \frac{(\lambda_y + \underline{\eta}'_{y,s}) G_{y,s} (1 - \alpha_{y,s})}{\text{Generation revenue}'_s}$$

1754 and plug in (H10), (H6),

$$1755 \Theta_{y,s} = \frac{\underline{\lambda}_y \text{surplus } \underline{G}_{y,h,scar,s}}{\text{surplus scarcity revenue in scarcity hours}_s} + \frac{(\underline{MV}'_{y,s} - \underline{J}'_y + \lambda_y) G_{y,s} (1 - \alpha_{y,s})}{\text{Generation revenue}'_s}$$

1756 Plugging in (H4),

1757  $\underline{\Theta}_{y,s} = \underline{\lambda}_{y,surplus} \underline{G}_{y,h,scar,s} + \sum_{h \neq h_{scar}} \underline{G}_{y,h,s} \underline{\lambda}_{y,h} + \underline{G}_{y,h,scar,s} * \max(\underline{\lambda}_{y,h|h \neq h_{scar}}) - \underline{J}'_y G_{y,s} (1 - \alpha_{y,s}) + \lambda_y G_{y,s} (1 - \alpha_{y,s})$

1758 Lastly, plug in the definition for  $\underline{\lambda}_{y,surplus}$  (Eq. (H3)),

1759  $\Theta_{y,s} = \sum_h \underline{\lambda}_{y,h} \underline{G}_{y,h,s} - \underline{J}'_y G_{y,s} (1 - \alpha_{y,s}) + \lambda_y G_{y,s} (1 - \alpha_{y,s}). \quad (H11)$

1760 Since the single-year revenue  $\Theta_{y,s}$  in REMIND should be aligned with DIETER due to harmonization condition (h3), and the  
 1761 DIETER revenue is  $\underline{\Theta}_{y,s} = \sum_h \underline{\lambda}_{y,h} \underline{G}_{y,h,s}$ , that means the last two terms in (H11) should sum to 0. Therefore REMIND  
 1762 electricity price  $\lambda_y$  should be equal to  $\underline{J}'_y$ .

1763 **H.2 Stabilization techniques using prefactors**

1764 In this Appendix, we describe the detailed implementations of prefactors for information exchanged from DIETER to REMIND.

1765 1. Markup prefactor:

1766 In order to facilitate convergence in REMIND, we implement an endogenous prefactor  $f_{y,s}^\eta$  for MV in the REMIND  
 1767 markup equation Eq. (5):

1768  $\eta_{y,s}(i) = f_{y,s}^\eta(i) * \underline{MV}'_{y,s}(i-1) - \underline{J}'_y(i-1). \quad (H12)$

1769 The endogenous prefactor  $f_{y,s}^\eta$  is dependent on the difference between in-iteration endogenous generation share and last-  
 1770 iteration DIETER generation share:

1771  $f_{y,s}^\eta(i) = 1 - \underline{b}_{y,s}(i-1) \Delta S_{y,s}, \quad (H13)$

1772 where  $\underline{b}_{y,s}$  is a positive parameter, equal to the ratio between market values and average price depending on their  
 1773 relationship in the last iteration DIETER,

1774  $\underline{b}_{y,s} = \frac{\underline{MV}'_{y,s}}{\underline{J}'_y} \text{ if } \underline{MV}'_{y,s} > \underline{J}'_y,$

1775  $\underline{b}_{y,s} = \frac{\underline{J}'_y}{\underline{MV}'_{y,s}} \text{ if } \underline{MV}'_{y,s} < \underline{J}'_y,$

1776 and where the generation share difference across models and consecutive iteration  $\Delta S_{y,s}$  is,

1777  $\Delta S_{y,s} = \frac{G_{y,s}(i)(1 - \alpha_{y,s}(i))}{\sum_s [G_{y,s}(i)(1 - \alpha_{y,s}(i))]} - \frac{\sum_h \underline{G}_{y,s}(i-1)}{\sum_{h,s} \underline{G}_{y,s}(i-1)}.$

1778 The values of  $\underline{b}_{y,s}$  are heuristically determined (see Sect. 6.2).

1779 When in-iteration REMIND solar generation share increases due to the price signal from the last-iteration DIETER market  
 1780 value, such that the REMIND share is larger than in the last DIETER iteration, the formula Eq. (H13) results in a prefactor  
 1781 smaller than one, decreasing in-iteration markup  $\eta_{y,s}(i)$ .

1782 2. Peak demand prefactor:

1783 The peak demand in REMIND  $d_{residual,y}$  depends on the last iteration DIETER peak hourly residual demand  
 1784  $\underline{d}_{residual}(y, i-1)$ . Implementing it in constraint (c7),

1785  $\sum_{dis} P_{y,dis} < d_{residual,y} * f_y^{d_{residual}}(i),$

1786 for iteration  $i$ , we use  $f_y^{d_{residual}}(i)$  as a prefactor for stabilization,

1787  $f_y^{d_{residual}}(i) = 1 - b_{y,peak} * \Delta S_{y,wind}.$

1788  $b_{y,peak}$  is a heuristic constant dependent on  $y$ ,  $\Delta S_{y,wind}$  is the wind generation share. We use the wind generation share in  
 1789 the current iteration of REMIND for stabilization, because in the peak residual demand hour, there usually is some wind  
 1790 production for the historical year we chose (but no solar). In general,  $b_{y,peak}$  is 0.5 for earlier years, and increasing to 1 for

1791 later years, under a baseline scenario. For climate scenarios,  $b_{y,peak}$  is around 1.5 for less stringent scenarios, and for more  
 1792 stringent scenarios, it is 0.5 for earlier years, and increasing to 3 for later years.

1793 3. Capacity factor prefactor:

1794 We set REMIND capacity factor  $\phi_{y,dis}$  to be equal to the DIETER annual average capacity factor from the last iteration  
 1795 multiplied by a prefactor:

1796 
$$\phi_{y,dis}(i) = \underline{\phi}_{dis}(y, i-1) * f_{y,s}^{\phi_{dis}}(i),$$

1797 where DIETER annual average capacity factor is  $\underline{\phi}_{dis} = \frac{\sum_h \underline{G}_{h,dis}}{\underline{P}_{dis} * 8760}$  for each year  $y$ . In order to facilitate convergence, a  
 1798 similar prefactor  $f_{y,s}^{\phi_{dis}}$  as in Eq. (H13) is implemented:

1799 
$$f_{y,s}^{\phi_{dis}}(i) = 1 - 0.5\Delta S_{y,s} \quad \text{if } \underline{\phi}_{dis}(y, i-1) < 0.5 \text{ (i.e. the plant is “peaker” or “mid-load” type in the last iteration),}$$

1800 
$$f_{y,s}^{\phi_{dis}}(i) = 1 + 0.5\Delta S_{y,s} \quad \text{if } \underline{\phi}_{dis}(y, i-1) \geq 0.5 \text{ (i.e. the plant is “base-load” type in the last iteration),}$$

1801 where 0.5 is a heuristic factor.

1802 The sign in the prefactor formula is determined based on the observation that under a system with variable renewable  
 1803 generations, for generator plants that have relatively high running cost and low investment cost, i.e. they are most  
 1804 economically operated as “peaker” plants or as “mid-load” plants of lower capacity factor, so when their generation share  
 1805 incrementally increases, their capacity factor decreases. Conversely, for generators with relatively low running cost and  
 1806 high investment cost, i.e. they are most economically operated as “base-load” plants, when their generation share  
 1807 incrementally increases, their capacity factor increases.

1808 4. Curtailment prefactor:

1809 The curtailment ratio in REMIND  $\alpha_{y,vre}$  is equal to last iteration DIETER curtailment ratio, multiplied by prefactor  $f_{y,vre}^\alpha$ :

1810 
$$\alpha_{y,vre}(i) = \frac{\sum_h \underline{Y}_{h,vre}(y, i-1)}{\sum_h \underline{G}_{h,vre}(y, i-1)} * f_{y,vre}^\alpha(i),$$

1811 where the prefactor is  $f_{y,vre}^\alpha(i) = 1 + \Delta S_{y,vre}$ .

1812 5. Capture price prefactor:

1813 Similar to the case of markup from the demand side, the markup for any demand-side technology given to REMIND is:

1814 
$$\eta_{y,s_d}(i) = f_{y,s_d}^\eta(i) * \underline{CP}_{y,s_d}(i-1) - \underline{J}_y(i-1),$$

1815 where  $\underline{J}_y$  is the annual average electricity price of all demand types  $s_d$  for period  $y$ ,

1816 
$$\underline{J} = \frac{\sum_h (\sum_{s_d} \underline{d}_{h,s_d}) * \underline{\lambda}_h}{\sum_h \sum_{s_d} \underline{d}_{h,s_d}},$$

1817 and  $f_{y,s_d}^\eta(i)$  is an endogenous stabilization prefactor for the flexible-demand markup based on shares of demand by  $s_d$  in  
 1818 total demand for each year.

1819 **Appendix I: Derivation for equilibrium condition for REMIND in the case of additional adjustment cost**

1820 Adjustment cost – an additional linear term in the objective function, acts as an inertia against fast or slow capacity additions or  
 1821 retirement. The implementation of positive adjustment costs mimics the challenges of scaling up the supply chains and of  
 1822 training new workers to do installation and construction. Adjustment costs are applied to all model time periods, so it is by  
 1823 nature intertemporal. The objective function for power sector including the adjustment cost  $\Xi_{y,s}$  is

1824 
$$Z = \sum_{y,s} (c_{y,s} P_{y,s} + o_{y,s} G_{y,s} + \Xi_{y,s}),$$

1825 where  $\Xi_{y,s}$  is a quadratic function of the difference between capacity additions of subsequent time periods  $y - \Delta y$  and  $y$ :

1826 
$$E_{y,s} = c_{y,s} k_s \left( \frac{\Delta P_{y,s} - \Delta P_{y-\Delta y,s}}{\Delta y^2} \right)^2 / \left( \frac{\Delta P_{y-\Delta y,s}}{\Delta y} + \beta_{y,s} \right),$$

1827 where  $\Delta P_{y,s}$  is as before the capacity addition during time period  $y$  of technology  $s$ ,  $\beta_{y,s}$  is an offset parameter to offset additions  
 1828 in initial time periods,  $k_s$  is a regional technological coefficient,  $c_{y,s}$  is the capital expenditure cost per capacity unit as before.  
 1829 Because the adjustment cost is a quadratic function of the endogenous variable  $P_{y,s}$ , it turns the power sector cost minimization  
 1830 in REMIND into a nonlinear problem.

1831 Similar to the case without adjustment costs in Sect. 3.2.3, the first stationary condition becomes:

1832 
$$\frac{\partial \mathcal{L}}{\partial P_{y,s}} = 0, \Rightarrow c_{y,s} + \omega_{y,s} - \mu_{y,s} \phi_{y,s} - \sigma_{y,s} + \gamma_{y,s} + 2c_{y,s} k_s \frac{\Delta P_{y,s} - \Delta P_{y-\Delta y,s}}{(\Delta P_{y-\Delta y,s} + \beta_{y,s}) \Delta y^2} = 0 ,$$

1833 simplifying,

1834 
$$c_{y,s} = -\omega_{y,s} + \mu_{y,s} \phi_{y,s} + \sigma_{y,s} - \gamma_{y,s} - a_{y,s} c_{y,s} ,$$

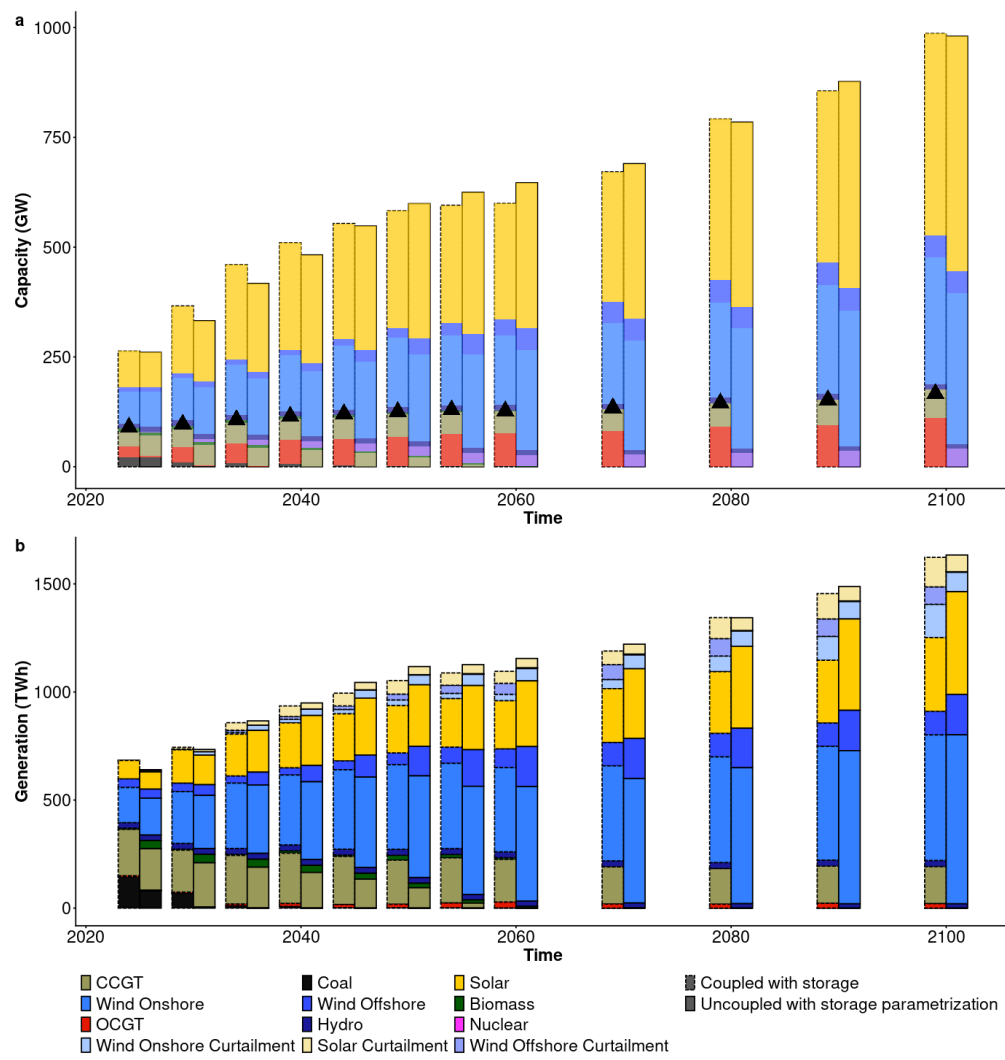
1835 where  $a_{y,s} = 2k_s \frac{\Delta P_{y,s} - \Delta P_{y-\Delta y,s}}{(\Delta P_{y-\Delta y,s} + \beta_{y,s}) \Delta y^2}$  is the endogenous adjustment factor of investment, and is a function of capacity.

1836 The new ZPR including the adjustment cost in terms of cost and revenue for technology  $s$ , can be derived

1837 
$$\sum_y [(c_{y,s} + a_{y,s} c_{y,s}) P_{y,s} + o_{y,s} G_{y,s} + \lambda_y \alpha_{y,s} G_{y,s} + (\omega_{y,s} - \sigma_{y,s} + \gamma_{y,s}) P_{y,s}] = \sum_y (\lambda_y G_{y,s}) .$$

1838 The adjustment cost  $a_{y,s} c_{y,s}$  can act as a disincentive or an incentive to capacity additions. If capacity addition in the current  
 1839 period is higher than in the last period  $\Delta P_{y,s} > \Delta P_{y-\Delta y,s}$ , i.e. a ramp-up case of capacity addition, the adjustment cost is positive  
 1840 and acts as a disincentive, so the ramp-up speed is slower. When added capacities are decreasing with time, i.e. a ramp-down  
 1841 case of capacity addition, adjustment cost is negative and acts as an incentive, and as a result, the ramp-down speed is slower.  
 1842 In the coupled run we see only a moderate adjustment cost which drops down fast as a function of time (see e.g. Fig.6).

## Appendix J: Comparing the coupled and uncoupled run



1845 **Figure J1: Under the 2C global scenario (no German net-zero goal), we compare (a) the capacity mix and (b) the**  
 1846 **generation mix of Germany for the DIETER-coupled version of REMIND with endogenous storage (dashed bar) and for**  
 1847 **the uncoupled version of REMIND with parametrized storage (solid bar). In (a), triangle dots indicate the peak residual**  
 1848 **demand of the year as determined in DIETER.**

## Appendix K: Complete list of mathematical symbols

The units used in the two models are usually different. Here we uniformly use MWh for energy units, and MW for capacity units. In the main text, underscore  $\_$  is used to denote DIETER parameters and variables. An apostrophe is used to indicate a modified version of the variable. An asterisk is used to indicate the values of variables at the optimum of objective functions.

Symbol	Description	Unit	Symbol	Description	Unit
$y, \Delta y$	REMIND time period, REMIND time step	-	$h$	Hour	-
$s$	Supply-side technology type	-	$dis, vre$	Dispatchable generators, Variable	-

				Renewable	
$s_d$	Demand-side technology type	-	$i$	Iteration	-
$reg$	Region	-	$\mathcal{L}$	Lagrangian	\$
$Z$	Objective function	\$	$G$	Generation	MWh
$c$	Fixed cost	\$/MW	$\psi$	Total annual renewable potential	MWh
$o$	Variable cost	\$/MWh	$\phi$	Capacity factor	1
$\alpha$	Annual curtailment to pre-curtailment generation ratio in REMIND model	1	$d$	Exogenous demand	MWh
$P$	Capacity	MW	$p$	Standing capacity in REMIND	MW
$\Gamma$	Curtailment	MWh	$\eta$	Markup	\$/MWh
$\lambda$	Shadow price of power supply-demand balance equation / power price	\$/MWh	MV	Market value	\$/MWh
$q$	Near-term ramp up constraint for capacities in REMIND	MW	$\theta$	revenue	\$
$M$	Difference in total revenues in the two models	\$	$\xi$	Shadow price due to positive generation	\$/MWh
$\omega$	Shadow price due to limited renewable potential	\$/MW	$\gamma$	Shadow price due to near-term ramp up constraint	\$/MW
$\mu$	Shadow price due to limit on generation from capacity	\$/MWh	$\varsigma$	DIETER shadow price due to standing capacity constraint from REMIND	\$/MW
$\sigma$	Shadow price due to standing capacities in REMIND	\$/MW	CP	Capture price of demand-side technologies	\$/MWh
$v$	Shadow price due to peak residual demand constraint	\$/MWh	$\Delta S$	Difference in generation shares between models	1
$f$	Prefactor for numeric stabilization	1	$W$	Economic welfare	-
$b, b_{peak}$	Multiplicative prefactors parameter	1	$\varrho$	Pure rate of time preference	1

$\Xi$	Adjustment cost	\$	$\beta$	Offset parameters in adjustment cost	\$
$\chi$	Consumption	\$	$a$	Adjustment factor of investment	1
$V$	Population	1	$k$	Regional technological coefficient for adjustment cost	1
$ER$	Early retirement rate in REMIND	1	$J$	Annual average DIETER electricity price	\$/MWh

1853 **Table K1: Complete list of mathematical symbols. For simplicity, in general, we only list the symbols, not their indices or**  
 1854 **in which model they are used.**

1855 **Appendix L: Complete list of abbreviations**

Abbreviation	Description	Abbreviation	Description
IAM	Integrated assessment model	LCOE	Levelized cost of electricity
PSM	Power sector model	MV	Market value
VRE	Variable renewable	O&M	Operation and maintenance
GHG	Greenhouse gas	OMF	Operation and maintenance fixed cost
NLP	Nonlinear programming	OMV	Operation and maintenance variable cost
LP	Linear programming	OCGT	Open cycle gas turbine
CES	Constant elasticity of substitution	CCGT	Combined cycle gas turbine
IPCC	Intergovernmental Panel on Climate Change	CP	Capture price
RLDC	Residual load duration curve	PtG	Power-to-Gas
ZPR	Zero-profit rule	PDC	Price duration curves
KKT	Karush–Kuhn–Tucker	CCS	Carbon capture and storage
EV	Electric Vehicles	GAMS	General Algebraic Modeling System

1856 **Table L1: Complete list of abbreviations.**

1857  
 1858 **Code and data availability:** The coupled and uncoupled REMIND code are implemented in GAMS, and the code and data  
 1859 management is done using R. The coupled and the uncoupled DIETER are entirely implemented in GAMS. The default

1860 uncoupled REMIND v3.0.0 code is available from the GitHub website: <https://github.com/remindmodel/remind> (last access: 1  
1861 September 2022), and is archived on Zenodo under the GNU Affero General Public License, version 3 (AGPLv3) (Luderer et  
1862 al., 2022b). The technical model documentation is available under <https://rse.pik-potsdam.de/doc/remind/3.0.0/> (last access: 1  
1863 September 2022). The coupled version of REMIND is available from <https://github.com/cchrisgong/remind-coupling-dieter-tree/couple> (last access: 2 September 2022); coupled DIETER is available from: <https://github.com/cchrisgong/dieter-coupling-remind> (last access: 2 September 2022). The two sets of coupling codes are archived at Zenodo under Creative  
1864 Commons Attribution 4.0 International License (Luderer et al., 2022c). The GAMS code, results, and scripts to produce the  
1865 figures shown in this paper are archived at Zenodo (Gong, 2022).

1868 **Author contribution:** Methodology development was done by CG, FU, and RP. CG designed and carried out the numerical  
1869 implementation, and performed theoretical analysis of the methodology. The methodology was first conceptualized by GL.  
1870 Supervision and funding acquisition were carried out by FU and GL. OA participated in development of model post-processing  
1871 and the overall structuring of the manuscript. MK and WPS performed theoretical and conceptual validation of the manuscript.  
1872 CG prepared the manuscript with contributions from all co-authors.

1873 **Competing interests:** The authors declare that they have no conflict of interest.

1874 **Acknowledgement:** The authors thank Professor Dr. Tom Brown at The Technical University of Berlin, and Dr. Marian  
1875 Leimbach, Dr. Renato Rodrigues, Dr. Nico Bauer at the Potsdam Institute for Climate Impact Research for discussion. We  
1876 gratefully received financial support by the German Federal Ministry of Education and Research (BMBF) via the project  
1877 Kopernikus-Ariadne (FKZ 03SFK5N0, FKZ 03SFK5A) and via the INTEGRATE project (FKZ 01LP1928A). We also received  
1878 financial support from the German Federal Environmental Foundation (Deutsche Bundesstiftung Umwelt).

## 1879 **References**

1880 Alimou, Y., Maïzi, N., Bourmaud, J.-Y., and Li, M.: Assessing the security of electricity supply through multi-scale modeling:  
1881 The TIMES-ANTARES linking approach, *Appl. Energy*, 279, 115717, <https://doi.org/10.1016/j.apenergy.2020.115717>, 2020.

1882 Data Platform – Open Power System Data: [https://data.open-power-system-data.org/renewable\\_power\\_plants/2017-02-16](https://data.open-power-system-data.org/renewable_power_plants/2017-02-16), last  
1883 access: 22 January 2022.

1884 openmod - Open Energy Modelling Initiative: <https://openmod-initiative.org/>, last access: 21 January 2022.

1885 Release REMIND v3.0.0 · remindmodel/remind: <https://github.com/remindmodel/remind/releases/tag/v3.0.0>, last access: 11  
1886 August 2022.

1887 Aryapur, V., O’Gallachoir, B., Dai, H., Chen, W., and Glynn, J.: A review of spatial resolution and regionalisation in national-  
1888 scale energy systems optimisation models, *Energy Strategy Rev.*, 37, 100702, <https://doi.org/10.1016/j.esr.2021.100702>, 2021.

1889 Azevedo, I., Bataille, C., Bistline, J., Clarke, L., and Davis, S.: Net-zero emissions energy systems: What we know and do not  
1890 know, *Energy Clim. Change*, 2, 100049, <https://doi.org/10.1016/j.egycc.2021.100049>, 2021.

1891 Bauer, N., Calvin, K., Emmerling, J., Fricko, O., Fujimori, S., Hilaire, J., Eom, J., Krey, V., Kriegler, E., Mouratiadou, I., Sytze  
1892 de Boer, H., van den Berg, M., Carrara, S., Daioglou, V., Drouet, L., Edmonds, J. E., Gernaat, D., Havlik, P., Johnson, N.,  
1893 Klein, D., Kyle, P., Marangoni, G., Masui, T., Pietzcker, R. C., Strubegger, M., Wise, M., Riahi, K., and van Vuuren, D. P.:  
1894 Shared Socio-Economic Pathways of the Energy Sector – Quantifying the Narratives, *Glob. Environ. Change*, 42, 316–330,  
1895 <https://doi.org/10.1016/j.gloenvcha.2016.07.006>, 2017.

1896 Baumstark, L., Bauer, N., Benke, F., Bertram, C., Bi, S., Gong, C. C., Dietrich, J. P., Dirnachner, A., Giannousakis, A., Hilaire,

1897 J., Klein, D., Koch, J., Leimbach, M., Levesque, A., Madeddu, S., Malik, A., Merfort, A., Merfort, L., Odenweller, A., Pehl, M.,  
1898 Pietzcker, R. C., Piontek, F., Rauner, S., Rodrigues, R., Rottoli, M., Schreyer, F., Schultes, A., Soergel, B., Soergel, D., Strefler,  
1899 J., Ueckerdt, F., Kriegler, E., and Luderer, G.: REMIND2.1: Transformation and innovation dynamics of the energy-economic  
1900 system within climate and sustainability limits, *Geosci. Model Dev. Discuss.*, 1–50, <https://doi.org/10.5194/gmd-2021-85>, 2021.  
1901 Bhaskar, A., Assadi, M., and Nikpey Somehsaraei, H.: Decarbonization of the Iron and Steel Industry with Direct Reduction of  
1902 Iron Ore with Green Hydrogen, *Energies*, 13, 758, <https://doi.org/10.3390/en13030758>, 2020.  
1903 Bistline, J. E. T.: The importance of temporal resolution in modeling deep decarbonization of the electric power sector, *Environ.*  
1904 *Res. Lett.*, 16, 084005, <https://doi.org/10.1088/1748-9326/ac10df>, 2021.  
1905 Blanford, G. J. and Weissbart, C.: A Framework for Modeling the Dynamics of Power Markets – The EU-REGEN Model, ifo  
1906 Working Paper Series, ifo Institute - Leibniz Institute for Economic Research at the University of Munich, 2019.  
1907 Böttger, D. and Härtel, P.: On wholesale electricity prices and market values in a carbon-neutral energy system, *Energy Econ.*,  
1908 106, 105709, <https://doi.org/10.1016/j.eneco.2021.105709>, 2022.  
1909 Brinkerink, M.: Assessing 1.5–2°C scenarios of integrated assessment models from a power system perspective - Linkage with a  
1910 detailed hourly global electricity model, Monograph, IIASA, Laxenburg, Austria, 2020.  
1911 Brinkerink, M., Zakeri, B., Huppmann, D., Glynn, J., Ó Gallachóir, B. and Deane, P.: Assessing global climate change  
1912 mitigation scenarios from a power system perspective using a novel multi-model framework, *Environ. Model Softw.*, 150,  
1913 105336, <https://doi.org/10.1016/j.envsoft.2022.105336>, 2022.  
1914 Brown, T. and Reichenberg, L.: Decreasing market value of variable renewables can be avoided by policy action, *Energy Econ.*,  
1915 100, 105354, <https://doi.org/10.1016/j.eneco.2021.105354>, 2021.  
1916 Brown, T., Hörsch, J., and Schlachtberger, D.: PyPSA: Python for Power System Analysis, *J. Open Res. Softw.*, 6, 4,  
1917 <https://doi.org/10.5334/jors.188>, 2018a.  
1918 Brown, T., Schlachtberger, D., Kies, A., Schramm, S., and Greiner, M.: Synergies of sector coupling and transmission  
1919 reinforcement in a cost-optimised, highly renewable European energy system, *Energy*, 160, 720–739,  
1920 <https://doi.org/10.1016/j.energy.2018.06.222>, 2018b.  
1921 Brunner, C., Deac, G., Braun, S., and Zöphel, C.: The future need for flexibility and the impact of fluctuating renewable power  
1922 generation, *Renew. Energy*, 149, 1314–1324, <https://doi.org/10.1016/j.renene.2019.10.128>, 2020. Butnar, I., Li, P.-H., Strachan,  
1923 N., Portugal Pereira, J., Gambhir, A., and Smith, P.: A deep dive into the modelling assumptions for biomass with carbon  
1924 capture and storage (BECCS): A transparency exercise., *Environ. Res. Lett.*, <https://doi.org/10.1088/1748-9326/ab5c3e>, 2019.  
1925 Calvin, K., Bond-Lamberty, B., Clarke, L., Edmonds, J., Eom, J., Hartin, C., Kim, S., Kyle, P., Link, R., Moss, R., McJeon, H.,  
1926 Patel, P., Smith, S., Waldhoff, S., and Wise, M.: The SSP4: A world of deepening inequality, *Glob. Environ. Change*, 42, 284–  
1927 296, <https://doi.org/10.1016/j.gloenvcha.2016.06.010>, 2017.  
1928 Chang, M., Thellufsen, J. Z., Zakeri, B., Pickering, B., Pfenninger, S., Lund, H., and Østergaard, P. A.: Trends in tools and  
1929 approaches for modelling the energy transition, *Appl. Energy*, 290, 116731, <https://doi.org/10.1016/j.apenergy.2021.116731>,  
1930 2021.  
1931 Cherp, A., Vinichenko, V., Tosun, J., Gordon, J. A., and Jewell, J.: National growth dynamics of wind and solar power  
1932 compared to the growth required for global climate targets, *Nat. Energy*, 6, 742–754, <https://doi.org/10.1038/s41560-021-00863-0>, 2021.  
1933 Clarke, L., Wei, Y.-M., De La Vega Navarro, A., Garg, A., Hahmann, A. N., Khennas, S., Azevedo, I. M. L., Löschel, A.,  
1934 Singh, A. K., Steg, L., Strbac, G., and Wada, K.: Energy Systems. In IPCC, 2022: Climate Change 2022: Mitigation of Climate  
1935 Change. Contribution of Working Group III to the Sixth Assessment Report of the Intergovernmental Panel on Climate Change,  
1936

1937 219, <https://doi.org/doi: 10.1017/9781009157926.008>, 2022.

1938 Conejo, A.J., Castillo, E., Mínguez R. and García-Bertrand, R.: Decomposition techniques in mathematical programming.

1939 Springer-Verlag Berlin Heidelberg, 2006.

1940 Creutzig, F., Agoston, P., Goldschmidt, J. C., Luderer, G., Nemet, G., and Pietzcker, R. C.: The underestimated potential of

1941 solar energy to mitigate climate change, *Nat. Energy*, 2, 17140, <https://doi.org/10.1038/nenergy.2017.140>, 2017.

1942 Deane, J. P., Chiodi, A., Gargiulo, M., and Ó Gallachóir, B. P.: Soft-linking of a power systems model to an energy systems

1943 model, *Energy*, 42, 303–312, <https://doi.org/10.1016/j.energy.2012.03.052>, 2012. National long-term strategies:

1944 <https://ec.europa.eu/info/energy-climate-change-environment/implementation-eu-countries/energy-and-climate-governance-and->

1945 reporting/national-long-term-strategies\_en

1946 last access: 15 January 2022.

1947 E3MLab, PRIMES Model Version 2018 - detailed model description, <http://www.e3mlab.ntua.gr/e3mlab/PRIMES>, last access:

1948 4 May 2023, 2018.

1949 Ellenbeck, S. and Lilliestam, J.: How modelers construct energy costs: Discursive elements in Energy System and Integrated

1950 Assessment Models, *Energy Res. Soc. Sci.*, 47, 69–770, <https://doi.org/10.1016/j.erss.2018.08.021>, 2019.

1951 Figueiredo, N. C. and Silva, P. P. da: The price of wind power generation in Iberia and the merit-order effect, *Int. J. Sustain.*

1952 *Energy Plan. Manag.*, 15, 21–30, <https://doi.org/10.5278/ijsepm.2018.15.4>, 2018.

1953 Frysztacki, M. M., Hörsch, J., Hagenmeyer, V., and Brown, T.: The strong effect of network resolution on electricity system

1954 models with high shares of wind and solar, *Appl. Energy*, 291, 116726, <https://doi.org/10.1016/j.apenergy.2021.116726>, 2021.

1955 Fuso Nerini, F., Keppo, I., Strachan, N.: Myopic decision making in energy system decarbonisation pathways. A UK case study.

1956 *Energy Strategy Rev.*, 17, 19–26, <https://doi.org/10.1016/j.esr.2017.06.001>, 2017.

1957 Gaete-Morales, C., Kittel, M., Roth, A., and Schill, W.-P.: DIETERpy: A Python framework for the Dispatch and Investment

1958 Evaluation Tool with Endogenous Renewables, *SoftwareX*, 15, 100784, <https://doi.org/10.1016/j.softx.2021.100784>, 2021.

1959 Gan, D., Feng, D., and Xie, J.: *Electricity Markets and Power System Economics*, CRC Press, Boca Raton, 220 pp.,

1960 <https://doi.org/10.1201/b15550>, 2013.

1961 Geels, F., Berkhout, F. and van Vuuren, D.: Bridging analytical approaches for low-carbon transitions, *Nat. Clim. Change*, 6,

1962 576–583, <https://doi.org/10.1038/nclimate2980>, 2016.

1963 Giarola, S., Mittal, S., Vielle, M., Perdana, S., Campagnolo, L., Delpiazzo, E., Bui, H., Kraavi, A. A., Kolpakov, A., Sognnaes,

1964 I., Peters, G., Hawkes, A., Köberle, A. C., Grant, N., Gambhir, A., Nikas, A., Doukas, H., Moreno, J., and van de Ven, D.-J.:

1965 Challenges in the harmonisation of global integrated assessment models: A comprehensive methodology to reduce model

1966 response heterogeneity, *Sci. Total Environ.*, 783, 146861, <https://doi.org/10.1016/j.scitotenv.2021.146861>, 2021.

1967 Gils, H. C., Gardian, H., Kittel, M., Schill, W.-P., Zerrahn, A., Murmann, A., Launer, J., Fehler, A., Gaumnitz, F., van

1968 Ouwerkerk, J., Bußar, C., Mikurda, J., Torralba-Díaz, L., Janßen, T., and Krüger, C.: Modeling flexibility in energy systems —

1969 comparison of power sector models based on simplified test cases, *Renew. Sustain. Energy Rev.*, 158, 111995,

1970 <https://doi.org/10.1016/j.rser.2021.111995>, 2022a.

1971 Gils, H. C., Gardian, H., Kittel, M., Schill, W.-P., Murmann, A., Launer, J., Gaumnitz, F., van Ouwerkerk, J., Mikurda, J., and

1972 Torralba-Díaz, L.: Model-related outcome differences in power system models with sector coupling—Quantification and

1973 drivers, *Renew. Sustain. Energy Rev.*, 159, 112177, <https://doi.org/10.1016/j.rser.2022.112177>, 2022b.

1974 Gong, C. C.: REMIND-DIETER - code, reportings, scripts, <https://doi.org/10.5281/zenodo.7072625>, 2022.

1975 Griffiths, S., Sovacool, B. K., Kim, J., Bazilian, M., and Uratani, J. M.: Industrial decarbonization via hydrogen: A critical and

1976 systematic review of developments, socio-technical systems and policy options, *Energy Res. Soc. Sci.*, 80, 102208,

1977 <https://doi.org/10.1016/j.erss.2021.102208>, 2021.

1977 Guivarch, C., Kriegler, E., Portugal-Pereira, J., and Bosetti, V.: IPCC, 2022: Annex III: Scenarios and modelling methods, In  
1978 IPCC, 2022:, in: Climate Change 2022: Mitigation of Climate Change. Contribution of Working Group III to the Sixth  
1979 Assessment Report of the Intergovernmental Panel on Climate Change, Cambridge University Press, Cambridge, United  
1980 Kingdom and New York, NY, USA, <https://doi.org/10.1017/9781009157926.022>, 2022.

1981 Günther, C., Schill, W.-P., and Zerrahn, A.: Prosumage of solar electricity: Tariff design, capacity investments, and power  
1982 sector effects, *Energy Policy*, 152, 112168, <https://doi.org/10.1016/j.enpol.2021.112168>, 2021.

1983 Guo, F., van Ruijven, B.J., Zakeri, B., Zhang, S., Chen, X., Liu, C., Yang, F., Krey, V., Riahi, K., Huang, H. and Zhou, Y.:  
1984 Implications of intercontinental renewable electricity trade for energy systems and emissions, *Nat. Energy*, 7, 1144–1156,  
1985 <https://doi.org/10.1038/s41560-022-01136-0>, 2022.

1986 Haydt, G., Leal, V., Pina, A., and Silva, C. A.: The relevance of the energy resource dynamics in the mid/long-term energy  
1987 planning models, *Renew. Energy*, 36, 3068–3074, 2011.

1988 Hildmann, M., Ulbig, A., and Andersson, G.: Empirical Analysis of the Merit-Order Effect and the Missing Money Problem in  
1989 Power Markets With High RES Shares, *IEEE Trans. Power Syst.*, 30, 1560–1570,  
1990 <https://doi.org/10.1109/TPWRS.2015.2412376>, 2015.

1991 Hirth, L.: The market value of variable renewables: The effect of solar wind power variability on their relative price, *Energy  
1992 Econ.*, 38, 218–236, <https://doi.org/10.1016/j.eneco.2013.02.004>, 2013.

1993 Hirth, L.: What caused the drop in European electricity prices? A factor decomposition analysis, *Energy J.*, 39,  
1994 <https://doi.org/10.5547/01956574.39.1.lhir>, 2018.

1995 Hirth, L. and Ueckerdt, F.: Redistribution effects of energy and climate policy: The electricity market, *Energy Policy*, 62, 934–  
1996 947, <https://doi.org/10.1016/j.enpol.2013.07.055>, 2013.

1997 Huppmann, D., Gidden, M., Fricko, O., Kolp, P., Orthofer, C., Pimmer, M., Kushin, N., Vinca, A., Mastrucci, A., Riahi, K., and  
1998 Krey, V.: The MESSAGEix Integrated Assessment Model and the ix modeling platform (ixmp): An open framework for  
1999 integrated and cross-cutting analysis of energy, climate, the environment, and sustainable development, *Environ. Model. Softw.*,  
2000 112, 143–156, <https://doi.org/10.1016/j.envsoft.2018.11.012>, 2019.

2001 ICCSD Tsinghua University: Power Sector, in: China's Long-Term Low-Carbon Development Strategies and Pathways:  
2002 Comprehensive Report, edited by: Institute of Climate Change and Sustainable Development of Tsinghua University et al.,  
2003 Springer, Singapore, 109–130, [https://doi.org/10.1007/978-981-16-2524-4\\_4](https://doi.org/10.1007/978-981-16-2524-4_4), 2022.

2004 IEA: World Energy Outlook 2021, <https://www.iea.org/reports/world-energy-outlook-2021>, 2021.

2005 IPCC: Climate change 2014: mitigation of climate change : Working Group III contribution to the Fifth assessment report of the  
2006 Intergovernmental Panel on Climate Change, edited by: Edenhofer, O., Pichs-Madruga, R., Sokona, Y., Farahani, E., Kadner, S.,  
2007 Seyboth, K., Alder, A., Baum, I., Brunner, S., Eikemeier, P., Kriemann, B., Salolainen, J., Schlömer, S., Stechow, C. von,  
2008 Zwicker, T., and Minx, J. C., Cambridge University Press, Cambridge, United Kingdom and New York, NY, USA, 2014.

2009 IRENA: Renewable power generation costs in 2019, International Renewable Energy Agency, 2020.

2010 Kannan, R. and Turton, H.: A Long-Term Electricity Dispatch Model with the TIMES Framework, *Environ. Model. Assess.*, 18,  
2011 325–343, <https://doi.org/10.1007/s10666-012-9346-y>, 2013.

2012 Karush, W.: Minima of functions of several variables with inequalities as side conditions., 1939.

2013 Keppo, I., Butnar, I., Bauer, N., Caspani, M., Edelenbosch, O., Emmerling, J., Fragkos, P., Guivarch, C., Harmsen, M., Lefèvre,  
2014 J., Le Gallic, T., Leimbach, M., McDowall, W., Mercure, J.-F., Schaeffer, R., Trutnevye, E., and Wagner, F.: Exploring the  
2015 possibility space: taking stock of the diverse capabilities and gaps in integrated assessment models, *Environ. Res. Lett.*, 16,  
2016 053006, <https://doi.org/10.1088/1748-9326/abe5d8>, 2021.

2017 Koch, J. and Leimbach, M.: Update of Ssp GDP Projections: Capturing Recent Changes in National Accounting, PPP  
2018 Conversion and Covid 19 Impacts, <https://doi.org/10.2139/ssrn.4011838>, 2022.

2019 Koutstaal, P. R. and va. Hout, M.: Integration costs and market value of variable renewables: A study for the Dutch power  
2020 market, 2017.

2021 Kuhn, H. W. and Tucker, A. W.: Nonlinear Programming, Proc. Second Berkeley Symp. Math. Stat. Probab., 2, 481–493, 1951.

2022 Lazard: Lazard's Levelized Cost of Energy Analysis - Version 15.0., 2021.

2023 Levesque, A., Pietzcker, R. C., Baumstark, L., De Stercke, S., Grüber, A., Luderer, G.: How much energy will buildings  
2024 consume in 2100? A global perspective within a scenario framework, Energy, 148, 514-527,  
2025 <https://doi.org/10.1016/j.energy.2018.01.139>, 2018.

2026 Leimbach, M., Bauer, N., Baumstark, L., Luken, M., and Edenhofer, O.: Technological Change and International Trade -  
2027 Insights from REMIND-R, Energy J., 31, 109–136, <https://doi.org/10.5547/ISSN0195-6574-EJ-Vol31-NoSI-5>, 2010.

2028 Li, P.-H. and Pye, S.: Assessing the benefits of demand-side flexibility in residential and transport sectors from an integrated  
2029 energy systems perspective, Appl. Energy, 228, 965–979, <https://doi.org/10.1016/j.apenergy.2018.06.153>, 2018.

2030 López Prol, J. and Schill, W.-P.: The Economics of Variable Renewable Energy and Electricity Storage, Annu. Rev. Resour.  
2031 Econ., 13, 443–467, <https://doi.org/10.1146/annurev-resource-101620-081246>, 2021.

2032 Luderer, G., Pietzcker, R. C., Carrara, S., de Boer, H. S., Fujimori, S., Johnson, N., Mima, S., and Arent, D.: Assessment of  
2033 wind and solar power in global low-carbon energy scenarios: An introduction, Energy Econ., 64, 542–551,  
2034 <https://doi.org/10.1016/j.eneco.2017.03.027>, 2017.

2035 Luderer, G., Vrontisi, Z., Bertram, C., Edelenbosch, O., Pietzcker, R. C., Rogelj, J., De Boer, H. S., Drouet, L., Emmerling, J.,  
2036 Fricko, O., Fujimori, S., Havlik, P., Iyer, G., Keramidas, K., Kitous, A., Pehl, M., Krey, V., Riahi, K., Saveyn, B., Tavoni, M.,  
2037 Van Vuuren, D. P., and Kriegler, E.: Residual fossil CO<sub>2</sub> emissions in 1.5–2°C pathways, Nat. Clim. Change, 8, 626–633,  
2038 <https://doi.org/10.1038/s41558-018-0198-6>, 2018.

2039 Luderer, G., Madeddu, S., Merfort, L., Ueckerdt, F., Pehl, M., Pietzcker, R., Rottoli, M., Schreyer, F., Bauer, N., Baumstark, L.,  
2040 Bertram, C., Dirnaichner, A., Humpenöder, F., Levesque, A., Popp, A., Rodrigues, R., Strefler, J., and Kriegler, E.: Impact of  
2041 declining renewable energy costs on electrification in low-emission scenarios, Nat. Energy, 7, 32–42,  
2042 <https://doi.org/10.1038/s41560-021-00937-z>, 2022a.

2043 Luderer, G., Bauer, N., Baumstark, L., Bertram, C., Leimbach, M., Pietzcker, R., Strefler, J., Aboumahboub, T., Abrahão, G.,  
2044 Auer, C., Benke, F., Bi, S., Dietrich, J., Dirnaichner, A., Giannousakis, A., Gong, C. C., Haller, M., Hasse, R., Hilaire, J.,  
2045 Hoppe, J., Klein, D., Koch, J., Körner, A., Kowalczyk, K., Kriegler, E., Levesque, A., Lorenz, A., Ludig, S., Lüken, M., Malik,  
2046 A., Manger, S., Merfort, A., Merfort, L., Moreno-Leiva, S., Mouratiadou, I., Odenweller, A., Pehl, M., Piontek, F., Popin, L.,  
2047 Rauner, S., Richters, O., Rodrigues, R., Roming, N., Rottoli, M., Schmidt, E., Schötz, C., Schreyer, F., Schultes, A., Sörgel, B.,  
2048 Ueckerdt, F., Verpoort, P., and Weigmann, P.: REMIND - REgional Model of INvestments and Development, Zenodo,  
2049 <https://doi.org/10.5281/zenodo.6794920>, 2022b.

2050 Luderer, G., Bauer, N., Gong, C. C., Odenweller, A., Baumstark, L., Bertram, C., Leimbach, M., Pietzcker, R., Strefler, J.,  
2051 Aboumahboub, T., Abrahão, G., Auer, C., Benke, F., Bi, S., Dietrich, J., Dirnaichner, A., Giannousakis, A., Haller, M., Hasse,  
2052 R., Hilaire, J., Hoppe, J., Klein, D., Koch, J., Kowalczyk, K., Kriegler, E., Levesque, A., Ludig, S., Malik, A., Merfort, A.,  
2053 Merfort, L., Moreno, S., Mouratiadou, I., Pehl, M., Piontek, F., Popin, L., Rauner, S., Richters, O., Schötz, C., Rodrigues, R.,  
2054 Ueckerdt, F., Zerrahn, A., Schreyer, F., Sörgel, B., Weigmann, P., Schill, W.-P., Verpoort, P., and Rottoli, M.: REMIND -  
2055 DIETER coupling, Zenodo, <https://doi.org/10.5281/zenodo.7053246>, 2022c.

2056 Ludig, S., Haller, M., Schmid, E., and Bauer, N.: Fluctuating renewables in a long-term climate change mitigation strategy,

2057 Energy, 36, 6674–6685, <https://doi.org/10.1016/j.energy.2011.08.021>, 2011.

2058 Martínez-Gordón, R., Morales-España, G., Sijm, J., and Faaij, A. P. C.: A review of the role of spatial resolution in energy  
2059 systems modelling: Lessons learned and applicability to the North Sea region, Renew. Sustain. Energy Rev., 141, 110857,  
2060 <https://doi.org/10.1016/j.rser.2021.110857>, 2021.

2061 Mills, A. D. and Wiser, R. H.: Strategies to mitigate declines in the economic value of wind and solar at high penetration in  
2062 California, Appl. Energy, 147, 269–278, <https://doi.org/10.1016/j.apenergy.2015.03.014>, 2015.

2063 Mowers, M., Mignone, B. K. and Steinberg, D. C.: Quantifying value and representing competitiveness of electricity system  
2064 technologies in economic models, Applied Energy, 329, 120132, <https://doi.org/10.1016/j.apenergy.2022.120132>, 2023.

2065 NGFS: NGFS Climate Scenarios for central banks and supervisors, Network for Greening the Financial System, 2020.

2066 van Ouwerkerk, J., Gils, H. C., Gardian, H., Kittel, M., Schill, W.-P., Zerrahn, A., Murmann, A., Launer, J., Torralba-Díaz, L.,  
2067 and Bußar, C.: Impacts of power sector model features on optimal capacity expansion: A comparative study, Renew. Sustain.  
2068 Energy Rev., 157, 112004, <https://doi.org/10.1016/j.rser.2021.112004>, 2022.

2069 Padhy, N. P.: Unit commitment-a bibliographical survey, IEEE Trans. Power Syst., 19, 1196–1205,  
2070 <https://doi.org/10.1109/TPWRS.2003.821611>, 2004.

2071 Pahle, M., Tietjen, O., Osorio, S., Egli, F., Steffen, B., Schmidt, T. S. and Edenhofer O.: Safeguarding the energy transition  
2072 against political backlash to carbon markets, Nat. Energy, 7, 290–296, <https://doi.org/10.1038/s41560-022-00984-0>, 2022.

2073 Palzer, A. and Henning, H.-M.: A Future German Energy System with a Dominating Contribution from Renewable Energies: A  
2074 Holistic Model Based on Hourly Simulation, Energy Technol., 2, 13–28, <https://doi.org/10.1002/ente.201300083>, 2014.

2075 Parra, D., Valverde, L., Pino, F. J., and Patel, M. K.: A review on the role, cost and value of hydrogen energy systems for deep  
2076 decarbonisation, Renew. Sustain. Energy Rev., 101, 279–294, <https://doi.org/10.1016/j.rser.2018.11.010>, 2019.

2077 Pietzcker, R. C., Ueckerdt, F., Carrara, S., de Boer, H. S., Després, J., Fujimori, S., Johnson, N., Kitous, A., Scholz, Y.,  
2078 Sullivan, P., and Luderer, G.: System integration of wind and solar power in integrated assessment models: A cross-model  
2079 evaluation of new approaches, Energy Econ., 64, 583–599, <https://doi.org/10.1016/j.eneco.2016.11.018>, 2017.

2080 Pina, A., Silva, C., and Ferrão, P.: Modeling hourly electricity dynamics for policy making in long-term scenarios, Energy  
2081 Policy, 39, 4692–4702, <https://doi.org/10.1016/j.enpol.2011.06.062>, 2011.

2082 Prina, M.G., Manzolini, G., Moser, D., Nastasi, B., and Sparber, W.: Classification and challenges of bottom-up energy system  
2083 models - A review, Renewable and Sustainable Energy Reviews, 129, 109917, <https://doi.org/10.1016/j.rser.2020.109917>, 2020.

2084 P.R. Shukla et al.: Climate Change 2022: Mitigation of Climate Change. Contribution of Working Group III to the Sixth  
2085 Assessment Report of the Intergovernmental Panel on Climate Change, <https://doi.org/10.1017/9781009157926>, 2022.

2086 Prol, J. L. and Schill, W.-P.: The Economics of Variable Renewables and Electricity Storage, ArXiv201215371 Econ Q-Fin,  
2087 2020.

2088 Ram, M., Bogdanov, D., Aghahosseini, A., Gulagi, A., Oyewo, S., Child, M., Caldera, U., Sadovskaia, K., Farfan Orozco, F.,  
2089 Noel, L., Fasihi, M., Maybodi, S., and Fell, H.-J.: Global Energy System based on 100% Renewable Energy: Energy Transition  
2090 in Europe Across Power, Heat, Transport and Desalination Sectors, <https://doi.org/10.13140/RG.2.2.10143.00160>, 2018.

2091 Ramsebner, J., Haas, R., Ajanovic, A., and Wietschel, M.: The sector coupling concept: A critical review, WIREs Energy  
2092 Environ., 10, e396, <https://doi.org/10.1002/wene.396>, 2021.

2093 Rechsteiner, R.: German energy transition (Energiewende) and what politicians can learn for environmental and climate policy,  
2094 Clean Technol. Environ. Policy, 23, 305–342, <https://doi.org/10.1007/s10098-020-01939-3>, 2021.

2095 Ringkjøb, H.-K., Haugan, P. M. and Solbrekke, I. M.: A review of modelling tools for energy and electricity systems with large  
2096 shares of variable renewables, Renewable and Sustainable Energy Reviews, 96, 440-459,

2097 <https://doi.org/10.1016/j.rser.2018.08.002>, 2018.

2098 Rodrigues, R., Pietzcker, R., Fragkos, P., Price, J., McDowall, W., Siskos, P., Fotiou, T., Luderer, G., and Capros, P.: Narrative-  
2099 driven alternative roads to achieve mid-century CO<sub>2</sub> net neutrality in Europe, *Energy*, 239, 121908,  
2100 <https://doi.org/10.1016/j.energy.2021.121908>, 2022.

2101 Rogelj, J., Shindell, D., Jiang, K., Fifita, S., Forster, P., Ginzburg, V., Handa, C., Kheshgi, H., Kobayashi, S., Kriegler, E.,  
2102 Mundaca, L., Séférian, R., and Vilariño, M. V.: Mitigation pathways compatible with 1.5°C in the context of sustainable  
2103 development, in: Special Report on the impacts of global warming of 1.5 °C, Intergovernmental Panel on Climate Change,  
2104 Geneva, 2018.

2105 Rotmans, J. and van Asselt, M. B. A.: Uncertainty in Integrated Assessment Modelling: A Labyrinthic Path, *Integr. Assess.*, 2,  
2106 43–55, <https://doi.org/10.1023/A:1011588816469>, 2001.

2107 Ruhnau, O.: How flexible electricity demand stabilizes wind and solar market values: The case of hydrogen electrolyzers, *Appl.*  
2108 *Energy*, 307, 118194, <https://doi.org/10.1016/j.apenergy.2021.118194>, 2022.

2109 Say, K., Schill, W.-P., and John, M.: Degrees of displacement: The impact of household PV battery prosumage on utility  
2110 generation and storage, *Appl. Energy*, 276, 115466, <https://doi.org/10.1016/j.apenergy.2020.115466>, 2020.

2111 Schill, W.-P., Roth, A., Guéret, A.: Ampel-Monitor Energiewende Shows the Pace of the Energy Transition Must Be  
2112 Accelerated Significantly. [https://doi.org/10.18723/diw\\_dwr:2022-26-1](https://doi.org/10.18723/diw_dwr:2022-26-1), 2022.

2113 Schill, W.-P. and Zerrahn, A.: Long-run power storage requirements for high shares of renewables: Results and sensitivities,  
2114 *Renew. Sustain. Energy Rev.*, 83, 156–171, <https://doi.org/10.1016/j.rser.2017.05.205>, 2018.

2115 Schill, W.-P. and Zerrahn, A.: Flexible electricity use for heating in markets with renewable energy, *Appl. Energy*, 266, 114571,  
2116 <https://doi.org/10.1016/j.apenergy.2020.114571>, 2020.

2117 Schill, W.-P., Pahle, M., and Gambardella, C.: Start-up costs of thermal power plants in markets with increasing shares of  
2118 variable renewable generation, *Nat. Energy*, 2, 1–6, <https://doi.org/10.1038/nenergy.2017.50>, 2017.

2119 Seljom, P., Rosenberg, E., Schäffer, L. E., and Fodstad, M.: Bidirectional linkage between a long-term energy system and a  
2120 short-term power market model, *Energy*, 198, 117311, <https://doi.org/10.1016/j.energy.2020.117311>, 2020.

2121 Sensfuß, F.: Assessment of the impact of renewable electricity generation on the German electricity sector: An agent-based  
2122 simulation approach, <https://doi.org/10.5445/IR/1000007777>, 2007.

2123 Sensfuß, F., Ragwitz, M., and Genoese, M.: The merit-order effect: A detailed analysis of the price effect of renewable  
2124 electricity generation on spot market prices in Germany, *Energy Policy*, 36, 3076–3084, 2008.

2125 Sepulveda, N. A., Jenkins, J. D., de Sisternes, F. J., and Lester, R. K.: The Role of Firm Low-Carbon Electricity Resources in  
2126 Deep Decarbonization of Power Generation, *Joule*, 2, 2403–2420, <https://doi.org/10.1016/j.joule.2018.08.006>, 2018.

2127 Sitarz, J., Pahle, M., Osorio, S., Luderer, G. and Pietzcker, R.: EU carbon prices signal high policy credibility and farsighted  
2128 actors, preprint, <https://doi.org/10.21203/rs.3.rs-2761645/v1>, 2023.

2129 Staub-Kaminski, I., Zimmer, A., Jakob, M. and Marschinski, R.: Climate policy in practice: a typology of obstacles and  
2130 implications for integrated assessment modeling, *Clim. Change Econ.*, 05, 1440004,  
2131 <https://doi.org/10.1142/S2010007814400041>, 2014.

2132 Stehfest, E., van Vuuren, D., Bouwman, L., and Kram, T.: Integrated assessment of global environmental change with IMAGE  
2133 3.0: Model description and policy applications, Netherlands Environmental Assessment Agency (PBL), 2014.

2134 Stöckl, F., Schill, W.-P., and Zerrahn, A.: Optimal supply chains and power sector benefits of green hydrogen, *Sci. Rep.*, 11,  
2135 14191, <https://doi.org/10.1038/s41598-021-92511-6>, 2021.

2136 Sullivan, P., Krey, V., and Riahi, K.: Impacts of considering electric sector variability and reliability in the MESSAGE model,

2137 Energy Strategy Rev., 1, 157–163, <https://doi.org/10.1016/j.esr.2013.01.001>, 2013.

2138 The White House: The Long-Term Strategy of the United States: Pathways to Net-Zero Greenhouse Gas Emissions by 2050,

2139 United States Department of State and the United States Executive Office of the President, Washington DC., 2021.

2140 Ueckerdt, F., Brecha, R., Luderer, G., Sullivan, P., Schmid, E., Bauer, N., Böttger, D., and Pietzcker, R.: Representing power

2141 sector variability and the integration of variable renewables in long-term energy-economy models using residual load duration

2142 curves, Energy, 90, Part 2, 1799–1814, <https://doi.org/10.1016/j.energy.2015.07.006>, 2015.

2143 Ueckerdt, F., Pietzcker, R., Scholz, Y., Stetter, D., Giannousakis, A., and Luderer, G.: Decarbonizing global power supply under

2144 region-specific consideration of challenges and options of integrating variable renewables in the REMIND model, Energy

2145 Econ., 64, 665–684, <https://doi.org/10.1016/j.eneco.2016.05.012>, 2017.

2146 UNEP: The Emissions Gap Report 2019, UNEP, Nairobi, Kenya, 2019.

2147 Welsch, M., Mentis, D., and Howells, M.: Chapter 17 - Long-Term Energy Systems Planning: Accounting for Short-Term

2148 Variability and Flexibility, in: Renewable Energy Integration, edited by: Jones, L. E., Academic Press, Boston, 215–225,

2149 <https://doi.org/10.1016/B978-0-12-407910-6.00017-X>, 2014.

2150 Weyant, J.: Some Contributions of Integrated Assessment Models of Global Climate Change, Rev. Environ. Econ. Policy, 11,

2151 115–137, <https://doi.org/10.1093/reep/rew018>, 2017.

2152 Wiese, F., Schlecht, I., Bunke, W.-D., Gerbaulet, C., Hirth, L., Jahn, M., Kunz, F., Lorenz, C., Mühlenfordt, J., Reimann, J.,

2153 and Schill, W.-P.: Open Power System Data – Frictionless data for electricity system modelling, Appl. Energy, 236, 401–409,

2154 <https://doi.org/10.1016/j.apenergy.2018.11.097>, 2019.

2155 Wilson, C., Guiavarch, C., Kriegler, E., van Ruijven, B., van Vuuren, D. P., Krey, V., Schwanitz, V. J., and Thompson, E. L.:

2156 Evaluating process-based integrated assessment models of climate change mitigation, Clim. Change, 166, 3,

2157 <https://doi.org/10.1007/s10584-021-03099-9>, 2021.

2158 Younis, A., Benders, R., Ramírez, J., de Wolf, M. and Faaij, A.: Scrutinizing the Intermittency of Renewable Energy in a Long-

2159 Term Planning Model via Combining Direct Integration and Soft-Linking Methods for Colombia’s Power System, Energies, 15,

2160 7604, <https://doi.org/10.3390/en15207604>, 2022.

2161 Zerrahn, A. and Schill, W.-P.: Long-run power storage requirements for high shares of renewables: review and a new model,

2162 Renew. Sustain. Energy Rev., 79, 1518–1534, <https://doi.org/10.1016/j.rser.2016.11.098>, 2017.

2163 Zerrahn, A., Schill, W.-P., and Kemfert, C.: On the economics of electrical storage for variable renewable energy sources, Eur.

2164 Econ. Rev., 108, 259–279, <https://doi.org/10.1016/j.eurocorev.2018.07.004>, 2018.